AN ANALYSIS OF THE MUTUAL COUPLING BETWEEN ANTENNAS ON A SMOOTH CONVEX SURFACE

P. H. Pathak and N. N. Wang

Final Report 784583-7

Contract No. N62269-76-C-0554

October 1978

Department of the Navy
Naval Air Development Center
Warminster, Pennsylvania 18974

UNCLASSIFIED
SECURITY CLASSIFICATION OF THIS PAGE (When Data Entered)

REPORT DOCUMENTATION PAGE		READ INSTRUCTIONS BEFORE COMPLETING FORM
1. REPORT NUMBER NADC-79046-30	2. GOVT ACCESSION NO.	3. RECIPIENT'S CATALOG NUMBER
4. TITLE (and Subtitle) AN ANALYSIS OF THE MUTUAL COUPLING BETWEEN ANTENNAS ON A SMOOTH CONVEX SURFACE		5. TYPE OF REPORT & PERIOD COVERED Final Report 6. PERFORMING ORG. REPORT NUMBER ESL 784583-7
7. AUTHOR(s) P. H. Pathak N. N. Wang		8. CONTRACT OR GRANT NUMBER(s) Contract N62269-76-C-0554
9. PERFORMING ORGANIZATION NAME AND ADDRESS The Ohio State University ElectroScience Laboratory, Department of Electrical Engineering Columbus, Ohio 43212		10. PROGRAM ELEMENT, PROJECT, TASK AREA & WORK UNIT NUMBERS 63206N,WR6-1154 WTW180000,RA702
11. CONTROLLING OFFICE NAME AND ADDRESS Department of the Navy Naval Air Development Center Warminster, Pennsylvania 18974		12. REPORT DATE October 1978 13. NUMBER OF PAGES 92
14. MONITORING AGENCY NAME & ADDRESS(if different from Controlling Office)		15. SECURITY CLASS. (of this report) Unclassified 15a. DECLASSIFICATION/DOWNGRADING SCHEDULE

16. DISTRIBUTION STATEMENT (of this Report)

Approved for public release; distribution unlimited

17. DISTRIBUTION STATEMENT (of the abstract entered in Block 20, if different from Report)

18. SUPPLEMENTARY NOTES

19. KEY WORDS (Continue on reverse side if necessary and identify by block number)

Mutual coupling
Antennas on convex bodies
GTD
Surface rays with torsion
Asymptotic solutions

20. ABSTRACT (Continue on reverse side if necessary and identify by block number)

A simple, approximate, asymptotic high frequency result is developed in this paper for the electromagnetic surface fields excited by infinitesimal electric or magnetic current sources which are placed on a smooth, perfectly-conducting convex surface of any shape. These surface fields propagate along Keller's surface ray paths, and their asymptotic description is uniformly valid along the ray including the immediate vicinity of the source. Furthermore, as the curvature of the surface becomes vanishingly small, this result recovers the known, exact result for the fields on

DD FORM 1 JAN 73 1473 EDITION OF 1 NOV 65 IS OBSOLETE

UNCLASSIFIED
SECURITY CLASSIFICATION OF THIS PAGE (When Data Entered)

20.

a planar, perfectly-conducting surface. The development of this result is heuristically based upon the form of the asymptotic solutions for the surface fields which are first obtained for the canonical circular cylinder and spherical geometries. These solutions are then generalized to the arbitrary convex surface via the local properties of wave propagation at high frequencies. The effect of torsion associated with the surface rays is clearly identified in this result through the presence of a factor T/κ, where T is the surface ray torsion and κ is the surface curvature along the ray direction. Some currently available numerical results based on this analysis are indicated for the circular cylinder case. Included in these numerical results are mutual admittance calculations for a pair of identical (axial or circumferential) slots in a circular cylinder; these numerical results show very good agreement with the results based on the exact (modal) series solution. Additional numerical calculations and experimental verifications for more general surface shapes are being planned for the near future.

TABLE OF CONTENTS

I. INTRODUCTION

An approximate asymptotic high frequency result is developed in this paper for describing the electromagnetic field in the immediate vicinity of a smooth, perfectly-conducting convex surface which is excited either by an infinitesimal electric current source located in the immediate vicinity of the surface, or by an infinitesimal magnetic current source located directly on the surface. The orientation of the electric current source is assumed to be along the surface normal; whereas, the orientation of the magnetic current source is assumed to be along the surface tangent. Thus, this result essentially constitutes an asymptotic approximation to the electric or magnetic type dyadic surface Green's function or its appropriate spatial derivatives, for the above orientations of the infinitesimal electric and magnetic current sources. One may therefore calculate the electromagnetic field in the immediate vicinity of a smooth, convex, conducting surface which is excited either by an aperture, or a thin short stub (monopole) antenna located on that surface by integrating this asymptotic dyadic surface Green's function (or it's appropriate derivatives) over the source distribution either in the aperture, or along the length of the stub, respectively. The source distribution in these cases may be defined in terms of an equivalent tangential magnetic current distribution in the aperture [1], or in terms of an equivalent electric current distribution along the stub, both of which are assumed known. This result for the electromagnetic field generated by an aperture or stub antenna on a convex, conducting surface may be employed to calculate the mutual coupling between a pair of aperture or stub antennas located on that surface via a procedure based on the reaction theorem [2]. The details of such an analysis of the mutual coupling between a pair of radiating elements on a smooth, convex conducting surface are presented in this paper for the case in which one of the radiating elements is an aperture with the other element being either an aperture, or a stub; and also for the case in which both of the radiating elements are stubs. These radiating elements are assumed to be short and thin for reasons that will be indicated later in Section V; in particular, the aperture is assumed to be a thin rectangular slot which is less than a half wavelength long, and the

stub (or monopole) is assumed to be a thin wire which is less than a quarter wavelength long. The problem of mutual coupling is of interest in the following way. A knowledge of the mutual coupling between antennas on a smooth convex surface is essential, for example, in the design of conformal arrays, or in estimating the electromagnetic compatibility of various multi-function antennas that are located on such a surface. In the present context, the smooth convex surface could locally model the region of an aircraft or spacecraft fuselage on which the conformal array, or a pair of multi-function antennas may be located.

In the present asymptotic solution the surface field due to an infinitesimal current source which is placed on a convex surface is associated with Keller's surface rays [3,4,5] which traverse geodesic paths on the surface between the source and the field points, respectively. In particular, the field of these surface rays is expressed in terms of Fock type integrals, and this field representation is uniform in the sense that it remains valid in the neighborhood of the source and within the shadow boundary transition (or penumbra) region; whereas, sufficiently far from the source it can be transformed via Cauchy's residue theorem into a rapidly converging series representation which is commonly referred to as the creeping wave modal series. Furthermore, as the curvature of the surface becomes vanishingly small, this result in terms of the Fock type integrals recovers the known, exact solution for the planar surface. Basically, this asymptotic result is valid provided that the surface curvature is neither large, nor rapidly varying. When the source and the field points are not directly on the surface, but are in the immediate vicinity of the surface, the field is expressed in terms of a Taylor expansion which involves the "soft" and "hard" type* Fock integrals for the surface field and its

*The "soft" and "hard" terminology employed here refers to the soft (or Dirichlet) and hard (or Neumann) boundary conditions encountered in acoustics. The application of these boundary conditions leads to the acoustic (or scalar) wave solutions of the soft and hard types.

derivatives. The soft and hard type Fock integrals denoted by $u(\xi)$ and $v(\xi)$ which appear in all of the field expressions developed here are tabulated by Logan [6], and their derivatives can be calculated numerically in an accurate manner. Thus, the present result not only imparts a simple physical interpretation in terms of surface rays, but it is also in a form which is convenient for engineering applications.

It is noted that several other asymptotic solutions for the surface currents excited by a tangential magnetic current moment on a convex conducting surface have been obtained previously by various authors. Hasserjian and Ishimaru presented an asymptotic solution pertaining to the convex cylinder geometry [7]; they obtained terms to lowest order in $\frac{1}{k\rho_g}$ and $\frac{1}{ks}$, where s is the arc length of the geodesic ray path on the surface from the source to the observation point, ρ_g is the radius of curvature of the surface along the ray direction, and k is the free space wavenumber. The nature of their solution is quite similar to that given earlier by Wait [8] for a large conducting sphere excited by a stub (or a short monopole) antenna. Later, Hwang and Kouyoumjian [9] constructed an asymptotic solution for the convex cylinder case within the systematic framework of the geometrical theory of diffraction (GTD) [3,4,5]. In order to perform this extension of the GTD, they introduced the modal launching and attachment coefficients for torsional surface rays. The launching and attachment coefficients are proportional to Keller's surface ray modal diffraction coefficients [4,5]; these launching and attachment coefficients were introduced earlier in [1] for the case of non-torsional surface rays. The result developed in [9] has been used in [10] for analyzing a simple, conformal, cylindrical array problem. In [9], the vector nature of the surface current (or the tangential surface magnetic field) is expressed rather compactly in a dyadic form by employing the unit tangent and binormal vectors fixed in the local surface ray coordinates at the source and the field points, respectively. As a result, this GTD formulation in [9] provides a simple physical interpretation for the manner in which the surface magnetic field is excited by a tangential magnetic current source on a convex cylindrical surface. As the field point approaches the

neighborhood of the source, the creeping wave modal series representation; i.e., the GTD representation in terms of the modal launching and attachment coefficients becomes slowly convergent, and it is then transformed in [9] into the same Fock type integrals as those employed in [7,8] and in this paper. Such a procedure was mentioned earlier where it was noted that these Fock type integrals can be transformed via the Cauchy residue theorem into the creeping wave residue (or modal) series which are rapidly convergent for large ks. In conformal array applications, the radiating elements are not necessarily far apart so that in the calculation of the mutual coupling between two closely spaced array elements it becomes necessary to evaluate the surface field for small values of ks. In the latter case, higher order terms in 1/ks become significant in the surface field calculation, and they therefore must be included for accuracy; these higher order terms in 1/ks are not present in [7], [8] and [9]. Also, the result in [9] and [10] based on the GTD indicates that the component of the surface magnetic field along the tangent to the ray path may be expressed only in terms of the acoustic soft type surface ray field, and likewise the component along the binormal direction to the ray may be expressed only in terms of the acoustic hard type surface ray field; however, such a simplified field decomposition does not appear to provide a sufficiently complete field description as indicated in some of the more recent analyses [11,12]. The GTD analysis of [9] which represents an asymptotic approximation only to first order nevertheless presents very useful and important concepts. In [11], Chan et. al. obtain asymptotic expressions for the surface fields on a convex cylinder, and also on a semi-infinite cone. The solution* in [11] is expressed in the local surface ray coordinates as in [9], and it contains terms (involving the Fock type integrals) to lowest order in $1/k\rho_g$ and to two orders in 1/(ks). As the curvature of the convex surface becomes vanishingly small, the solution in [11] thus recovers the exact solution

*Three different solutions are presented in [11]; here we refer to their solution which is designated as Full Formula (and it's variant for the circumferential current element).

for the planar surface only to terms in $1/(ks)^2$, but not to terms in $1/(ks)^3$. The solutions in [7], [9] and [11] for the convex cylindrical surface are obtained via a generalization of their respective asymptotic solutions which were developed first for the simpler, canonical circular cylinder geometry. Such a generalization of the canonical solutions is based on the principle of locality of wave propagation at high frequencies as employed in the GTD procedure. Further generalizations to conical surfaces as in [11], or to arbitrary convex surfaces may be performed heuristically in a similar fashion. More recently, Lee [12] has presented an approximate asymptotic solution for an arbitrary convex surface such that it recovers the exact planar result, i.e., up to terms in $1/(ks)^3$, as the surface curvature becomes vanishingly small. The solution in [12] is also expressed in terms of the unit vectors fixed in the surface ray coordinates of [9]. The solution in [12] is obtained by first modifying an asymptotic solution pertaining to the canonical sphere geometry; this "modified" sphere solution is then subsequently generalized heuristically to treat an arbitrary convex surface via the principle of locality of high frequency wave propagation. In particular, an additive type term is introduced into the solution for the sphere problem in [12] in an ad hoc fashion, to construct that "modified" sphere solution. As indicated in [12], the only justification for including this "ad hoc" term is that it is essential for the purposes of obtaining accurate results when the "modified" sphere solution is applied to the circular cylinder geometry; furthermore, when this modified solution is applied back to the sphere geometry, it does not yield numerical values which are significantly different from those based on the un-modified sphere solution. Due to the fact that the solution for the arbitrary convex surface, and hence for the convex cylinder case in [12] is based on the sphere solution to begin with, it therefore always contains both, the acoustic "hard" and "soft" type Fock integrals corresponding to the two types of scalar potentials from which the sphere solution is constructed. However, it is well known that for an axially directed magnetic current source on a perfectly-conducting cylinder, only the scalar potential corresponding to the acoustic "hard" function is required to completely describe the electromagnetic field which is generated by that source.

It is noted that the field solutions in [7], [9],and [11], contain only the acoustic hard type potential for the case of an axial magnetic current source on a convex cylinder. An interesting difference between the cylinder result in [11] and the result in [12] is that a "cross term" exists in the dyadic representation for the surface field of [11]; whereas, it is absent in [12] since the latter solution is based on the sphere solution. Such a cross term which involves higher order range (or $(ks)^{-2}$) dependent terms is also absent in [7] and [9], because the cylinder solutions in [7] and [9] do not contain these higher order range terms.

In this paper, an asymptotic result for the surface fields on an arbitrary, convex, perfectly-conducting convex surface is obtained by generalizing asymptotic solutions which are first constructed in Appendices I and II for the surface fields on canonical, perfectly-conducting, circular cylinder and spherical geometries, respectively. The solution for the sphere problem in Appendix II is essentially based on the method employed by Fock [13]. The excitation for these canonical circular cylinder and sphere problems analyzed in Appendices I and II includes not only a magnetic current source, but also an electric current source. On the other hand, only the case corresponding to the magnetic current source excitation is considered in [7,9,11,12]. The canonical solutions developed in the Appendices are summarized in a dyadic form similar to that in [9,11,12] in terms of the surface ray tangent and binormal vectors. It is noted that the dyadic surface field representation for the canonical cylinder geometry contains a cross term similar to that present in [11], but the form of this cross term is not identical to that in [11]. Furthermore, the solution for the axially directed magnetic current on the cylinder contains only the acoustic hard type potential as in [7,9,11]. The case of magnetic current source excitation is summarized in Section II, and likewise the electric current source excitation case is summarized in Section III. Based on the information present in the results for both, the canonical cylinder geometry and the canonical sphere geometry, these results are in turn heuristically generalized with the aid of the local properties of high frequency wave propagation, to treat an arbitrary convex surface

geometry as indicated in Section IV. Only terms to lowest order in $\frac{1}{k\rho_g}$ are retained in this analysis. The effect of torsion associated with the surface rays is clearly identified in this solution through the presence of a factor T/κ, where T is the surface ray torsion and $\kappa=(\rho_g)^{-1}$. As the surface curvature becomes vanishingly small, the present solution recovers all terms in the known, exact solution for the planar geometry. Expressions for mutual coupling between slots and/or stubs (monopoles) are presented in Section V in terms of the results obtained earlier in Section IV. Some preliminary numerical calculations indicating the accuracy of the results developed in this paper are also shown in Section V.

II. SUMMARY OF ASYMPTOTIC SOLUTIONS TO THE CANONICAL PROBLEMS FOR THE MAGNETIC CURRENT SOURCE CASE

As mentioned earlier, the problems involving the electric and magnetic current source excitation of the circular cylinder and sphere geometries which have been analyzed in Appendices I and II, respectively, serve as canonical problems in the sense that their solutions are instrumental to the development of a solution for an arbitrary convex surface, as indicated in Section IV. Hence, the results obtained in Appendices I and II are summarized in this section for the case of magnetic current source excitation; whereas, corresponding results for the electric current source excitation are summarized in Section III.

The results for the circular cylinder are summarized in part A of this section, and the results for the sphere case are summarized in part B. These results are expressed below in an invariant form in terms of the local surface ray coordinates as in [9].

A. Asymptotic Results for the Canonical Circular Cylinder Problem

The circular cylinder geometry of interest is illustrated in Figure 1. The infinitesimal magnetic current source, $\bar{M}$ which excites the circular cylinder may be represented in terms of the Dirac delta function by

$$\overline{M} = \overline{p}_m \, \delta(|\overline{r}-\overline{r}'|). \tag{1}$$

The source $\overline{M}$ is assumed to be placed at P_N' on the surface of the cylinder and it is oriented tangential to the surface. The quantity p_m refers to the strength of the infinitesimal magnetic current (or current moment), and $\overline{r}$ is an arbitrary position vector; whereas, $\overline{r}'$ is the position vector at the source location P_N' on the circular cylinder.

First, expressions for the electric and magnetic fields are given for the case when the field point is located at a point P_N which is on the surface. Next, an expression is given for the normal component of the electric field when the field point is moved from P_N to the point P which lies above but in the close vicinity of the surface.

From the details of the analysis in Appendix I, it is observed that the field may be interpreted to arrive at P_N from the source point at P_N' via a geodesic ray propagation path on the surface. It is noted that in the case of the cylinder, the geodesic surface ray paths are helices. The vector nature of this field at P_N may be expressed compactly in terms of a triad of unit vectors fixed in the surface ray coordinates at P_N' and P_N. These unit vectors are defined as follows. Let $\hat{n}$ and $\hat{n}'$ denote the unit outward normal vectors to the surface at P_N and P_N', respectively; likewise, let $\hat{t}$ at P_N and $\hat{t}'$ at P_N' denote the unit vectors which are oriented along the forward tangent to the geodesic surface ray path from P_N' to P_N. Then the unit binormal vectors at P_N and P_N' associated with the geodesic ray path between these points are defined by $\hat{b} = \hat{t} \times \hat{n}$ and $\hat{b}' = \hat{t}' \times \hat{n}'$, respectively. These unit tangent, normal, and binormal vectors constitute the triad of unit vectors associated with a surface ray. The surface ray geodesic path between P_N' and P_N, and the associated triad of unit vectors at these end points are illustrated in Figure 1. In addition, the pair of unit vectors $(\hat{\tau}_1', \hat{\tau}_2')$ and $(\hat{\tau}_1, \hat{\tau}_2)$ along the principal directions on the cylinder surface at P_N' and P_N are also illustrated in Figure 1. It is noted that the following relationships exist between the various unit vectors.

$$\cos\delta = \hat{t}'\cdot\hat{\tau}_1' = \hat{\tau}_2'\cdot\hat{b}' = \hat{t}\cdot\hat{\tau}_1 = \hat{\tau}_2\cdot\hat{b} \quad , \tag{2a}$$

$$\sin\delta = \hat{t}'\cdot\hat{\tau}_2' = -(\hat{\tau}_1'\cdot\hat{b}') = -(\hat{\tau}_1\cdot\hat{b}) = \hat{t}\cdot\hat{\tau}_2. \tag{2b}$$

Referring to (2a;2b), and (A-34) of Appendix I, one may now express the tangential magnetic field $\bar{H}_t^m$ at P_N on the surface due to the source $\bar{M}$ at P_N' in terms of the unit vectors defined above as follows.

$$\bar{H}_t^m(P_N) \sim \bar{p}_m \cdot \Bigg[\hat{\tau}_1'\hat{\tau}_1' \cdot \Bigg(\hat{b}'\hat{b} \left[1 - \frac{j}{ks}\left(1 - \frac{j}{ks}\right)\right] v(\xi) + \hat{t}'\hat{t}\left[\frac{2j}{ks}\left(1 - \frac{j}{ks}\right)\right] v(\xi) \Bigg) +$$

$$+ \hat{\tau}_2'\hat{\tau}_2' \cdot \Bigg(\hat{b}'\hat{b} \Bigg\{ \left[1 - \frac{j}{ks}\left(1 - \frac{j}{ks}\right)\right] v(\xi) + (f)\,\frac{j}{ks}\,[u(\xi) - v(\xi)] \Bigg\} +$$

$$+ \hat{t}'\hat{t} \Bigg\{ \left[\frac{2j}{ks}\left(1 - \frac{j}{ks}\right)\right] v(\xi) + (f)\,\frac{j}{ks}\,[u(\xi) - v(\xi)] \Bigg\} \Bigg) \Bigg] G(ks) \tag{3}$$

where a = radius of the circular cylinder,

$$G(ks) = \frac{k^2 Y_o}{2\pi j}\,\frac{e^{-jks}}{ks} \quad , \tag{4}$$

$$\xi = \frac{ms}{\rho_g} \; ; \quad \text{with } m = \left(\frac{k\rho_g}{2}\right)^{1/3} \text{ and } \rho_g = a/\sin^2\delta. \tag{5}$$

The factor f is defined as $1/\sin^2\delta$ in (A-27b) of Appendix I.

The quantity Y_o is the free space admittance. The quantities k and s refer to the free space wavenumber and the length of the surface ray geodesic path from P_N' to P_N; whereas, ρ_g denotes the radius of curvature of the surface along the ray (or $\hat{t}$) direction, as indicated previously in Section I. The result in Equation (3) represents $\bar{H}_t^m$ along a given geodesic ray path from P_N' to P_N. In the circular cylinder problem, there are two, dominant, helical geodesic paths from P_N' to P_N, and only one such path is indicated in Figure 1; the other geodesic path (not indicated) encircles the cylinder in the opposite sense with respect to the one shown in Figure 1.

The total field is then the sum of the fields of each of these rays. The result in Equation (3) also applies to the other geodesic path provided that the unit vectors $\hat{t}', \hat{b}', \hat{t}, \hat{b}, \hat{n}$, and the quantities s, and ξ are now associated with this other ray path. In addition, infinitely many geodesic surface ray paths corresponding to multiple encirclements of the cylinder (before reaching the field point) do exist; however, their contribution is negligible for large ka. The functions $u(\xi)$ and $v(\xi)$ refer to the "soft" and "hard" Fock type integrals which are defined in Equations (A-22a) and (A-29) of Appendix I. As mentioned earlier, Logan has provided tabulated values of the Fock integrals $u(\xi)$ and $v(\xi)$; in addition, he has also given rapidly convergent series expansions to accurately represent these functions [6]. The series expansions for $u(\xi)$ and $v(\xi)$ are also indicated in [11,12]. Although the series expansions in $u(\xi)$ and $v(\xi)$ are available in [6,11,12], they are presented in Appendix V for the sake of completeness; it is noted that separate expansions exist for large and small values of ξ, and these separate expansions provide numerical values which do overlap for moderate values of ξ as shown in [11]. The result in Equation (3) is therefore in terms of functions which can be computed rather easily. One may express this result in Equation (3) more compactly as

$$\bar{H}_t^m(P_N) \sim \bar{p}_m \cdot \left(\hat{b}'\hat{b} \left[1 - \frac{j}{ks}\left(1 - \frac{j}{ks}\right) \right] v(\xi) + \hat{t}'\hat{t} \left[\frac{2j}{ks}\left(1 - \frac{j}{ks}\right) \right] v(\xi) \right) G(ks)$$

$$+ \bar{p}_m \cdot \hat{\tau}_2' \hat{\tau}_2 \; (f) \; \frac{j}{ks}[u(\xi) - v(\xi)] \Big) G(ks) \quad , \tag{6}$$

since $\hat{\tau}_1'\hat{\tau}_1' + \hat{\tau}_2'\hat{\tau}_2' = \bar{\bar{I}}_s$, where $\bar{\bar{I}}_s$ denotes an identity dyad on a surface so that $\bar{p}_m \cdot \bar{\bar{I}}_s = \bar{p}_m$, and $(\hat{\tau}_2' \cdot \hat{b}')\hat{b} + (\hat{\tau}_2' \cdot \hat{t}')\hat{t} = \hat{\tau}_2$. Even though the result in Equation (6) is more compact than the one in Equation (3), the expression in Equation (3) indicates more directly the fact that the field $\bar{H}_t^m$ which is produced by the axial or the $\hat{\tau}_1'$-component of the source $\bar{p}_m$ is substantially different from that which is produced by the circumferential or the $\hat{\tau}_2'$-component of $\bar{p}_m$. In particular, the $\hat{\tau}_1'$ or the axial component of $\bar{p}_m$ generates a field $\bar{H}_t^m$ which contains only the hard type Fock integral $v(\xi)$

as expected; whereas, the $\hat{\tau}_2'$-component of $\bar{p}_m$ generates both, $u(\xi)$ and $v(\xi)$ type terms. That the $\hat{\tau}_1'$ component of $\bar{p}_m$ generates only a $v(\xi)$ type term is in agreement with the results in [7,9,11]; on the other hand, the result in [12] indicates that this axial component of $\bar{p}_m$ generates both, $u(\xi)$ and $v(\xi)$ type functions in the cylinder problem. Also, the "cross" term of the type $\bar{p}_m \cdot \hat{\tau}_2' \hat{\tau}_2 (---) G(ks)$ in Equation (6) is also present in [11], except that the functional form of this term in [11] is somewhat different from that in Equation (6). Such a "cross term" is not present in the result of [12]. Furthermore, except for the important difference which exists in the functional form of this "cross term", the result given in [11] otherwise agrees with that of Equation (6) up to terms in $1/ks$ and $1/(ks)^2$. It is noted that terms of order $1/(ks)^3$ are present in Equation (6), but they are not present in [11].

From Equation (A-36b) of Appendix I, and the relationships in Equation (2a;b), one may similarly express the component of the electric field $\bar{E}_n^m$ which is normal to the surface at P_N, and which is excited by the source $\bar{M}$ at P_N', in terms of the surface ray coordinates as follows.

$$\bar{E}_n^m(P_N) \sim (Y_o)^{-1} \bar{p}_m \cdot \left(\hat{b}' \hat{n} \left[1 - \frac{j}{ks} \right] v(\xi) + \hat{\tau}_2' \cos\delta \, \hat{n} \, f \, \frac{j}{ks} [u(\xi) - v(\xi)] \right) G(ks). \quad (7)$$

As before, Equation (7) represents the field of a "typical" surface ray path from P_N' to P_N; there are of course, two such dominant ray paths and the field of both of these rays must be included to obtain the total field.

The results in Equation (7) may now be generalized such that the field $\bar{E}_n^m$ is evaluated not on the surface at P_N, but is instead evaluated at a point P which lies above the surface. It is assumed that the point P lies in the immediate neighborhood of the surface. In particular, the point P_N on the surface represents the projection of the point P along the normal to the surface, and the height of the point P above P_N is denoted by d_2 as shown in Figures 1 and 2. Thus,

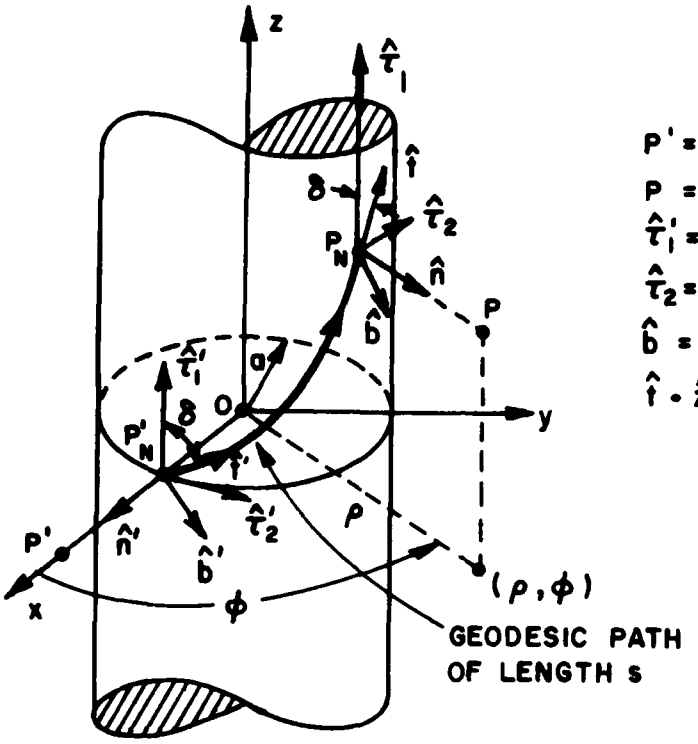

$P' = P'(a+d_1, 0, 0)$

$P = P(a+d_2, \phi, z)$

$\hat{\tau}_1' = \hat{z}$ AT P_N'; $\hat{\tau}_1 = \hat{z}$ AT P_N

$\hat{\tau}_2 = \hat{\phi}$ AT P_N'; $\hat{\tau}_2 = \hat{\phi}$ AT P_N

$\hat{b} = \hat{t} \times \hat{n}$; $\hat{b}' = \hat{t}' \times \hat{n}'$

$\hat{t} \cdot \hat{z} = \cos\delta = \hat{t}' \cdot \hat{z}'$

Figure 1. Circular cylinder geometry.

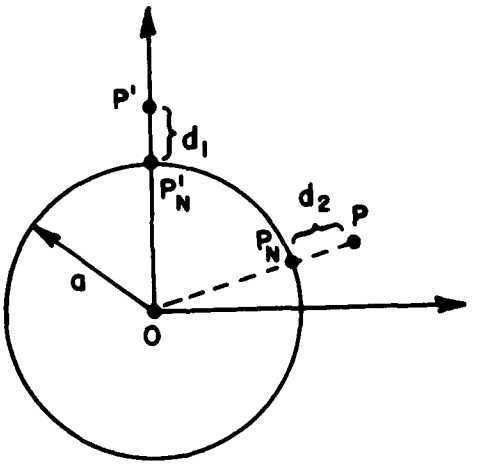

Figure 2. Cross sectional view indicating the heights d_1 and d_2 of the points p' and P above the surface.

$$\overline{P_N P} = |\overline{P_N P}|\hat{n} = d_2\hat{n}. \tag{8}$$

From the comments at the end of Appendix I, it is seen that the results for $E_n^m(P)$ is the same as that in Equation (7) with the exception that the functions $u(\xi)$ and $v(\xi)$ must now be replaced by the more general Fock functions $F_s(\xi,y_1,y_2)$ and $F_h(\xi,y_1,y_2)$, respectively, which are defined in Equation (A-139) and Equation (A-138) of Appendix V. Hence,

$$E_n^m(P) \sim (Y_o)^{-1}\bar{p}_m \cdot \left(\hat{b}'\hat{n}\left[1 - \frac{j}{ks}\right]F_h(\xi,0,y_2) + \hat{\tau}_2' \cos\delta \;\; \hat{n} \; f \;\; \frac{j}{ks}[F_s(\xi,0,y_2) - F_h(\xi,0,y_2)] \right) \cdot G(ks) \tag{9a}$$

The quantities y_1 and y_2 can be shown to be related to d_1 and d_2 as follows.

$$y_1 = m^{-1}kd_1 = 0 \text{ (since } \overline{M} \text{ is at } P_N'); \qquad y_2 = m^{-1}kd_2 \; . \tag{9b;9c}$$

Since kd_2 is assumed to be much smaller than ka in the present case (i.e., P is in the immediate neighborhood of the surface), a Taylor series approximation for the functions $F_s(\xi,y_1,y_2)$ and $F_h(\xi,y_1,y_2)$ may be employed as indicated in Equations (A-146) and (A-145) of Appendix V. Such an approximation appears to be valid only if the value of ξ is not too close to zero; however, it has the advantage that for sufficiently small ky_1 and ky_2, the functions F_s, and F_h may be evaluated in terms of the derivatives of the functions $-j\sqrt{\frac{\pi}{j\xi^3}}\,u(\xi)$, and $\sqrt{\frac{4\pi}{j\xi}}\,v(\xi)$, respectively; these derivatives with respect to the argument ξ may be easily computed numerically in an accurate fashion; on the other hand, accurate approximations for these functions and their derivatives are available (see Appendix V).

B. Asymptotic Results for the Canonical Sphere Problem

The sphere geometry is illustrated in Figure 3. The infinitesimal magnetic current source $\overline{M}$ is located at P_N' on the sphere and it has been

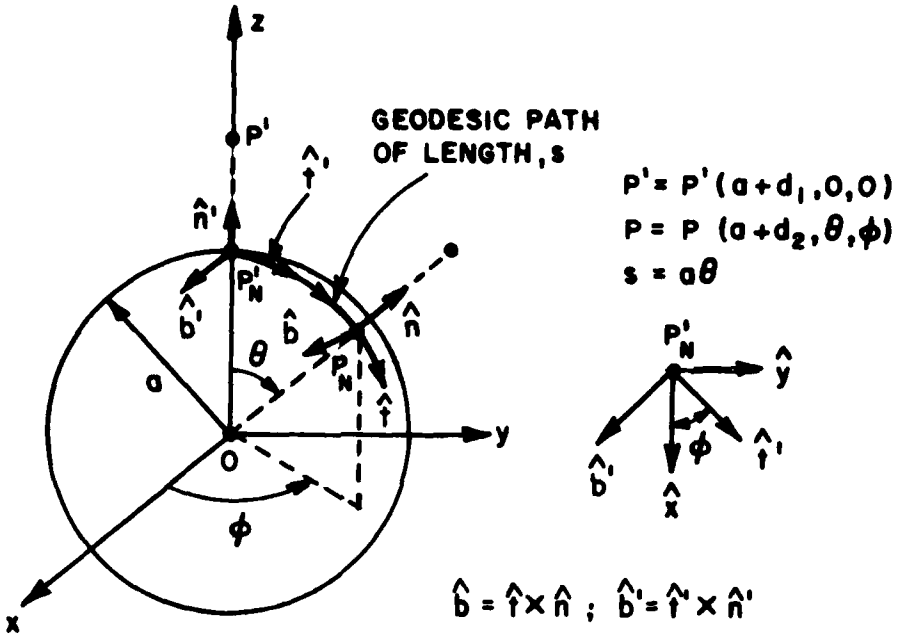

Figure 3. Sphere geometry.

defined previously in Equation (1). Following the development in Part A for the circular cylinder, the tangential magnetic field $\overline{H}_t^m$ at P_N on a perfectly-conducting spherical surface which is excited by $\overline{M}$ may also be expressed in terms of the local, geodesic surface ray coordinates as follows. Firstly, it is noted that the geodesic surface ray paths on the sphere are great circles. The triad of unit vectors, $(\hat{t}',\hat{n}',\hat{b}')$ at P_N', and $(\hat{t},\hat{n},\hat{b})$ at P_N, which are associated with a geodesic (great circle) path that connects these points are illustrated in Figure 3. Secondly, the following relationships exist between the unit vector triad associated with a surface ray path, and the usual triad of unit vectors $(\hat{r},\hat{\theta},\hat{\phi})$ associated with the spherical coordinates.

$$\left.\begin{aligned} &\hat{\theta} = \hat{t} \;\; ; \;\; \hat{\phi} = -\hat{b} \;\; ; \;\; \hat{r} = \hat{n} \;\; . \qquad\qquad 0 \le \theta \le \pi \qquad \text{(10a);(10b);(10c)} \\ &\text{Also,} \\ &\overline{p}_m \cdot \hat{t}' = \cos\phi \;\; ; \;\; \overline{p}_m \cdot \hat{b}' = -\sin\phi \;\; . \qquad\qquad \text{(10d);(10e)} \end{aligned}\right\}$$

When Equations (10a-10e) above are incorporated into Equations (A-104a;b;c) of Appendix II, one obtains

$$\bar{H}_t^m(P_N) \sim \bar{p}_m \cdot \left(\hat{b}'\hat{b} \left[(1 - \frac{j}{ks}) v(\xi) + D^2 (\frac{j}{ks})^2 u(\xi) \right] + \hat{t}'\hat{t} \left[D^2 \frac{j}{ks} v(\xi) + \frac{j}{ks} (1 - \frac{2j}{ks}) u(\xi) \right] \right) D \cdot G(ks), \tag{11}$$

where

$$D = \sqrt{\frac{\theta}{\sin\theta}}, \text{ a quantity which is related to the surface ray divergence factor,} \tag{12}$$

and

$$\xi = \frac{ms}{a}, \quad \text{with } s = a\theta. \tag{13}$$

As in Equation (6), the above result in Equation (11) is associated with only one geodesic (great circle) path between P_N' and P_N as shown in Figure 3. A second geodesic (great circle) path also exists between P_N' and P_N; this path is not shown in Figure 3, and it corresponds to the one which arrives at P_N after being launched at P_N' in a direction opposite to the path shown in Figure 3. The result in Equation (11) applies also to the other geodesic path provided the unit vectors, $\hat{t}', \hat{b}', \hat{t}, \hat{b}$, and $\hat{n}$, and the quantities, s, θ, D and ξ are now associated with this other ray path. The contribution from additional, multiply encircling surface rays is negligible for large ka. Except for the factor D^2 which appears with the square brackets in Equation (11), this result agrees with the one obtained by Lee [12]. It appears that D^2 has been approximated by unity in [12]. It is noted that $\theta = \pi$, or $ks = ka\pi$ is the position of a focal caustic of the surface rays on a sphere. At $\theta = \pi$, D is unbounded, and the result in Equation (11) must be modified as indicated in Appendix III. In particular, the total surface magnetic field, $\bar{H}_t^{m(total)}$; i.e., the sum of the fields $\bar{H}_t^m$ associated with "both" of the great circle geodesic paths from P_N' to P_N must be replaced by

$$H_t^{m(\text{total})}(P_N) \Big|_{\substack{P_N \text{ in the close} \\ \text{neighborhood} \\ \text{of } \theta=\pi}} \sim -\bar{p}_m \cdot \left(\hat{b}' \hat{\phi} \left[(1 - \frac{j}{ks}) v(\xi) \right] - \hat{t}' \hat{\theta} \left[\frac{j}{ks} (1 - \frac{2j}{ks}) u(\xi) \right] \right) T_{c1}$$

$$- \bar{p}_m \cdot \left(\hat{b}' \hat{\phi} \left[(\frac{j}{ks})^2 u(\xi) \right] - \hat{t}' \hat{\theta} \left[\frac{j}{ks} v(\xi) \right] \right) T_{c3} \quad , \qquad (14)$$

where the caustic correction factors T_{c1} and T_{c3} are given in Equations (A-128) and (A-130) of Appendix III. Away from $\theta=\pi$, the result in Equation (14) accurately approximates the sum of the field associated with each of the two geodesic (great circle) ray paths from P_N' to P_N in which the field of either one of these rays is typically given by Equation (11).

From Equation (10), and Equation (A-109) of Appendix II, one may also write the normal component of the electric field E_n^m, at P_N due to the source $\bar{M}$ at P_N', in terms of the surface ray coordinates associated with a typical geodesic surface ray path between P_N' and P_N as follows.

$$E_n^m(P_N) \sim (Y_o)^{-1} \bar{p}_m \cdot \left(\hat{b}' \hat{n} \left[1 - \frac{j}{ks} \right] v(\xi) \right) D\, G(ks). \qquad (15)$$

Actually, the total field at P_N is the sum of the fields associated with the two dominant geodesic (great circle) paths which exist between the points P_N' and P on the sphere; the form of the field along each of these paths is as in Equation (15).

The result in Equation (15) may be generalized to include the case in which the field point is no longer on the surface at P_N, but is moved to a point P which lies above the surface; it is assumed in this generalization however, that P is in the close neighborhood of the surface. As before, P_N is the normal projection on the surface of the Point P which is located a distance, d_2 above the surface. The relationship between P_N and P is as given in Equation (8). From the discussion at the end of

Appendix II, it is seen that when $d_2 \neq 0$, the $v(\xi)$ in Equation (15) must be replaced by $F_h(\xi, y_1, y_2)$ of Equation (A-138) with $y_1 = 0$. The quantities y_1 and y_2 are as in Equations (9b) and (9c), respectively. Since kd_2 is assumed to be much smaller than ka, $F_h(\xi, y_1, y_2)$ may be approximated by a Taylor series for small y_2 as in Equation (A-145) provided that ξ is not allowed to approach too close to zero. As $\theta \to \pi$, $D \to \infty$, and the total surface electric field $\bar{E}_n^{m(\text{total})}$; i.e., the sum of the fields $\bar{E}_n^m$ associated with "both" of the great circle geodesic paths from P_N' to P_N must be replaced by

$$\bar{E}_n^{m(\text{total})}(P_N)\Big|_{\theta \approx \pi} \sim (Y_o)^{-1} \bar{p}_m \cdot \left(\hat{b}' \hat{n} \left[1 - \frac{j}{ks} \right] v(\xi) \right) T_{c2} \tag{16}$$

where the caustic correction factor T_{c2} is given in Equation (A-129) of Appendix III. If P_N is changed to P in Equation (16), then $v(\xi)$ must be replaced by $F_h(\xi, y_1, y_2)$ with $y_1 = 0$.

III. SUMMARY OF ASYMPTOTIC SOLUTIONS TO THE CANONICAL PROBLEMS FOR THE ELECTRIC CURRENT SOURCE CASE

In this section, asymptotic solutions for the fields in the immediate vicinity of the canonical perfectly-conducting circular cylindrical, and spherical geometries are summarized for the case when they are excited by an infinitesimal electric current source. The electric current source is placed in the close neighborhood of the cylindrical and spherical geometries, and the orientation of this source is assumed to be along the surface normal. As mentioned previously, the asymptotic solutions to these canonical problems are developed in detail in Appendices I and II for the circular cylindrical and spherical geometries, respectively. The results for the circular cylinder case are presented in Part A of this section, and corresponding results for the spherical case are presented subsequently in part B.

A. Asymptotic Results for the Canonical Circular Cylinder Problem

The circular cylinder geometry is illustrated as before in Figure 1. The source and the field points are initially chosen to lie at P_N' and P_N on the surface. The electric current source $\overline{J}$ is defined as

$$\overline{J} = \overline{p}_e \, \delta(|\overline{r}-\overline{r}'|). \tag{17}$$

It is noted that $\overline{r}'$ is the position vector of the source at P_N' on the cylinder surface, and the quantity p_e represents the strength of the infinitesimal electric current (or current moment). From Equation (A-39) of Appendix I, the tangential magnetic field $\overline{H}_t^e$ at P_N due to $\overline{J}$ at P_N' propagates along a typical geodesic surface ray path as shown in Figure 1. This field may be expressed in terms of the unit vectors t',n',b' and t,n,b fixed in the surface ray as,

$$\overline{H}_t^e(P_N) \sim -(\gamma_o)^{-1} \overline{p}_e \cdot \left(\hat{n}'\hat{b}\left[1 - \frac{j}{ks}\right] v(\xi) + \hat{n}' \cos\delta \, \hat{\tau}_2 \, f \, \frac{j}{ks}[u(\xi)-v(\xi)] \right) G(ks). \tag{18}$$

There are of course two dominant geodesic surface ray paths as mentioned earlier; only one such path is shown in Figure 1. The field of either of these rays is given by Equation (18).

If the source at P_N' is now raised a distance d_1 above the surface to the point P' as shown in Figure 1, where P' is in the close vicinity of the surface, then the result in Equation (18) must be replaced as before by

$$\overline{H}_t^e(P_N) \sim -(\gamma_o)^{-1} \overline{p}_e \cdot \left(\hat{n}'\hat{b}\left[1 - \frac{j}{ks}\right] F_h(\xi,y_1,0) + \hat{n}' \cos\delta \, \hat{\tau}_2 \, f \, \frac{j}{ks}[F_s(\xi,y_1,0)-F_h(\xi,y_1,0)] \right) \cdot G(ks) \tag{19}$$

It is noted that $y_2 = m^{-1}kd_2 = 0$ in $F_{s\atop h}(\xi,y_1,y_2)$ which appears in Equation

(19) since P_N is on the surface. Only $y_1 = m^{-1}kd_1$ may be non-zero. Furthermore, $\overline{P'_N P'} = |P'_N P'|\hat{n}' = d_1\hat{n}'$. As before, the $F_{s,h}(\xi,y_1,0)$ functions may be approximated by a Taylor series valid for sufficiently small kd_1 ($kd_1 << ka$) and for ξ not too close to zero, as indicated in Equations (A-145) and (A-146) of Appendix V.

From Equation (A-42) of Appendix I, the component of the electric field $\overline{E}^e_n$, which is normal to the surface at P_N, due to $\overline{J}$ at P'_N, may be expressed in terms of the surface ray coordinates associated with a "typical" geodesic surface ray path between P'_N and P_N as follows.

$$\overline{E}^e_n(P_N) \sim -(Y_o)^{-2}\overline{p}_e \cdot \hat{n}'\hat{n}\left(\left[1 - \frac{j}{ks}\left(1 - \frac{j}{ks}\right)\right] v(\xi) + f\,\frac{j}{ks}\,[u(\xi)-v(\xi)] - \right.$$

$$\left. - \frac{j}{ks}\left(1 - \frac{j}{ks}\right)[u(\xi)-v(\xi)]\right) G(ks), \qquad (20a)$$

or

$$\overline{E}^e_n(P_N) \sim -(Y_o)^{-2}\overline{p}_e \cdot \hat{n}'\hat{n}\left(v(\xi) - \frac{j}{ks}\left(1 - \frac{j}{ks}\right)u(\xi) + f\,\frac{j}{ks}[u(\xi)-v(\xi)]\right) G(ks) \qquad (20b)$$

One notes that if source and observation points at P'_N and P_N are both moved to the points P' and P, respectively which lie above the surface such that $\overline{P'_N P'} = d_1\hat{n}'$ with $kd_1 << ka$, and $\overline{P_N P} = d_2\hat{n}$ with $kd_2 << ka$, then the $u(\xi)$ and $v(\xi)$ in Equation (20) must be replaced by $F_s(\xi,y_1,y_2)$ and $F_h(\xi,y_1,y_2)$, respectively. Thus,

$$\overline{E}^e_n(P) \sim -(Y_o)^{-2}\overline{p}_e \cdot \hat{n}'\hat{n}\left(\left[1 - \frac{j}{ks}\left(1 - \frac{j}{ks}\right)\right] F_h(\xi,y_1,y_2) + f\,\frac{j}{ks}[F_s(\xi,y_1,y_2) - \right.$$

$$\left. - F_h(\xi,y_1,y_2)] - \frac{j}{ks}\left(1 - \frac{j}{ks}\right)[F_s(\xi,y_1,y_2) - F_h(\xi,y_1,y_2)]\right) G(ks), \qquad (21)$$

with $y_{1,2} = m^{-1}kd_{1,2}$.

B. Asymptotic Results for the Canonical Sphere Problem

The geometry of the sphere problem is illustrated in Figure 3. The source $\bar{J}$ as defined in Equation (17) is initially located at P_N' on the spherical surface. From Equations (10a-10e), and (A-110) of Appendix II, the tangential magnetic field $\bar{H}_t^e$ at P_N on the sphere due to the source $\bar{J}$ at P_N' may be expressed in terms of the surface ray coordinates associated with a typical geodesic great circle ray path between P_N' and P_N as indicated below.

$$\bar{H}_t^e(P_N) \sim -(Y_o)^{-1} \bar{p}_e \cdot \left(\hat{n}' \hat{b} \left[1 - \frac{j}{ks} \right] v(\xi) \right) D\, G(ks) \quad . \tag{22}$$

As before, the total field at P_N is the sum of the fields associated with the two dominant geodesic surface ray paths which exist between the points P_N' and P_N on the sphere; the form of the field along each of these paths is given by Equation (22). As $\theta \to \pi$, P_N approaches the focal caustic of the surface rays; hence, the total surface magnetic field $\bar{H}_t^{e(total)}$; i.e., the sum of the fields $\bar{H}_t^e$ associated with "both" of the great circle surface ray paths from P_N' to P_N must be replaced by:

$$\bar{H}_t^{e(total)}(P_N) \Big|_{\theta \approx \pi} \sim +(Y_o)^{-1} \bar{p}_e \cdot \left(\hat{n}' \hat{\phi} \left[1 - \frac{j}{ks} \right] v(\xi) \right) T_{c2} \quad . \tag{23}$$

The factor T_{c2} is defined in Equation (A-129) of Appendix III. Also, if P_N' is moved to P' with $\overline{P_N'P'} = d_1 \hat{n}'$, and $kd_1 << ka$ as before, then $v(\xi)$ in Equation (22) must be replaced by $F_h(\xi, y_1, y_2)$ with $y_2 = 0$.

From Equations (10a-10e), and (A-112) of Appendix II, the normal component of the electric field, $\bar{E}_n^e$ at P_N due to $\bar{J}$ at P_N' is expressed as follows

$$\bar{E}_n^e(P_N) \sim -(Y_o)^{-2} \bar{p}_e \cdot \hat{n}' \hat{n} \left(\left[1 - \frac{j}{ks} \left(1 - \frac{j}{ks} \right) \right] v(\xi) \right) D\, G(ks). \tag{24}$$

Again, the result in Equation (24) represents the field associated with a "typical" geodesic surface ray path between the points P_N' and P_N on a sphere. If the source and observation points at P_N' and P_N are both moved to the points P' and P, respectively which lie above the surface such that $\overline{P_N'P'}=d_1\hat{n}'$ with $kd_1<<ka$, and $\overline{P_NP}=d_2\hat{n}$ with $kd_2<<ka$, then $v(\xi)$ in Equation (24) must be replaced by $F_h(\xi,y_1,y_2)$. Finally, if $\theta\to\pi$, the result in Equation (24) becomes singular, and the total electric field $\overline{E}_n^{e(total)}$; i.e., the sum of the fields $\overline{E}_n^e$ associated with "both" of the great circle paths between P_N' and P_N must be replaced by

$$\overline{E}_n^{e(total)}(P_N) \sim -(Y_o)^{-2}\overline{p}_e\cdot\left(\hat{n}'\hat{n}\left[1-\frac{j}{ks}\left(1-\frac{j}{ks}\right)\right]v(\xi)\right)T_{cl}, \tag{25}$$

where the caustic correction factors T_{cl} is as given by Equation (A-128) of Appendix III.

IV. GENERALIZATION TO ARBITRARY CONVEX SURFACES

In this section, the results which were presented in Sections II and III for the canonical circular cylinder and spherical geometries will be generalized to the arbitrary convex surface case. In particular, the results pertaining to the surface fields which are excited by infinitesimal electric or magnetic current sources located on a smooth, perfectly-conducting convex surface of arbitrary shape will be developed in this section.

The generalization of the canonical solutions to treat the arbitrary convex surface case is based on the locality of high frequency wave propagation as employed in the GTD procedure. Thus, the results pertaining to the canonical circular cylinder geometry which were presented in Sections II-A and III-A for the magnetic and electric source excitations, respectively may be generalized via the GTD procedure to treat the arbitrary convex cylinder with a slowly varying curvature, by assuming that the neighborhood of each point on the convex cylinder can be approximated by a circular

cylinder of the same local radius of curvature as the convex cylinder. While such a generalization to the convex cylindrical surface of variable curvature is fairly direct, an analogous generalization presented here to treat a smooth convex surface of any shape is somewhat less direct, and more heuristic in nature for the following reasons. The circular cylinder constitutes a "developable" surface; thus, it possesses an infinite radius of curvature along its "generator" which also constitutes one of the "principal directions" on the surface. In addition, the surface geodesics are always straight lines on the "developed" surface. The arbitrary convex cylinder and the cone also belong to the class of developable surfaces; hence, they possess all of the properties of developable surfaces mentioned above in connection with the circular cylinder geometry. As a result of these common geometrical properties which characterize the cylinder and cone, it is therefore reasonable to conjecture that a GTD type generalization of the results pertaining to the canonical circular cylinder geometry would be accurate for treating not only the convex cylinder, but also the cone geometry. This conjecture has of course been verified by Keller [4] in the case of the GTD analysis of the scattering of waves by a smooth convex cylinder wherein the GTD solution based on the generalization of the corresponding canonical circular cylinder solution was found to agree with the rigorous asymptotic high frequency solutions to the problem of scattering of waves by elliptic, and parabolic cylinder geometries. Recently, Chan et. al. [11] have indicated that they are indeed able to verify that the GTD prescription for the surface ray field on a cone which is based on a generalization of the canonical circular cylinder result, is in agreement with the corresponding rigorous asymptotic high frequency solution for the surface field on a cone; this verification in [11] pertains to a cone with an acoustic hard (or the Neumann) boundary condition. On the other hand, a convex surface with an arbitrary shape is in general neither a surface of revolution, nor a developable surface; hence, a generalization of only the results for the canonical circular cylinder geometry is expected to be inaccurate to treat an arbitrary convex surface; clearly, additional information is required in order to construct an asymptotic result which is useful for treating this case since one notes that the two

principal radii of curvatures on an arbitrary convex surface are in general different and finite. In addition, the torsion associated with the geodesics on an arbitrary convex surface is generally not a constant. In contrast, the canonical circular cylinder geometry possesses a constant principal radius of curvature along the circumferential direction on the surface; whereas, it exhibits an infinite radius of curvature along the other (or the axial) principal direction. Furthermore, the torsion is constant along a given geodesic path on a circular cylinder. Of course, a simple canonical geometry for which both principal radii of curvatures are finite is the sphere. The canonical problem of the radiation by an infinitesimal electric or a magnetic current source on a perfectly-conducting sphere has been treated in Appendix II as mentioned earlier. However, the sphere has a constant curvature, and hence the surface geodesics on a sphere are great circle paths which possess no torsion. A third canonical problem for which a well known, exact solution is available is the problem of the radiation by an infinitesimal electric or a magnetic current source on a perfectly-conducting planar surface of infinite extent. The planar geometry has zero curvature; and the surface geodesics for this case are straight lines which are obviously torsionless. Even though the convex cylinder, and the canonical sphere geometries do not possess all of the general properties associated with a convex surface of an arbitrary shape, the asymptotic solutions pertaining to these geometries including the exact solution for the planar case nevertheless do provide some useful information based on which an approximate asymptotic solution may be constructed for the arbitrary smooth convex surface. Thus, an asymptotic solution for the surface fields excited by infinitesimal electric or magnetic currents located on a smooth, perfectly-conducting convex surface of any shape is developed here on the basis of certain assumptions. Some of these assumptions are completely heuristic in nature. In particular, the development of this asymptotic solution is based on the following properties and assumptions:

(a) An asymptotic solution for the arbitrary convex surface should be expected to recover the solutions pertaining to the canonical circular cylinder and sphere geometries when it is specialized to the latter cases,

respectively. This solution should also be expected to reduce to the well known result for the planar surface in the limit as the curvature of the convex surface becomes vanishingly small.

(b) Since the sphere geometry exhibits uniform (or isotropic) surface properties along different directions on the surface that correspond to the different geodesic paths which originate from a source on the sphere, the scalar components of the dyadic transfer function relating the surface field at the receiving (or observation) point to the launching (or source) point are also independent of these directions as seen from the canonical sphere results of Sections II-B and III-B, respectively. On the other hand, the circular cylinder exhibits non-uniform (or non-isotropic) surface properties along the different directions that again correspond to the different geodesic paths originating from a source on this surface. As a result, the scalar components of the dyadic transfer function for the surface field on a circular cylinder in general are a function of the launching/receiving direction on the surface. It is easily seen from the canonical circular cylinder geometry that this non-uniform surface property results directly from the variation of the geodesic radius of curvature, ρ_g as the launching/receiving direction of this geodesic path is changed at the source/receiver location. Thus, as the launching direction of the geodesic ray path is changed at the source (launch) point on a circular cylinder, from the principal direction along the circumference to the other principal direction along the generator (axial direction), the radius of curvature ρ_g in the direction of the geodesic path increases monotonically from ρ_g=a to $\rho_g \to +\infty$. As a result of the change in ρ_g, the torsion associated with the geodesic path also increases from zero to a maximum value as ρ_g increases from a to 2a. As expected, however, the torsion then decreases back to zero as ρ_g increases from 2a to infinity, since the geodesics along the principal directions on a convex surface must be torsionless. Referring to the results for the surface fields on a circular cylinder as given in Sections II-A and III-A, one notes that the dependence of the scalar components of the surface field dyadic transfer function upon variations in ρ_g, resulting from a change in the launching direction of the geodesic

path at the source can be identified more definitely if the unit vectors $\hat{\tau}_2'$ and $\hat{\tau}_2$ in Equations (6), (7), (18), and (20a) are expressed in terms of the unit vectors $\hat{t}'$, $\hat{b}'$, $\hat{t}$ and $\hat{b}$ fixed in the surface rays. The corresponding results in Equations (11), (15), (22), and (24) for the sphere case have been completely expressed in the surface ray coordinates. Once the cylinder results are also completely expressed in an invariant form in terms of the same surface ray coordinates, the precise differences between the cylinder and sphere solutions should become apparent. Since the goedesic surface ray paths in general posses non-zero torsion in the case of the cylinder; whereas, they are torsionless in the case of the sphere, it is therefore also reasonable to expect that any differences between the cylinder and sphere solutions may be primarily caused by the effects of torsion associated with the surface rays on a cylinder.

In order to express Equations (6), (7), (18), and (20a) completely in terms of the surface ray coordinates, one makes use of the following relationships.

$$\hat{\tau}_1' = \cos\delta\hat{t}'-\sin\delta\hat{b}' \quad ; \quad \hat{\tau}_1 = \cos\delta\hat{t}-\sin\delta\hat{b} \tag{26a;26b}$$

$$\hat{\tau}_2' = \sin\delta\hat{t}'+\cos\delta\hat{b}' \quad ; \quad \hat{\tau}_2 = \sin\delta\hat{t}+\cos\delta\hat{b} \tag{26c;26d}$$

$$\hat{\tau}_2'\hat{\tau}_2 = \sin^2\delta\hat{t}'\hat{t}+\cos^2\delta\hat{b}'\hat{b}+\sin\delta\cos\delta(\hat{t}'\hat{b}+\hat{b}'\hat{t}) \tag{26e}$$

Incorporating Equation (26e) into Equation (6) yields

$$\begin{aligned}\overline{H}_t^m(P_N)\sim\overline{p}_m\cdot\Big(&\hat{b}'\hat{b}\left[(1-\tfrac{j}{ks})v(\xi)+D^2(\tfrac{j}{ks})^2v(\xi)+T_o^2\,\tfrac{j}{ks}\{u(\xi)-v(\xi)\}\right]+\\&+\hat{t}'\hat{t}\left[D^2\,\tfrac{j}{ks}\,v(\xi)+\tfrac{j}{ks}\,u(\xi)-2(\tfrac{j}{ks})^2v(\xi)\right]+\\&+[\hat{t}'\hat{b}+\hat{b}'\hat{t}]T_o\,\tfrac{j}{ks}\{u(\xi)-v(\xi)\}\Big)D\,G(ks)\ .\end{aligned} \tag{27}$$

The factor D which is related to the surface ray divergence factor is unity for the circular cylinder; however, it is introduced symbolically in Equation (27) above to facilitate a direct comparison with the sphere results. The factor $T_o(=\cot\delta)$ is identified as a ratio of the surface ray torsion T and

the surface curvature $\kappa(=1/\rho_g)$ along the ray direction. It is easily verified that for a given helical geodesic surface ray path on a circular cylinder,

$$T_o = \cot\delta = T/\kappa \; ; \; T = \frac{\sin 2\delta}{2a} \; ; \; \kappa = (\rho_g)^{-1} = \frac{\sin^2\delta}{a} \; . \quad (28a;28b;28c)$$

Thus, the quantity T_o is a constant for a given helical surface ray on the cylinder, and indeed, it serves to uniquely specify that helical geodesic path. When T (and hence T_o) is allowed to vanish as in the case of the sphere, the above result in Equation (27) for the cylinder reduces exactly to the result in Equation (11) for the sphere, except for the $(\frac{j}{ks})^2 v(\xi)G(ks)$ term which is different from the $(\frac{j}{ks})^2 u(\xi)G(ks)$ present in the sphere case. As expected, the significant differences between Equations (27) and (11) are thus attributed to the presence of the torsion factor $T_o=T/\kappa$. Proceeding next to rewrite Equation (7) completely in terms of the surface ray coordinates, one obtains

$$\bar{E}_n^m(P_N) \sim (Y_o)^{-1} \bar{p}_m \cdot \left(\hat{b}'\hat{n} \left\{ \left[1 - \frac{j}{ks} \right] v(\xi) + T_o^2 \frac{j}{ks} [u(\xi) - v(\xi)] \right\} + \right.$$
$$\left. + \hat{t}'\hat{n} \, T_o \frac{j}{ks} [u(\xi) - v(\xi)] \right) D \, G(ks) \quad . \quad (29)$$

As in Equation (27), it is noted that D in Equation (29) is unity for the cylinder. When the torsion T is allowed to vanish, the above result in Equation (29) for the cylinder also reduces exactly to the corresponding result in Equation (15) for the sphere. One may next rewrite Equation (18) in the same way that Equation (7) was rewritten to obtain (29). Thus

$$\bar{H}_t^e(P_N) \sim -(Y_o)^{-1} \bar{p}_e \cdot \left(\hat{n}'\hat{b} \left\{ \left(1 - \frac{j}{ks} \right) v(\xi) + T_o^2 \frac{j}{ks} (u(\xi) - v(\xi)) \right\} + \right.$$
$$\left. + \hat{n}'\hat{t} T_o \frac{j}{ks} [u(\xi) - v(\xi)] \right) D \, G(ks). \quad (30)$$

Finally, Equation (20a) may be rewritten as

$$\bar{E}_n^e(P_N) \sim (Y_o)^{-2} \bar{p}_e \cdot \hat{n}'\hat{n} \left(\left\{ v(\xi) - \frac{j}{ks} v(\xi) + (\frac{j}{ks})^2 u(\xi) \right\} + T_o^2 \frac{j}{ks} [u(\xi) - v(\xi)] \right) D \, G(ks), \quad (31)$$

after noting that $f-1=T_0^2$ for the circular cylinder. Again the factor D in Equations (30) and (31) is unity for the circular cylinder and it is introduced symbolically in the above equations to facilitate a direct comparison between the cylinder and the sphere solutions. Clearly, Equation (30) reduces directly to the sphere result of Equation (22) when the torsion is allowed to vanish; on the other hand Equation (31) reduces exactly to the sphere result of Equation (24) if T (and hence T_0) is set equal to zero except for the term $(\frac{j}{ks})^2 u(\xi)G(ks)$ which is different from the term $(\frac{j}{ks})^2 v(\xi)G(ks)$ present in the sphere result. However, the dominant differences between the sphere and the cylinder solutions are clearly attributed to the presence of torsion associated with the surface rays. The only other differences that exist between the cylinder and sphere solutions involve terms with different Fock functions; i.e., they involve terms of the type $(\frac{j}{ks})^2 u(\xi)G(ks)$ and $(\frac{j}{ks})^2 v(\xi)G(ks)$. One of these terms occurs in the sphere solution; whereas, only the other occurs in the cylinder solution, and vice versa. Notice that both, $(\frac{j}{ks})^2 u(\xi)G(ks)$ and $(\frac{j}{ks})^2 v(\xi)G(ks)$ behave essentially as $(\frac{j}{ks})^2 G(ks)$ when ks is small; furthermore, these terms of order $(\frac{1}{ks})^3$ are important only for very small ks values. Consequently, the failure of the cylinder solution to exactly reduce to the sphere solution to terms in $(\frac{1}{ks})^3$, when T is set to zero, is not a serious problem from the point of view of being able to generalize these canonical solutions to the arbitrary convex surface. The following heuristic procedure is proposed for generalizing the cylinder results in Equations (27), (29), (30), and (31), and the corresponding sphere results in Equations (11), (15), (22), (24) to treat the arbitrary convex surface. The results in Equations (27), (29), (30), and (31) for the cylinder may be assumed to be applicable for treating an arbitrary convex surface as well via the local properties of propagation and diffraction at high frequencies, provided the geometrical properties of the arbitrary surface are slowly varying with respect to the wavelength. The geodesic ray paths on an arbitrary convex surface in general possess non-zero torsion. The effects of torsion on the surface ray field are then accounted for by the factor T_0 present in Equations (27), (29), (30), and (31). The torsion T and curvature κ appearing in T_0 of Equation (28a) are given by Equations (28b) and (28c), respectively for a circular cylinder. For an arbitrary convex surface one may write

$$T_o = \frac{T}{\kappa} \; ; \quad T = \frac{\sin 2\delta}{2}(\kappa_2 - \kappa_1) \; ; \quad \kappa = \cos^2\delta\kappa_1 + \sin^2\delta\kappa_2 \qquad (32a;32b;32c)$$

with

$$\hat{t}\cdot\hat{\tau}_1 = \cos\delta \; ; \quad \hat{t}\cdot\hat{\tau}_2 = \sin\delta \quad , \qquad (32d;32e)$$

in which $\hat{\tau}_1$ and $\hat{\tau}_2$ are now the principal directions at any point on an arbitrary convex surface, and κ_1 and κ_2 are the principal surface curvatures. It will be assumed for the sake of definiteness that

$$\kappa_1 \leq \kappa_2 \quad ; \quad \left\{ \begin{matrix} \kappa_1 \geq 0 \\ \kappa_2 \geq 0 \end{matrix} \right\} \quad . \qquad (32f)$$

The result for torsion (or T) in Equation (32b) which applies to a geodesic surface ray path on an arbitrary convex surface has been obtained in a simple manner through the use of differential geometry; whereas, the result in Equation (32c) for the curvature (or $\kappa=1/\rho_g$) is simply a statement of Euler's theorem. For surfaces with slowly varying geometrical properties, one may symmetrically split the factor T_o between the launch (or source) point and the receiving (or field) point on the surface to represent an averaging type effect. Such a symmetrical split is also essential for preserving reciprocity. Thus*

$$T_o = \pm\sqrt{\frac{|T(P_N')| \cdot |T(P_N)|}{|\kappa(P_N')| \cdot |\kappa(P_N)|}} \qquad (33)$$

Next, one introduces the dimensionless shape factors Λ_s and Λ_c to appropriately weight the $(\frac{j}{ks})^2 u(\xi)\, G(ks)$, and the $(\frac{j}{ks})^2 v(\xi) G(ks)$ type terms, such that only one or the other type term is correctly present when the results for the arbitrary convex surface are specialized to either the circular cylinder or the sphere. In particular, this would require that Λ_s and Λ_c have the following properties:

* The - sign is chosen in (33) if $\frac{T}{\kappa}$ is negative at P_N' and/or P_N; otherwise the + sign is chosen

$$\Lambda_s+\Lambda_c = 1 \tag{34a}$$

$$\Lambda_s = \begin{cases} 1, \text{ sphere} \\ 0, \text{ cylinder} \end{cases} \tag{34b}$$

$$\Lambda_c = \begin{cases} 1, \text{ cylinder} \\ 0, \text{ sphere} \end{cases} . \tag{34c}$$

As will be seen later, the property in Equation (34a) is also essential for recovering the planar surface result as $\kappa \to 0$. A simple choice of Λ_s would be to define it as the ratio of the principal curvatures; thus,

$$\Lambda_s = \frac{\kappa_1}{\kappa_2} = \begin{cases} 1, \text{ for a sphere (since } \kappa_1=\kappa_2) \\ 0, \text{ for a cylinder (since } \kappa_1=0) \end{cases} . \tag{34d}$$

From Equation (34a), Λ_c must then be defined as

$$\Lambda_c = \frac{\kappa_2-\kappa_1}{\kappa_2} = \begin{cases} 1, \text{ for a cylinder (since } \kappa_1=0) \\ 0, \text{ for a sphere (since } \kappa_1=\kappa_2) \end{cases} . \tag{34e}$$

Furthermore, the above Λ_s and Λ_c will also be symmetrically split between the launching and receiving points to preserve reciprocity and to represent an averaging type effect for surfaces with slowly varying geometrical properties. It follows that,

$$\Lambda_s = \sqrt{\frac{\kappa_1(P_N')}{\kappa_2(P_N')} \cdot \frac{\kappa_1(P_N)}{\kappa_2(P_N)}} \quad ; \quad \Lambda_c=1-\Lambda_s \text{ (with } \Lambda_s \text{ as in Equation (35a)} \tag{35a;35b}$$

The shape factors Λ_s and Λ_c essentially serve to smoothly interpolate between the cylinder and sphere solutions; this role of the shape factors together with the relation in Equation (35a) guarantees that the conditions set forth in part (a) are satisfied by the solution for the arbitrary convex surface.

As is evident from the cylinder and the sphere solutions, the variation of the surface field between the launching and receiving points is primarily governed by the Fock type functions $u(\xi)$ and $v(\xi)$. In the case of the cylinder, the Fock parameter $\xi = \frac{ms}{\rho_g} = ms\kappa$; whereas, $\xi = \frac{ms}{a}$ for the sphere. This Fock parameter ξ may be readily generalized in the usual manner to treat the arbitrary convex surface case by employing the local properties of wave propagation at high frequencies as follows.

$$\xi = \int_{P_N'}^{P_N} \frac{m}{\rho_g}\, ds \quad ; \quad m = \left(\frac{k\rho_g}{2}\right)^{1/3} , \tag{36}$$

in which the integral is evaluated over the geodesic surface ray path from P_N' to P_N. It is assumed in the development of the result in Equation (36) that m and hence ρ_g vary slowly with a change in the geodesic arc length; i.e., the surface properties are slowly varying. Besides the dependence on ρ_g (or $1/\kappa$), the variation of the surface field between P_N' and P_N also depends upon the surface radius of curvature, $\rho_{tn}=(\kappa_1 \sin^2\delta+\kappa_2\cos^2\delta)^{-1}$ in the binormal direction to the surface ray path; this dependence occurs through the presence of the spatial factor, D which is related to the surface ray divergence factor. For an arbitrary convex surface, it can be shown that

$$D = \sqrt{\frac{s\,d\psi_o}{\rho_c\, d\psi}} , \tag{37}$$

where $d\psi_o$ is the angle extended by the surface ray tube at the launching point P_N', and likewise, $d\psi$ is the angle extended by the same ray tube (or pencil) at the receiving point P_N as shown in Figure 4. Also illustrated in Figure 4 is the caustic distance, ρ_c of the wavefront associated with the surface ray tube. The caustic distance ρ_c is the geodesic (or tangent) radius of curvature of the geodesic circle at P_N. It can be shown through the use of differential geometry that,

$$(\rho_c)^{-1} = \frac{\partial G/\partial s}{2\sqrt{E}\,G} \quad , \tag{38}$$

where E, F and G are the usual "first fundamental coefficients" which arise in the development of the first fundamental form associated with the differential arc length along a curve on a surface. It is easily verified that ρ_c=s on a cylinder and also on a plane; whereas ρ_c=atanθ=atan($\frac{s}{a}$) for a sphere (see Figure 3). This concludes the discussion corresponding to the assumptions and postulates of part (b).

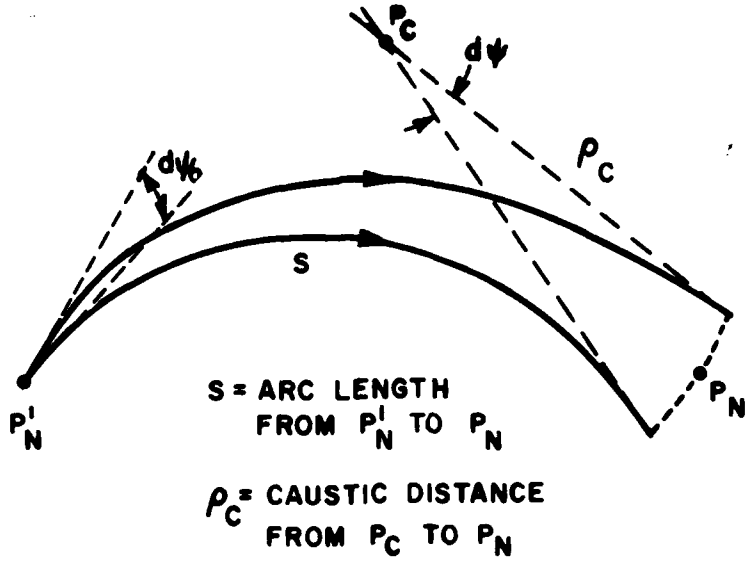

Figure 4. Caustic distance associated wit the spreading of the surface ray field.

A. Surface Fields of an Infinitesimal Magnetic Current Source on a Convex Surface

In this section, an asymptotic solution is presented for the field on an arbitrary convex surface excited by an infinitesimal magnetic current source. The construction of this solution is heuristic in nature, and it follows directly via the postulates and assumptions outlined in parts (a) and (b) above. An analogous solution for the field on an arbitrary convex surface excited by an infinitesimal electric current source will be presented later in Section B. Thus, the field, $\overline{H}_t^m$ for an arbitrary convex surface becomes via Equations (11), (27), and the postualtes in parts (a) and (b), the following,

$$\overline{H}_t^m(P_N) \sim \overline{p}_m \cdot \overline{\overline{y}}_m \quad , \tag{39a}$$

where the dyadic $\overline{\overline{y}}_m$ is given by

$$\begin{aligned}\overline{\overline{y}}_m = \Bigg(&\hat{b}'\hat{b}\left\{\left[1-\frac{j}{ks}\right]v(\xi)+D^2\left(\frac{j}{ks}\right)^2\left[\Lambda_s u(\xi)+\Lambda_c v(\xi)\right]+T_o^2\,\frac{j}{ks}\left[u(\xi)-v(\xi)\right]\right\} + \\ &+ \hat{t}'\hat{t}\left\{D^2\,\frac{j}{ks}\,v(\xi)+\frac{j}{ks}\,u(\xi)-2\left(\frac{j}{ks}\right)^2\left[\Lambda_s u(\xi)+\Lambda_c v(\xi)\right]\right\} + \\ &+ (\hat{t}'\hat{b}+\hat{b}'\hat{t})\left\{T_o\,\frac{j}{ks}\left[u(\xi)-v(\xi)\right]\right\}\Bigg)\, D\, G(ks) \quad . \end{aligned} \tag{39b}$$

The quantities ξ, D, Λ_s, Λ_c, T_o and G(ks) are as defined in Equations (36), (37), (35a), (35b), (33), and (4), respectively. One similarly obtains $\overline{E}_n^m$ for an arbitrary convex surface as

$$\overline{E}_n^m(P_N) \sim \overline{p}_m \cdot \overline{\overline{L}}_m \quad , \tag{40a}$$

where the dyadic $\overline{\overline{L}}_m$ is given by

$$\begin{aligned}\overline{\overline{L}}_m = (Y_o)^{-1}\Bigg(&\hat{b}'\hat{n}\left\{\left[1-\frac{j}{ks}\right]v(\xi)+T_o^2\,\frac{j}{ks}\left[u(\xi)-v(\xi)\right]\right\} + \\ &+ \hat{t}'\hat{n}\left\{T_o\,\frac{j}{ks}\left[u(\xi)-v(\xi)\right]\right\}\Bigg)\, D\, G(ks) \quad . \end{aligned} \tag{40b}$$

It is easily verified that Equation (39) reduces to Equation (27) for a circular cylinder when $\kappa_1=0$ and $\kappa_2=1/a$ (a=radius), and it reduces to Equation (11) for a sphere when $\kappa_1=\kappa_2=1/a$ and $T_o=C$. Likewise Equation (40) reduces to

Equation (29) when it is specialized to the circular cylinder case, and it reduces to Equation (15) when it is specialized to the sphere case. Furthermore, both Equations (39) and (40) properly reduce to the corresponding results for a planar surface when $\kappa \to 0$.

B. Surface Fields of an Infinitesimal Electric Current Source on a Convex Surface

The field $\overline{H}_t^e$ for an arbitrary convex surface becomes via Equations (22) and (30), and the postulates in parts (a) and (b), the following,

$$\overline{H}_t^e(P_N) \sim \overline{p}_e \cdot \overline{\overline{L}}_e \quad , \tag{41a}$$

where the dyadic $\overline{\overline{L}}_e$ is given by

$$\overline{\overline{L}}_e = -(Y_o)^{-1}\left(\hat{n}'\hat{b}\left\{\left[1-\frac{j}{ks}\right]v(\xi)+T_o^2\frac{j}{ks}[u(\xi)-v(\xi)]\right\} + \hat{n}'\hat{t}\left\{T_o\frac{j}{ks}[u(\xi)-v(\xi)]\right\}\right) D\,G(ks) \quad . \tag{41b}$$

Likewise, the field $\overline{E}_n^e$ for an arbitrary convex surface is

$$\overline{E}_n^e(P_N) \sim \overline{p}_e \cdot \overline{\overline{Z}}_e \quad , \tag{42a}$$

where the dyadic $\overline{\overline{Z}}_e$ is given by

$$\overline{\overline{Z}}_e = -(Y_o)^{-2}\,\hat{n}'\hat{n}\left(\left[v(\xi)-\frac{j}{ks}v(\xi)\right]+\left(\frac{j}{ks}\right)^2[\Lambda_s v(\xi)+\Lambda_c u(\xi)] + T_o^2\frac{j}{ks}[u(\xi)-v(\xi)]\right) D\,G(ks) \quad . \tag{42b}$$

Again, it is easily verified that Equation (41) reduces to Equation (30) when it is specialized to the circular cylinder case, and it reduces to Equation (22) when it is specialized to the sphere case. Also, Equation (42) reduces to Equation (31) when specialized to the circular cylinder case, and it reduces to Equation (24) when specialized to the sphere case. Finally, both Equations (41) and (42) reduce to the corresponding results for a planar surface as $\kappa \to 0$.

It is noted that for a convex surface of revolution in which the source $\overline{p}_e$ or $\overline{p}_m$ on the surface is located on the axis of revolution, there exists a

caustic of the surface rays at a point which is antipodal to the source point. In this case, the caustic matching functions T_{c1}, T_{c2} and T_{c3} must be introduced in the results of Equations (39), (40), (41), and (42), in exactly the same fashion as done in Sections II-B and III-B for the canonical sphere geometry. Also, in the case that the field point is raised from P_N on the surface to the point P which is a small distance above the surface, the functions $u(\xi)$ and $v(\xi)$ in Equations (39), (40), (41), and (42) must be replaced by $F_s(\xi,0,y_2)$ and $F_h(\xi,0,y_2)$, respectively. In addition, if the source $\overline{p}_e$ at P'_N on the surface is also raised slightly above the surface to the point P', then $F_s(\xi,y_1,y_2)$ and $F_h(\xi,y_1,y_2)$ must be used instead, as indicated previously.

Finally, if the surface changes continuously but not sufficiently slowly from an almost spherical surface at one point on a geodesic surface ray path to an almost cylindrical surface at another point on that geodesic path, then the results given in Equations (39), (40), (41), and (42) may not be valid because the GTD procedure upon which they are based is not strictly valid for rapidly varying surface properties. However, if the change in surface properties is not too rapid, then it would be interesting to study if one could heuristically take such moderately rapid changes into account by allowing the factors T_o, Λ_s, and Λ_c to also change continuously along the geodesic path. Thus, one may conjecture that

$$T_o = \frac{1}{s}\int_{P'_N}^{P_N} (T/\kappa)ds \quad ; \quad \Lambda_s = \frac{1}{s}\int_{P'_N}^{P_N} (\kappa_1/\kappa_2)ds \tag{43a;43b}$$

and

$$\Lambda_c = \frac{1}{s}\int_{P'_N}^{P_N} (1-(\kappa_1/\kappa_2))ds \quad . \tag{43c}$$

It is noted that the results in Equations (39), (40), (41), and (42) appear to be accurate, but they still are being tested carefully; as such, they may be subject to further improvements or modifications in the future. Equations (43a;b;c) are added simply as something of interest to study in the future, and it is not recommended that they be used until sufficient tests on their validity have been completed.

V. NUMERICAL RESULTS AND DISCUSSION

In this section, general expressions will be indicated for the mutual coupling between a pair of antennas located on a smooth, perfectly-conducting convex surface of any shape. These expressions will of course make use of the results developed in Section IV. The type of antennas considered in this paper are thin, rectangular slots which are less than half a wavelength long, and thin stubs which are less than a quarter wavelength long. The reason for selecting such short and thin slot, or stub antennas is that the shape of the field distribution in the slot or the current distribution along the stub may then be assumed to be that of the dominant mode. Furthermore, a short circuit placed in a waveguide feeding the slot such that it is an integral number of "dominant mode" half wavelengths from the slot aperture would effectively produce a short circuit at the aperture. Thus, a surface field which propagates along a geodesic surface ray path over such a short circuited aperture would for all practical purposes be unaltered by the presence of the slot since the scattering of the surface field by the short circuited slot would then be vanishingly small. This fact is particularly useful if one is interested in the calculation of the mutual admittance between a pair of slots in a slot array environment. A similar simplification results in the calculation of the mutual impedance between a pair of thin and short stub (or monopole) antennas in a stub array environment since such an open circuited stub, placed in the path of the surface field would perturb this field negligibly. It is noted that the conditions imposed by the above assumptions on the size of the radiating elements are not stringent; in fact, these conditions are commonly met in practice. The calculation of the mutual coupling between a pair of slot or wire type radiating elements on a convex surface which do not satisfy the above assumptions and conditions can still be performed on the basis of the results developed in Section IV provided the aperture field distribution (for the case when the radiating element is a slot antenna which may not be sufficiently small) and the current distribution along a wire (for the case of a stub antenna which may not be sufficiently short and thin) is known in

the coupled environment. In the latter cases, one could employ measurements, or numerical techniques (such as the method of moments) for solving the coupled integral equations for these problems in order to obtain the field or current distributions on these radiating elements. These integral equations could be simplified so that the only unknowns are the fields on the antennas and not on the electrically large structure upon which the antennas are located, by appropriately employing the surface field dyadics introduced in Section IV, in the construction of these integral equations. These dyadics would actually constitute asymptotic approximations to the appropriate surface dyadic Green's functions or their spatial derivatives which constitute the kernels of these integral equations.

Some numerical results will be presented in this section for the calculation of the mutual admittance between a pair of rectangular slots in a perfectly-conducting circular cylinder; both, axial and circumferential slots will be considered. These numerical results which are based on the development in Section IV, will be compared with the corresponding numerical results obtained by others [11,12].

The general expressions for the mutual coupling between a pair of radiating elements on a smooth, perfectly-conducting convex surface are presented in the following discussion. In particular, let antennas designated ① and ② constitute a pair of radiating elements on a convex surface. The mutual coupling between these antennas may be calculated via an application of the reaction theorem [2]. Thus, if antenna ② is an aperture (or slot), the dominant mode current I_{21} induced in this aperture by antenna ① when antenna ② is short circuited is given by [2]

$$I_{21} = - \frac{\iint_{S_2} ds_2 \, \bar{H}_{21} \cdot \bar{M}_2}{V_{22}} \quad , \tag{44}$$

where $\overline{M}_2 = \overline{E}_2 \times \hat{n}_2$, and $\overline{E}_2$ is the dominant mode electric field distribution in the aperture of the slot antenna ② with $\hat{n}_2$ being the unit outward normal vector to the surface of the aperture of antenna ②. The integration in Equation (44) is over the surface area s_2 of the aperture corresponding to slot antenna ②. Furthermore,

$$\overline{E}_2 = v_{22}\overline{e} = v_{22}\hat{u}_y \sqrt{\frac{2}{d\ell}} \cos\left(\frac{\pi}{\ell} u_x\right) \quad . \tag{45}$$

In Equation (45) above, v_{22} is the dominant mode voltage associated with the dominant vector mode function $\overline{e}$ for a rectangular slot. The local, orthogonal coordinates u_x and u_y whose origin is at the center of the slot are indicated in Figure 5 together with the slot dimensions d and ℓ,

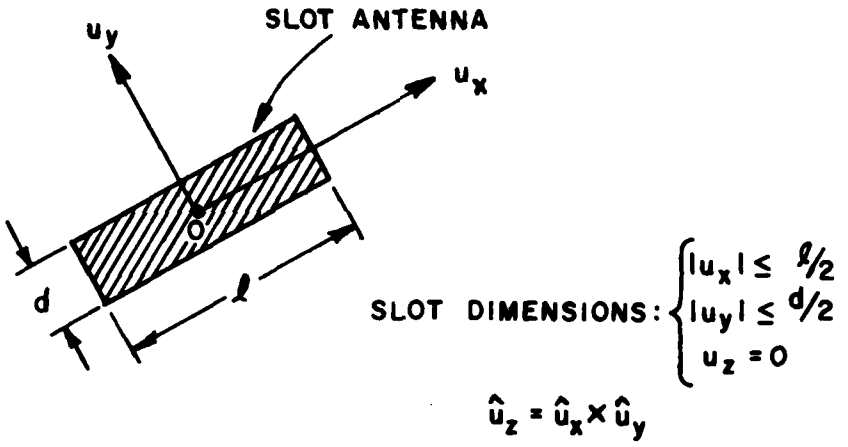

Figure 5. Local coordinates associated with the slot antenna.

respectively. The field $\overline{H}_{21}$ is the magnetic field at antenna ②, which is produced by antenna ① with antenna ② short circuited. From the development in Section IV, it is easily seen that when antenna ① is also a slot, then $\overline{H}_{21} = \iint_{s_1} ds_1 \, \overline{M}_1 \cdot \overline{\overline{y}}_m$, where the integration is over the surface s_1 of the aperture corresponding to slot antenna ①, with $\overline{\overline{y}}_m$ as given in Equation (39b), and $\overline{M}_1 = \overline{E}_1 \times \hat{n}_1$. Of course, $\hat{n}_1$ is the outward

unit normal vector to the surface area s_1 of the aperture corresponding to slot antenna ①, and

$$\bar{E}_1 = v_{11}\,\bar{e} \quad . \tag{46}$$

v_{11} is the dominant mode voltage associated with slot antenna ①. On the other hand, if antenna ① is a stub, then $\bar{H}_{21} = \iiint_{v_1} dv_1\, \bar{J}_1 \cdot \bar{\bar{L}}_e$, where the integration is on volume v_1 just encapsulating stub ①, with $\bar{\bar{L}}_e$ as given in Equation (41b), and

$$\bar{J}_1 = I_{11}\bar{h} = I_{11}\hat{u}_z \delta(u_x)\delta(u_y) I(u_z) \quad . \tag{47a}$$

In Equation (47a) above, I_{11} is the mode current on the stub, which is associated with the vector mode function $\bar{h}$ for the stub. The vector $\bar{h}$ involves the 2-D Dirac delta function $\delta(u_x)\delta(u_y)$ and a distribution $I(u_z)$ which is generally assumed to be

$$I(u_z) = \frac{\sin[k(\ell - |u_z|)]}{\sin(k\ell)} \quad ; \qquad 0 < u_z < \ell \quad . \tag{47b}$$

The local orthogonal coordinates (u_x, u_y, u_z) whose origin is at the base (or feed point) of the stub are illustrated in Figure 6. From the above discussion, it follows that

$$I_{21}\Big|_{\substack{\text{Slot ② Short Circuited, or } v_{21}=0}} = -\frac{\iint_{s_2} ds_2 \iint_{s_1} ds_1\, \bar{M}_1 \cdot \bar{\bar{y}}_m \cdot \bar{M}_2}{v_{22}} \quad , \quad \begin{array}{l}\text{if antenna} \\ \text{① is also} \\ \text{a slot,}\end{array} \tag{48}$$

and

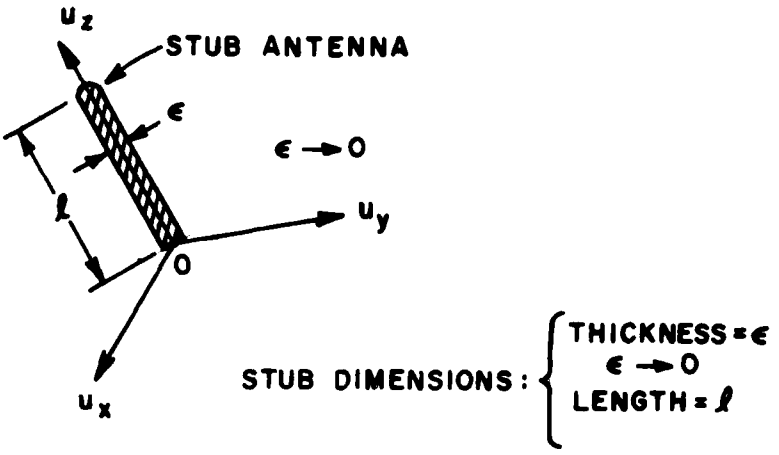

Figure 6. Local coordinates associated with the stub antenna.

$$I_{21}\Big|_{\substack{\text{Slot } (2) \\ \text{Short} \\ \text{Circuited,} \\ \text{or } v_{21}=0}} = -\frac{\iint_{S_2} ds_2 \iiint_{V_1} dv_1 \, \bar{J}_1 \cdot \bar{\bar{L}}_e \cdot \bar{M}_2}{v_{22}} \quad , \quad \text{if antenna (1) is a stub.} \tag{49}$$

It follows from Equation (48), that the mutual admittance Y_{21} between a pair of slots (slot antenna (1) and slot antenna (2)) is given by I_{21}/v_{11} with $v_{21}=0$, or

$$Y_{21} = -\frac{\iint_{S_2} ds_2 \iint_{S_1} ds_1 \, \bar{M}_1 \cdot \bar{\bar{y}}_m \cdot \bar{M}_2}{v_{11} v_{22}} \; ; \qquad Y_{21} = Y_{12} \; . \tag{50}$$

A similar set of results may be obtained if antenna (2) is a stub. Thus, the mode voltage v_{21} induced in stub antenna (2) by antenna (1) when antenna (2) is open circuited is given as [2]

$$V_{21} = - \frac{\iiint_{v_2} dv_2 \, \bar{E}_{21} \cdot \bar{J}_2}{I_{22}} \quad , \tag{51}$$

where v_2 is the volume just encapsulating stub antenna ②, and $\bar{J}_2 = I_{22}\,\bar{h}$ on this stub. $\bar{E}_{21}$ is the electric field at stub antenna ②, which is produced by antenna ① when antenna ② is open circuited. It follows from the development in Section IV that $\bar{E}_{21} = \iint_{s_1} ds_1 \, \bar{M}_1 \cdot \bar{\bar{L}}_m$ if antenna ① is a slot, and $\bar{E}_{21} = \iiint_{v_1} dv_1 \, \bar{J}_1 \cdot \bar{\bar{Z}}_e$ if antenna ① is also a stub. The dyadics $\bar{\bar{L}}_m$ and $\bar{\bar{Z}}_e$ are given in Equations (40b) and (42b). Summarizing the results for the open circuit voltage v_{21} at stub antenna ②, one has

$$V_{21}\Big|_{\substack{\text{Stub ②} \\ \text{Open Circuited,} \\ \text{or } I_{21}=0}} = - \frac{\iiint_{v_2} dv_2 \iint_{s_1} ds_1 \, \bar{M}_1 \cdot \bar{\bar{L}}_m \cdot \bar{J}_2}{I_{22}} \quad , \quad \text{if antenna ① is a slot,} \tag{52}$$

and

$$V_{21}\Big|_{\substack{\text{Stub ②} \\ \text{Open Circuited,} \\ \text{or } I_{21}=0}} = - \frac{\iiint_{v_2} dv_2 \iiint_{v_1} dv_1 \, \bar{J}_1 \cdot \bar{\bar{Z}}_e \cdot \bar{J}_2}{I_{22}} \quad , \quad \text{if antenna ① is also a stub.} \tag{53}$$

It is evident from Equation (53), that the mutual impedance Z_{21} between a pair of stubs (monopoles) is given by V_{21}/I_{11} with $I_{21}=0$, or

$$Z_{21} = - \frac{\iiint_{V_1} dv_2 \iiint_{V_1} dv_1 \, \bar{J}_1 \cdot \bar{\bar{Z}}_e \cdot \bar{J}_2}{I_{11} I_{22}} ; \quad Z_{21} = Z_{12}. \tag{54}$$

Some numerical results are indicated below for Y_{12} between a pair of identical rectangular slots in a perfectly-conducting circular cylinder. In particular, Figures 7 and 8 indicate the surface field on a circular cylinder due to an infinitesimal circumferential slot; whereas Figures 9 and 10 indicate the isolation, s_{12} (related to Y_{12}) between a pair of axial slots. These numerical results are marked as OSU on the plots. Furthermore, these results are compared with the exact (modal) results as well as those in [11,12]; in particular, the results of [11] are marked as PINY in these figures; whereas, those of [12] are marked as UI results. Additional comparison between the OSU, PINY, and UI results for Y_{12} are indicated in Tables I and II for the circumferential slots. It is seen from these comparisons that firstly the OSU results agree very well with the results based on the exact (modal) solution given in [12], which also contains the Hughes modal solution. Secondly, it appears that the results based on all three asymptotic solutions; namely those based on the OSU, PINY and UI solutions are for all practical purposes quite accurate and not noticeably different except when ks becomes small, and/or the pair of slots are in each other's paraxial regions for the case of circumferential type slots. Thus, when ks becomes very small, the PINY solution becomes inaccurate because only terms up to and including $\frac{1}{(ks)^2}$ appear in that solution; whereas, the OSU and UI results which include the effects of $(\frac{1}{ks})^3$ terms remain accurate even for ks very small. The OSU and PINY asymptotic solutions for the circular cylinder are not strictly valid within paraxial regions since the approximation for the field in terms of Fock type Airy functions cannot be completely justified in these regions. On the other hand, the UI solution bypasses this difficulty by conjecturing an asymptotic solution for the circular cylinder via a heuristic modification of an asymptotic solution for the sphere geometry. As mentioned previously

TABLE I

Y_{12} Between a Pair of Circumferential Slots in a Circular Cylinder of Radius, a=1.991"; frequency=9 GHz, and δ=0 (E-plane)

	Modal Solutions		Asymptotic Solutions			
(Inches)	Hughes	UI	UI	OSU	PINY	Planar a=∞
.5	- 7.27 dB -72°	- 7.27 -72°	- 7.31 -77.77°	- 7.86 -69.71°	- 6.46 -68.17°	- 8.16 -66.85°
2	-16.52 -117°	-16.43 -117°	-16.36 -115.67°	-17.56 -110.08°	-15.66 -117.88°	-18.10 -105.84°
8	-26.95 33°	-26.49 34°	-26.54 36.77°	-28.78 46.20°	-25.51 33.60°	-28.97 53.6°
16		-31.13 -4°	-31.31 -.9°	-34.28 10.19°	-30.04 -4.2°	-35.98 19.96°
40		-36.60 -115°	-37.17 -109.44°	-41.29 -96.97°	-35.58 -112.59°	-43.93 -83.17°

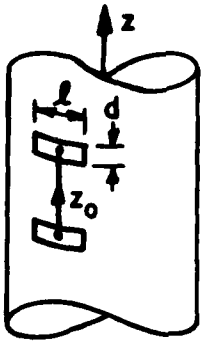

ℓ = 0.9"
d = 0.4"

TABLE II

Y_{12} Between a Pair of Circumferential Slots in a Circular Cylinder of Radius a=1.991"; Frequency=9 GHz and for $\delta=\pi/2$; $z_o=0$ (H-Plane)

	Modal	Asymptotic Solutions		
Degree	Hughes	UI	OSU	PINY
30°	-25.98 dB -77°	-25.98 -76.77°	-26.07 -75.73°	-77.93 -64.81°
40°	-34.52 108°	-34.63 169.58°	-34.67 170.07	-35.72 179.40
50°	-40.96 58°	-41.32 59.88°	-41.76 60.33°	-42.03 68.31°
60°	-46.62 -49°	-47.08 -47.85°	-46.92 -47.55°	-47.55 -40.48°

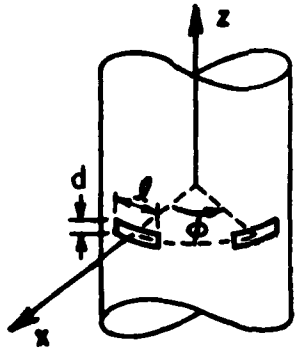

ℓ = 0.9"
d = 0.4"

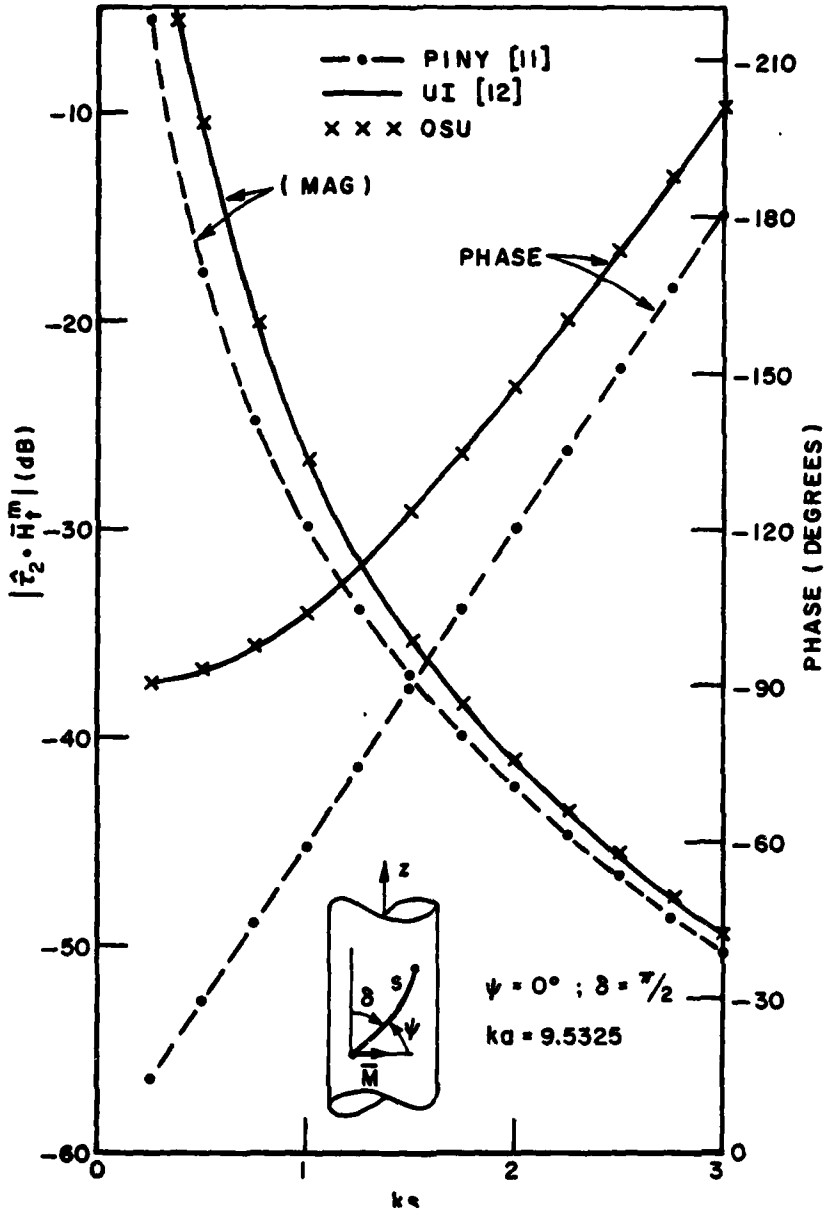

Figure 7. Variation of $\hat{\tau}_2 \cdot \bar{H}_t^m$ along a path for which $\psi=0°$ on a circular cylinder which is excited by a $\hat{\tau}_2'$ directed magnetic current point source.

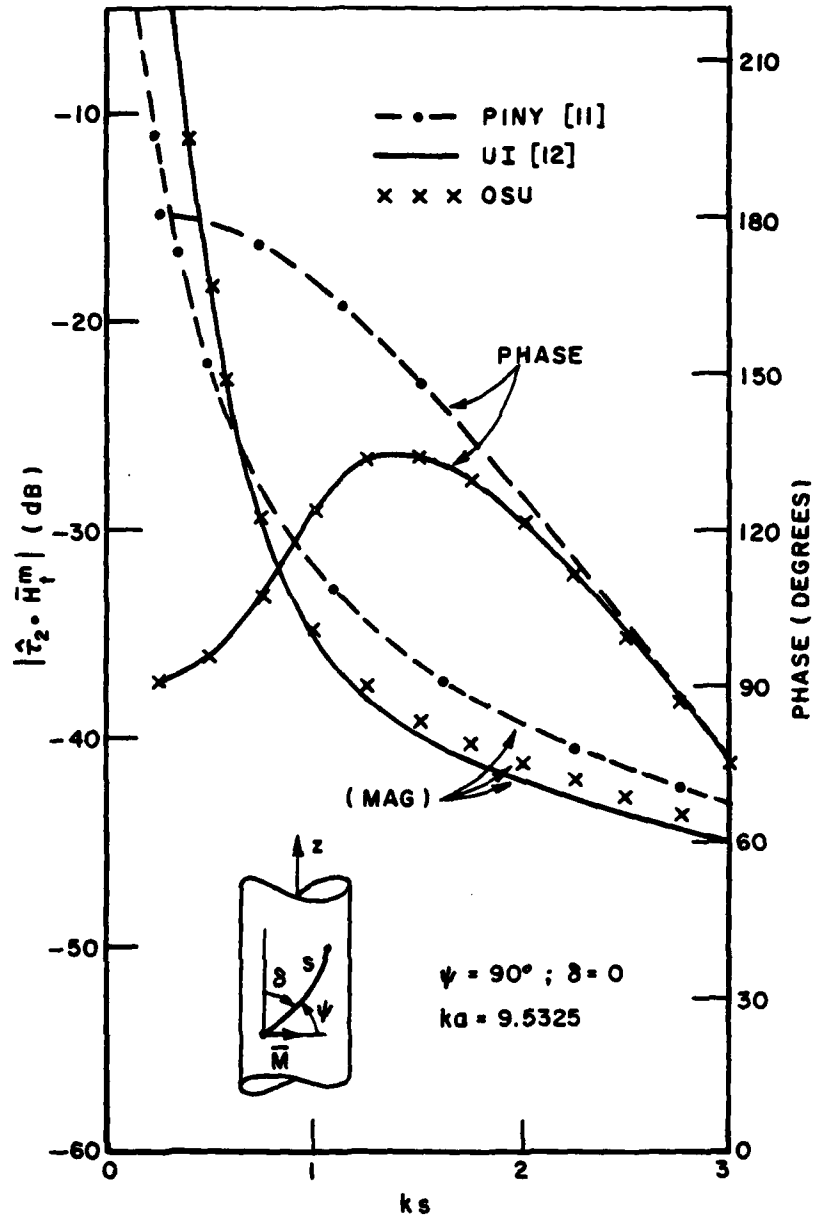

Figure 8. Variation of $\hat{\tau}_2 \cdot \bar{H}_t^m$ along a path for which ψ=90° on a circular cylinder which is excited by a $\hat{\tau}_2'$ directed magnetic current point source.

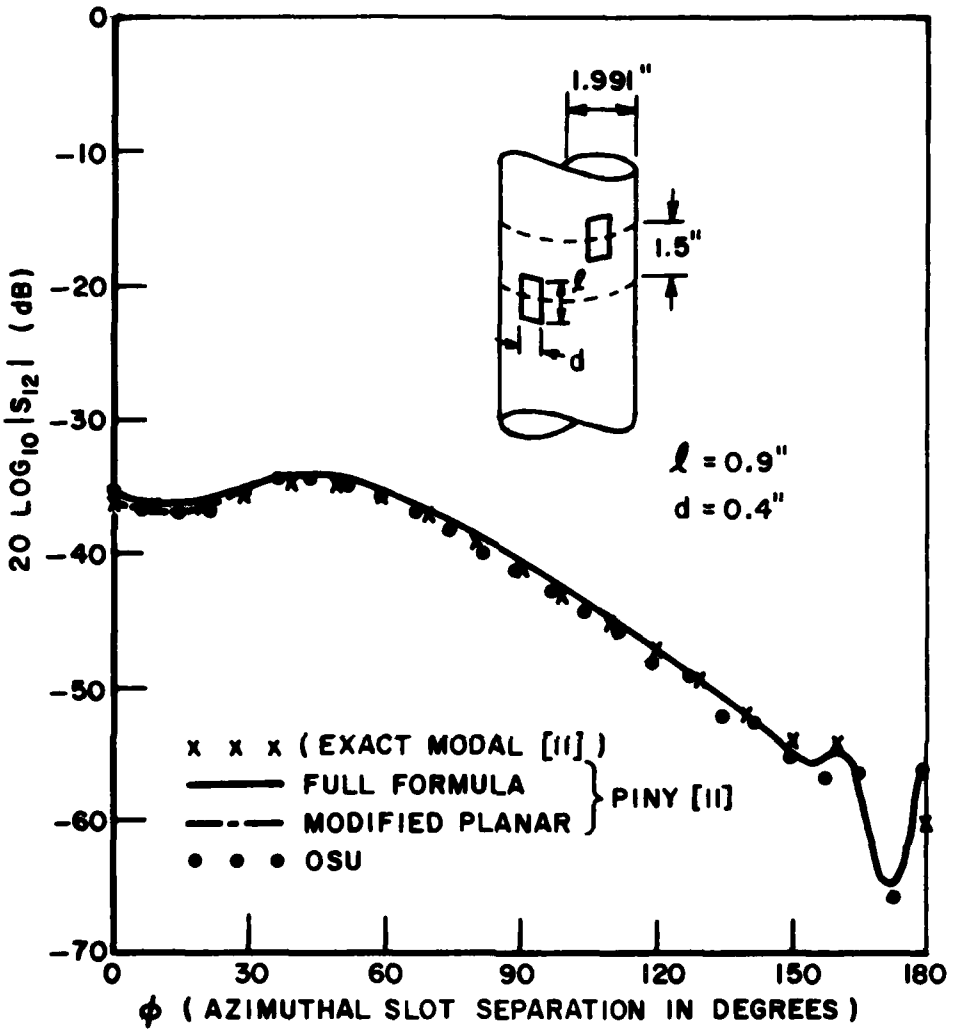

Figure 9. Isolation of axial slots on a conducting cylinder a = 1.991"; Z_0 = 1.50"; Frequency = 9 GHz.

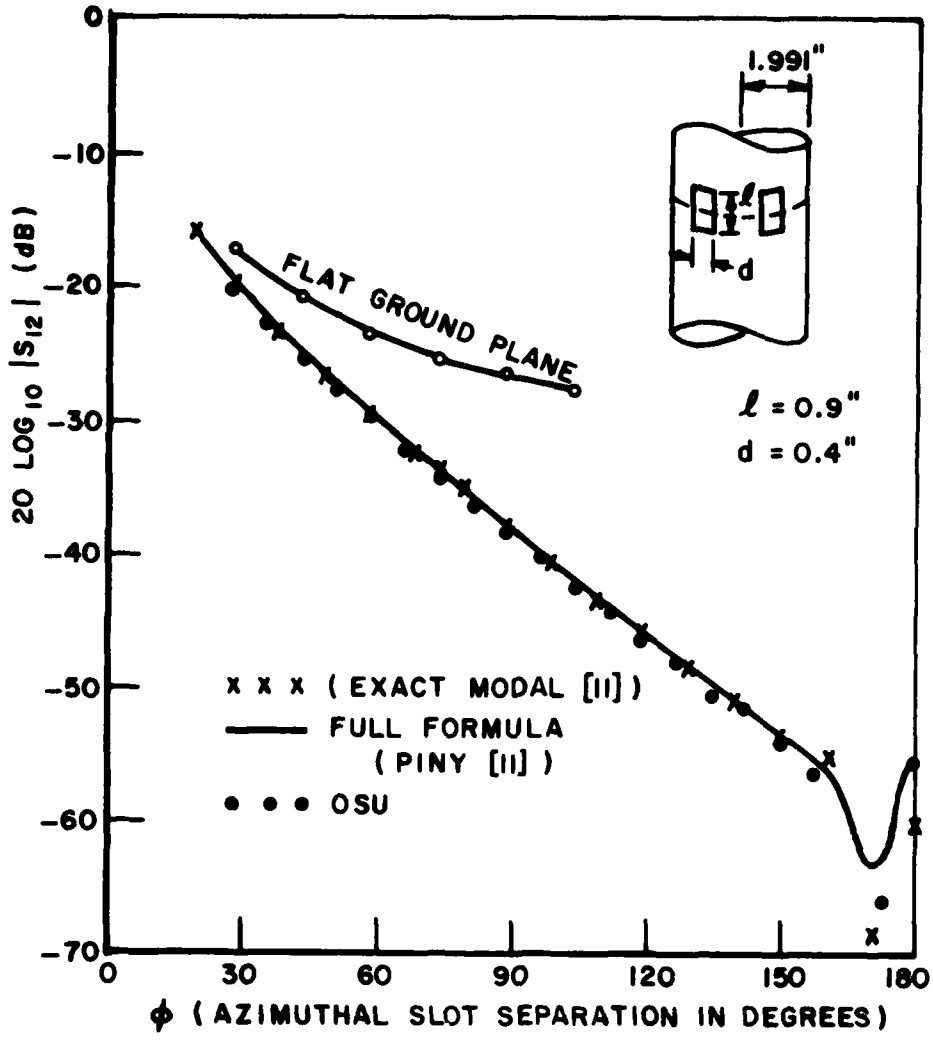

Figure 10. Isolation of axial slots on a conducting cylinder, a = 1.991"; Z_0 = 0; Frequency = 9 GHz.

(Section I), this modification of the sphere solution in [12] results from the introduction of an extra term via an ad hoc procedure. This extra term improves the accuracy of the modified sphere result when it is specialized to the circular cylinder case; and the improvement is especially noticeable in the paraxial regions of the cylinder. As a result, the UI solution appears to be quite accurate even in the paraxial regions, i.e., in the immediate vicinity of the axial direction on a circular cylinder for the circumferential slot case. Although the OSU and PINY solutions for the circular cylinder are not strictly valid within te paraxial regions, they still provide accurate results for the axial slot case, and they are reasonably accurate even for the circumferential slot case; thus, these solutions may be employed even within the paraxial regions. Actually, the OSU results for the paraxial regions corresponding to the circumferential slot case differs from the exact (modal) results by less than 10% in amplitude, and by less than 5% in phase.*

It is evident from the results in Sections II and III, that the asymptotic solutions for the cylinder are somewhat different from those for the sphere as one might expect, since the two geometries are different. Also, it is noted that the OSU solution for the circular cylinder case (as presented in Section II-A) is actually identical to the corresponding PINY solution to terms in $\frac{1}{ks}$ and $\frac{1}{(ks)^2}$, except for the cross term (i.e., the $\hat{\tau}_2^i\hat{\tau}_2$ type term) whose functional form is different in the OSU and PINY solutions. A cross term of this type is absent in the UI solution. Furthermore, it is this cross term which dominates the solution in the paraxial regions for the circumferential slot case. Thus, the numerical results based on the OSU and PINY solutions are slightly different in the paraxial regions for the circumferential slot case. While the UI solution surprisingly yields good accuracy for the circular cylinder case, it raises some interesting questions which were also indicated previously in Section I. In particular, the UI solution when specialized to the circular cylinder geometry excited by an axial slot will contain both, the soft and hard type Fock functions $u(\xi)$ and $v(\xi)$, respectively.

*It is expected that further improvements in the paraxial region field calculations are possible if higher order terms in $\frac{1}{k\rho_g}$ are included in the analysis. However, as indicated above, the leading (or lowest order) terms in $\frac{1}{k\rho_g}$ which are the only ones that have been retained in this analysis are sufficiently accurate even for paraxial region calculations.

However, it is well known, that only the potential corresponding to the "hard" or $v(\xi)$ type function is required to completely describe the fields of an axial slot in a circular cylinder. Secondly, the "ad hoc" procedure employed to modify the asymptotic solution for the sphere in order to obtain an asymptotic solution for the circular cylinder geometry may need further justification, In this sense, the present approximate (OSU) asymptotic solution for the circular cylinder is not based on a heuristic procedure as the one in [12],* and it may be viewed as an extension of the approximate PINY asymptotic solution [11] and the previous OSU solution [9]. It is noted that the OSU asymptotic solution for the circular cylinder could be improved even further in the paraxial regions for the circumferential slot case by employing a different asymptotic evaluation which would be more accurate in these regions; however, this analysis will not be pursued at the present time since the solution derived in this paper appears to be sufficiently accurate even for this special case.

It is noted that in addition to the asymptotic solutions pertaining to the surface fields on the canonical circular cylinder and the sphere geometries, an approximate asymptotic solution is also heuristically constructed in this paper for the arbitrary smooth convex surface. Also, the effect of torsion associated with the surface rays is clearly identified in this solution through the presence of the factor T/κ. Furthermore, the excitation of this convex surface by both infinitesimal electric and magnetic type current moments are considered in this paper. Numerical results for both the electric and magnetic type source excitation of spheroidal geometries will hopefully be presented in the near future along with experimental results for comparison in order to test the validity of the present asymptotic solution for the arbitrary convex surface.

*During the editing of the final version of this paper, we have received from Professor S. W. Lee (at University of Illinois) a set of handwritten notes by Professor J. Boersma which deal with a new and more rigorous asymptotic solution (that is valid within the paraxial regions) for the surface fields of slots on cylinders. These notes are soon expected to be published as a UI report [16]. It is interesting to note that the solution in our paper agrees exactly with the one in Professor Boersma's notes to all orders in $(\frac{1}{ks})$ and to leading terms in $(\frac{1}{k\rho_g})$, even though it is derived via a different asymptotic procedure. The effect of torsion associated with the surface rays has not been specifically identified in Prof. Boersma's notes.

REFERENCES

[1] P. H. Pathak and R. G. Kouyoumjian, "An Analysis of the Radiation from Apertures in Curved Surfaces by the Geometrical Theory of Diffraction," Proc. IEEE, Vol. 62, pp. 1438-1461, November 1974.

[2] J. H. Richmond, "A Reaction Theorem and It's Application to Antenna Impedance Calculations," IRE Trans., Vol. AP-9, No. 6, pp. 515-520, November 1961.

[3] J. B. Keller, "Geometrical Theory of Diffraction," J. Opt. Soc. Amer., Vol. 52, pp. 116-130, 1962.

[4] J. B. Keller, "Diffraction by a Convex Cylinder," IRE Trans., Vol. AP-24, pp. 312-321.

[5] B. R. Levy and J. B. Keller, "Diffraction by a Smooth Object," Comm. Pure and Appl. Math., Vol. 12, pp. 159-209, 1959.

[6] N. A. Logan, "General Research in Diffraction Theory," Missiles and Space Div., Lockheed Aircraft Corp., Vol. 1, Report LMSD-288087, and Vol. 2, Report LMSD-288088, December 1959.

[7] G. Hasserjian and A Ishimaru, "Excitation of a Conducting Cylindrical Surface of Large Radius of Curvature," IRE Trans., Vol. AP-10, pp. 2640273, 1962.

[8] J. R. Wait, "Currents Excited on a Conducting Surface of Large Radius of Curvature," IRE Trans., Vol. MTT-4, No. 3, pp. 143-145, 1956.

[9] Y. Hwang and R. G. Kouyoumjian, "The Mutual Coupling Between Slots on an Arbitrary Convex Cylinder," Report 2902-21, March 1975, The Ohio State University ElectroScience Laboratory, Department of Electrical Engineering; prepared under Grant No. NGL 36-008-138 for National Aeronautics and Space Administration.

[10] P. H. Pathak, "Analysis of a Conformal Receiving Array of Slots in a Perfectly-Conducting Cylinder by the Geometrical Theory of Diffraction," Report 3735-2, January 1975, The Ohio State University ElectroScience Laboratory, Department of Electrical Engineering; prepared under Contract N00140-74-C-6017 for Naval Regional Procurement Office.

[11] Z. W. Chang, L. B. Felsen, and A. Hessel, "Surface Ray Methods for Mutual Coupling in Conformal Arrays on Cylinder and Conical Surfaces," Polytechnic Institute of New York, Final Report (Sept. 1975-Feb. 1976), 1976; prepared under Contract N00123-76-C-0236. - Also see K. K. Chan, L. B. Felsen, A. Hessel, and J. Shmoys, "Creeping Waves on a Perfectly-Conducting Cone," IEEE Trans., Vol. AP-25, No. 5, pp. 661-670, September 1977.

[12] S. W. Lee and R. Mittra, "Mutual Admittance Between Slots on a Cylinder or Cone," Electromagnetics Lab., Univ. of Illinois, Dept. of Electrical Engineering, Tech. Rept. 77-24, 1977, prepared under Contract N00019-77-C-0127. - Also see S. W. Lee and S. Naini, "Approximate Asymptotic Solution of Surface Field due to a Magnetic Dipole on a Cylinder," IEEE Trans., Vol. AP-26, No. 4, pp. 593-597, July 1978.

[13] V. A. Fock, Electromagnetic Diffraction and Propagation Problems, New York: Pergamon, 1965.

[14] R. F. Harrington, Time Harmonic Electromagnetic Fields, New York: McGraw-Hill, 1961.

[15] J. J. Bowman, T. B. A. Senior, and P. L. E. Uslenghi, Electromagnetic and Acoustic Scattering by Simple Shapes, Amsterdam: North Holland Publishing Co., 1969.

[16] J. Boersma and S. W. Lee, "Asymptotic Solution of Surface Field due to a Magnetic Dipole on a Cylinder," to appear as an Electromagnetic Lab., University of Illinois, technical report. See footnote at bottom of page 49.

APPENDIX I

ASYMPTOTIC ANALYSIS OF THE SURFACE FIELDS EXCITED BY INFINITESIMAL ELECTRIC OR MAGNETIC CURRENT SOURCES ON A PERFECTLY-CONDUCTING CIRCULAR CYLINDER

The geometry of this canonical problem is illustrated in Figure 1. The case of a tangential magnetic current source at P_N' will be analyzed first; the analysis for a radial electric current source at P_N' will be performed subsequently.

Let a magnetic current source $\bar{M}$ generate the surface fields $\bar{E}_n^m$ and $\bar{H}_t^m$ on the surface, where $\bar{E}_n^m$ is the radial component of the electric field, and $\bar{H}_t^m$ is the tangential component of the magnetic field. The source $\bar{M}$ is defined as

$$\bar{M} = \bar{p}_m \, \delta(|\bar{r} - \bar{r}'|) \quad , \tag{A-1}$$

where $\bar{r}'$ is the position vector of P_N' and $\bar{r}$ is an arbitrary position vector. The quantity p_m is the strength of the infinitesimal magnetic current moment which is oriented tangential to the surface.

The fields $\bar{E}_n^m$ and $\bar{H}_t^m$ can be constructed from a suitable set of electric and magnetic vector potentials $\bar{F}$ and $\bar{A}$, respectively [14]. Following the development in [14] for an $e^{j\omega t}$ time dependence which is assumed and suppressed, one obtains,

$$\bar{A} = \hat{z} \frac{1}{2\pi} \sum_{-\infty}^{\infty} e^{jn\phi} \int_{-\infty}^{\infty} a_n(h) \, H_n^{(2)}(k_t\rho) e^{jhz} \, dh = A_z \hat{z}, \tag{A-2}$$

and

$$\bar{F} = \hat{z} \frac{1}{2\pi} \sum_{-\infty}^{\infty} e^{jn\phi} \int_{-\infty}^{\infty} b_n(h) \, H_n^{(2)}(k_t\rho) e^{jhz} \, dh = F_z \hat{z}, \tag{A-3}$$

where $H_n^{(2)}(k_t\rho)$ is the Hankel function of the second kind and of order n. The k_t appearing in the argument of this Hankel function is defined by

$$k_t^2 = k^2 - h^2 \quad . \tag{A-4}$$

The unknown coefficients $a_n(h)$ and $b_n(h)$ in the above expansions may be obtained by an application of the electromagnetic boundary conditions on the surface. From the usual relationships between the vector potentials and the electromagnetic fields, one obtains [14]

$$H_z = \frac{1}{jkz_o} \left(\frac{\partial^2}{\partial z^2} + k^2\right) F_z \tag{A-5}$$

$$H_\phi = -\frac{\partial A_z}{\partial \rho} + \frac{1}{jkz_o\rho} \frac{\partial^2 F_z}{\partial \phi \, \partial z} \tag{A-6}$$

$$E_\rho = \frac{1}{jkY_o} \frac{\partial^2 A_z}{\partial \rho \partial z} - \frac{1}{\rho} \frac{\partial F_z}{\partial \phi} \quad . \tag{A-7}$$

In the above equations, z_o = free space impedance, and $Y_o = 1/z_o$. Then, $\bar{H}_t^m = H_\phi \hat{\phi} + H_z \hat{z}$, and $\bar{E}_n^m = \hat{\rho}\, E_\rho$. In Equations (A-5), (A-6) and (A-7), the fields are not necessarily on the surface. For convenience of analysis, $\bar{p}_m$ is decomposed as follows.

$$\bar{p}_m = p_m^a \hat{\tau}_1' + p_m^c \hat{\tau}_2' \quad ; \qquad \begin{cases} \hat{\tau}_1' = \hat{z} \text{ at } P_N' \\ \hat{\tau}_2' = \hat{\phi} \text{ at } P_N' \end{cases} \quad . \tag{A-8}$$

From the boundary condition $\bar{E}^m \times \hat{n} = \bar{M}$ at $\rho = a$, where $\bar{E}^m$ is the total electric field and $\bar{M}$ is as in Equation (A-1), it can be shown that

$$\bar{A} = A_z \hat{z} = \frac{\hat{z}}{2\pi} \sum_{-\infty}^{\infty} e^{jn\phi} \int_{-\infty}^{\infty} \left[\frac{jkY_o \, p_m^c}{2\pi k_t^2 a}\right] \cdot \frac{H_n^{(2)}(k_t\rho)}{H_n^{(2)}(k_t a)} \, e^{jhz} \, dh \tag{A-9}$$

and

$$\bar{F} = F_z\hat{z} = \frac{\hat{z}}{2\pi}\sum_{-\infty}^{\infty} e^{jn\phi}\int_{-\infty}^{\infty}\left[\frac{-p_m^a}{2\pi k_t a}\right]\frac{H_n^{(2)}(k_t\rho)}{H_n^{(2)'}(k_t a)}\, e^{jhz}\, dh$$

$$+\frac{\hat{z}}{2\pi}\sum_{-\infty}^{\infty} e^{jn\phi}\int_{-\infty}^{\infty}\left[\frac{nh\, p_m^c}{2\pi k_t^3 a^2}\right]\frac{H_n^{(2)}(k_t\rho)}{H_n^{(2)'}(k_t a)}\, e^{jhz}\, dh\ . \qquad \text{(A-10)}$$

In order to evaluate Equations (A-5), (A-6) and (A-7) asymptotically for large $k_t a$, one begins by employing the usual Watson transformation [5] to Equations (A-9) and (A-10). Thus,

$$\bar{A}=\hat{z}A_z=\frac{\hat{z}}{2\pi}\int_{-\infty}^{\infty} dh e^{jhz}\int_{-\infty-j\varepsilon}^{\infty-j\varepsilon} d\nu\left[\frac{jkY_o p_m^c}{2\pi k_t^2 a}\right]\frac{H_\nu^{(2)}(k_t\rho)}{H_\nu^{(2)}(k_t a)}\cdot\left[\sum_{\ell=0}^{\infty}\left(e^{-j\nu\phi}+e^{-j\nu(2\pi-\phi)}\right)e^{-j2\pi\ell\nu}\right] \qquad \text{(A-11)}$$

and

$$\bar{F}=\hat{z}F_z=\frac{\hat{z}}{2\pi}\int_{-\infty}^{\infty} dh e^{jhz}\int_{-\infty-j\varepsilon}^{\infty-j\varepsilon} d\nu\left[\frac{-p_m^a}{2\pi k_t a}\right]\frac{H_\nu^{(2)}(k_t\rho)}{H_\nu^{(2)'}(k_t a)}\left[\sum_{\ell=0}^{\infty}\left(e^{-j\nu\phi}+e^{-j\nu(2\pi-\phi)}\right)e^{-j2\pi\ell\nu}\right]$$

$$+\frac{\hat{z}}{2\pi}\int_{-\infty}^{\infty} dh e^{jhz}\int_{-\infty-j\varepsilon}^{\infty-j\varepsilon} d\nu\left[\frac{\nu h p_m^c}{2\pi k_t^3 a^2}\right]\frac{H_\nu^{(2)}(k_t\rho)}{H_\nu^{(2)'}(k_t a)}\left[\sum_{\ell=0}^{\infty}\left(e^{-j\nu\phi}+e^{-j\nu(2\pi-\phi)}\right)e^{-j2\pi\ell\nu}\right] \qquad \text{(A-12)}$$

It is assumed that ka is sufficiently large so that one may retain only the $\ell=0$ term in Equations (A-11) and (A-12), as the $\ell>0$ terms correspond to the field which multiply encircles the cylinder and contributes insignificantly for large ka. The contours of integration in the complex h and ν planes are shown in Figures A-I, and A-II, respectively. The dominant contribution to the ν integrals in Equations (A-11) and (A-12) will occur for $\nu\sim O(k_t a)$ in the deep shadow region and also in the shadow boundary

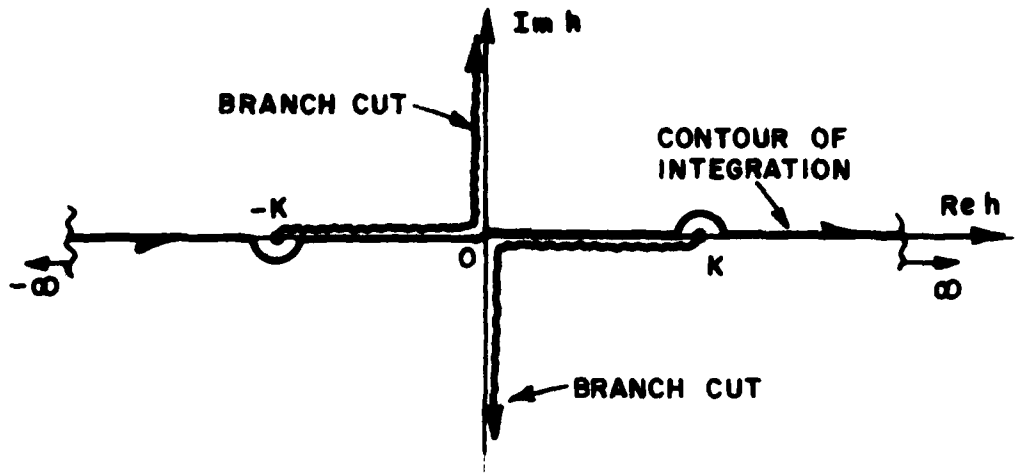

Figure A-I. Contour of integration in the complex h plane.

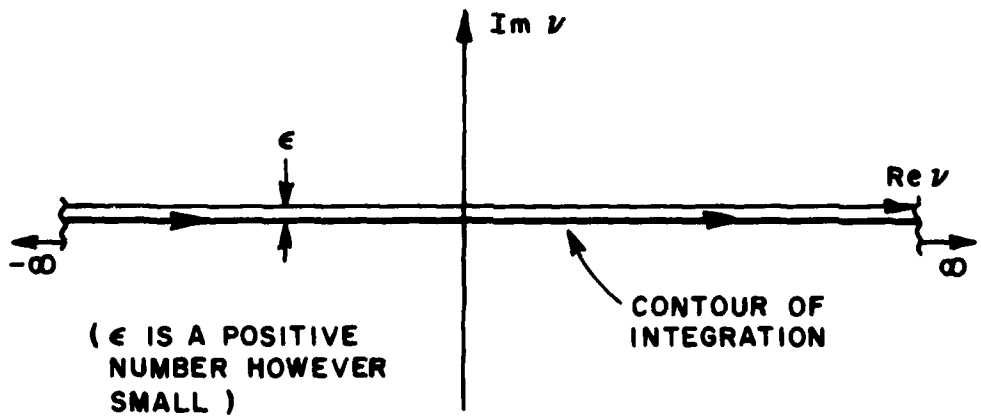

Figure A-II. Contour of integration in the complex ν plane.

transition region. Since the surface fields are of interest, and $\bar{M}$ lies on the cylinder, the field point is always in the shadow region. Thus, one may approximate the Hankel functions by the Fock type Airy functions [6,15] for $\nu \sim 0(k_t a)$ as follows.

$$H_\nu^{(2)}(k_t a) \sim \frac{j}{\sqrt{\pi}} (m_t^{-1})\, W_2(\tau) \tag{A-13}$$

$$H_\nu^{(2)'}(k_t a) \sim \frac{-j}{\sqrt{\pi}} (m_t^{-2})\, W_2'(\tau) \tag{A-14}$$

with

$$\nu = k_t a + m_t \tau \; ; \qquad m_t = \left(\frac{k_t a}{2}\right)^{1/3} . \tag{A-15a;A-15b}$$

It is noted that $W_2'(\tau)$ is the derivative of $W_2(\tau)$ with respect to the argument τ. The functions $W_1(\tau)$, $W_2(\tau)$ and their derivatives are discussed in Appendix V. Introducing the transformation of Equation (A-15a) into Equations (A-11) and (A-12) together with the approximations in Equations (A-13) and (A-14), one obtains,

$$\left.\frac{\partial A_z^+}{\partial \rho}\right|_{\rho=a} \simeq -\frac{jkY_o p_m^c}{4\pi^2 a} \int_{-\infty}^{\infty} dh\, \frac{e^{jhz}}{k_t} \int_{-\infty}^{\infty} d\tau\, \frac{W_2'(\tau)}{W_2(\tau)}\, e^{-jk_t a\phi - jm_t \tau\phi} \tag{A-16}$$

and

$$\left.F_z^+\right|_{\rho=a} \simeq \frac{+p_m^a}{4\pi^2 a} \int_{-\infty}^{\infty} dh\, \frac{e^{jhz}}{k_t} \left\{ m_t^2 \int_{-\infty}^{\infty} d\tau\, \frac{W_2(\tau)}{W_2'(\tau)}\, e^{-jk_t a\phi - jm_t \tau\phi} \right\} +$$

$$+ \frac{-p_m^c}{4\pi^2 a} \int_{-\infty}^{\infty} dh\, \frac{e^{jhz}}{k_t^3 a} h \left\{ m_t^2 \int_{-\infty}^{\infty} d\tau (k_t a + m_t \tau)\, \frac{W_2(\tau)}{W_2'(\tau)}\, e^{-jk_t a\phi - jm_t \tau\phi} \right\} . \tag{A-17}$$

The superscript "+" on A_z^+ and F_z^+ in Equations (A-16) and (A-17) signifies that only the term corresponding to $e^{-j\nu\phi}$ in Equations (A-11) and (A-12) are considered for convenience; the expressions for the $e^{-j\nu(2\pi-\phi)}$ terms are similar and may be designated by A_z^- and F_z^- with the understanding that

$$A_z = A_z^+ + A_z^- \quad ; \qquad F_z = F_z^+ + F_z^- \quad . \tag{A-18a;A-18b}$$

In order to evaluate the integrals with respect to the variable h, it is convenient to introduce the usual polar transformations given by,

$$h = k\sin\alpha, \quad k_t = + k\cos\alpha; \quad d \equiv a\phi = s\cos\psi; \quad z = s\sin\psi. \tag{A-19a;A-19b A=19c;A-19d}$$

Thus, Equation (A-16) becomes the following via Equation (A-19).

$$\left.\frac{\partial A_z^+}{\partial \rho}\right|_{\rho=a} \approx -\frac{jkY_o p_m^c}{4\pi^2 a} \int_{C_\alpha} d\alpha\, e^{-jks\cos(\alpha-\psi)} \int_{-\infty}^{\infty} d\tau\, \frac{W_2'(\tau)}{W_2(\tau)}\, e^{-jm_t\tau\phi} \quad . \tag{A-20}$$

The contour of integration, C_α is indicated in Figure A-III. The dominant

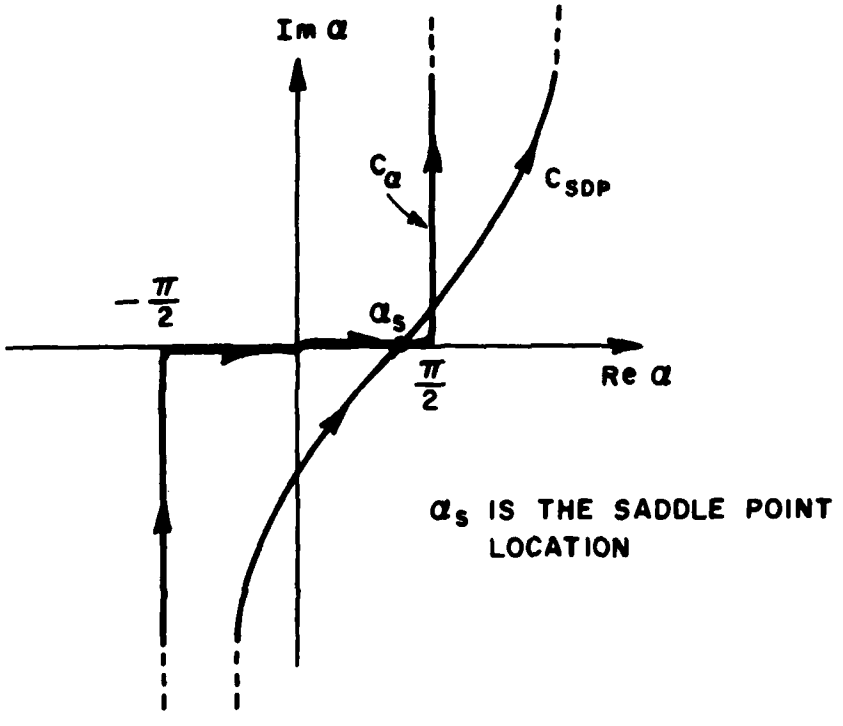

Figure A-III. Contours C_α and C_{SDP} in the complex α plane.

contribution to the integral over α occurs for $\alpha = \alpha_s = \psi$ for large ks where α_s is the saddle point in the complex α plane. The integral over τ yields

a slowly varying function of α in the neighborhood of α_s. The contour C_α may be continuously deformed into the steepest descent path C_{SDP} since no singularities are enclosed (for $\psi < \pi/2$), and the contributions from the paths connecting C_α with C_{SDP} are vanishingly small. Therefore, Equation (A-20) becomes

$$\left.\frac{\partial A_z^+}{\partial \rho}\right|_{\rho=a} \approx -\frac{jkY_o p_m^c}{4\pi^2 a} u(\xi)\, e^{-j\frac{3\pi}{4}} \xi^{-3/2} \sqrt{\pi} \int_{C_{SDP}} d\alpha e^{-jks\cos(\alpha-\psi)}; \qquad \text{(A-21)}$$

where the Fock type function $u(\xi)$ is discussed in Appèndix V; it is defined as,

$$u(\xi) = e^{j\frac{3\pi}{4}} \xi^{3/2} \frac{1}{\sqrt{\pi}} \int_{-\infty}^{\infty} d\tau \frac{W_2'(\tau)}{W_2(\tau)} e^{-j\xi\tau} \quad ; \qquad \text{(A-22a)}$$

with

$$\xi = \frac{ms}{\rho_g} \; ; \quad m = \left(\frac{k\rho_g}{2}\right)^{1/3} \; ; \quad \rho_g = \frac{a}{\cos^2\psi} \; . \qquad \text{(A-22b;A-22c;A-22d)}$$

The geometrical interpretation of the angle ψ is illustrated in Figure 1 in terms of the angle δ where

$$\delta = \frac{\pi}{2} - \psi = \frac{\pi}{2} - \cos^{-1}(\hat{t}'.\hat{\tau}_2') \quad . \qquad \text{(A-23)}$$

It can be shown that the leading term in the steepest descent approximation for large ks yields the following relationship for the C_{SDP} integral in Equation (A-21).

$$\frac{1}{2j}\sqrt{\frac{2jk\cos\psi}{\pi d}} \int_{C_{SDP}} d\alpha\, e^{-jks\cos(\alpha-\psi)} \sim \frac{e^{-jks}}{s} \; . \qquad \text{(A-24)}$$

It is interesting to note that the left hand side of Equation (A-24) is directly related to another integral as follows

$$\frac{1}{2j}\int_{-\infty}^{\infty} dh\, H_o^{(2)}(k_t d)\, e^{jhz} \approx \frac{1}{2j}\sqrt{\frac{2jk\cos\psi}{\pi d}}\int_{C_{SDP}} d\alpha\, e^{-jks\cos(\alpha-\psi)}, \quad \text{(A-25a)}$$

for $|k_t d| >> 1$
with $k_t = \sqrt{k^2-h^2}$.

Furthermore, it is well known that the left hand side of Equation (A-25a) is exactly given by

$$\frac{1}{2j}\int_{-\infty}^{\infty} dh\, H_o^{(2)}(k_t d)e^{jhz} = \frac{e^{-jks}}{s} \quad ; \quad s = \sqrt{d^2+z^2} \quad . \qquad \text{(A-25b)}$$

Now the approximation arrived at on the right hand side of Equation (A-24) is identical to the result on the right hand side of Equation (A-25b). Thus, the leading term of the asymptotic approximation to the C_{SDP} integral in Equation (A-25a) is identical to the exact result in Equation (A-25b). Based on these observations, it would appear that the final result in Equation (A-24) is therefore valid even for ks small. Equation (A-21) may now be written as,

$$\left.\frac{\partial A_z^+}{\partial \rho}\right|_{\rho=a} \approx - p_m^c \quad f \quad \frac{j}{ks}\, u(\xi)\, G(ks) \qquad \text{(A-26)}$$

with

$$G(ks) = \frac{k^2 Y_o}{2\pi j} \quad \frac{e^{-jks}}{ks} \quad , \qquad \text{(A-27a)}$$

and

$$f = 1/\cos^2\psi = 1/\sin^2\delta \quad . \qquad \text{(A-27b)}$$

Similarly, one can show that Equation (A-17) becomes

$$F_z^+\Big|_{\rho=a} \approx \frac{P_m^a}{4\pi^2}\,\frac{m^2}{\rho_g}\cdot\sqrt{\frac{4\pi}{j\xi}}\cdot v(\xi)\cdot\int_{C_{SDP}} d\alpha e^{-jk\xi\cos(\alpha-\psi)}$$

$$-\frac{P_m^c}{8\pi^2}\,\frac{k\cot\delta}{m}\left[\int_{-\infty}^{\infty} d\tau\,\frac{W_2(\tau)}{W_2'(\tau)}\,e^{-j\xi\tau}+\frac{j\operatorname{cosec}^2\delta}{2m^2}\cdot\frac{\partial}{\partial\xi}\int_{-\infty}^{\infty} d\tau\,\frac{W_2(\tau)}{W_2'(\tau)}\,e^{-j\xi\tau}\cdot\right.$$

$$\left.\cdot\int_{C_{SDP}} d\alpha\, e^{-jk\xi\cos(\alpha-\psi)}\right], \qquad \text{(A-28)}$$

where the Fock type function $v(\xi)$ is discussed in Appendix V; it is also defined below.

$$v(\xi)=\sqrt{\frac{j\xi}{4\pi}}\int_{-\infty}^{\infty} d\tau\,\frac{W_2(\tau)}{W_2'(\tau)}\,e^{-j\xi\tau}\quad. \qquad \text{(A-29)}$$

The third term on the right hand side of Equation (A-28) is of higher order in $\frac{1}{ka}$ as compared to the other two terms; hence, this term will be discarded as only the lowest order terms in $\frac{1}{ka}$ are retained in this analysis. Consequently, Equation (A-28) may be written as

$$F_z^+\Big|_{\rho=a} \approx \frac{P_m^a}{4\pi^2}\,\frac{m^2}{\rho_g}\sqrt{\frac{4\pi}{j\xi}}\,v(\xi)\int_{C_{SDP}} d\alpha e^{-jk\xi\cos(\alpha-\psi)}$$

$$-\frac{P_m^c}{8\pi^2}\,\frac{k\cot\delta}{m}\cdot\sqrt{\frac{4\pi}{j\xi}}\,v(\xi)\int_{C_{SDP}} d\alpha e^{-jk\xi\cos(\alpha-\psi)}\quad. \qquad \text{(A-30)}$$

From Equation (A-24), and Equation (A-30), one obtains

$$F_z^+\Big|_{\rho=a} \approx \frac{P_m^a}{2\pi}\,v(\xi)\,\frac{e^{-jks}}{s}-\frac{P_m^c}{2\pi}\cot\delta\;\;v(\xi)\,\frac{e^{-jks}}{s}\quad. \qquad \text{(A-31)}$$

From Equations (A-5), (A-6), (A-26) and (A-31),

$$\bar{H}_t^m(P_N) \sim \hat{z}\,\frac{1}{jkz_o}\left[\left(\frac{\partial^2}{\partial z^2}+k^2\right)F_z^+\right]_{\rho=a} + \hat{\phi}\left[-\frac{\partial A_z^+}{\partial \rho}+\frac{1}{jkz_o\rho}\,\frac{\partial^2 F_z^+}{\partial\phi\partial z}\right]_{\rho=a} \tag{A-32}$$

with the understanding that $\bar{H}_t^m(P_N)$ in Equation (A-32) is associated only with the A_z^+ and F_z^+ terms; the total $\bar{H}_t^m(P_N)$ must be obtained from $(A_z^+ + A_z^-)$ and $(F_z^+ + F_z^-)$. However, the form of $\bar{H}_t^m(P_N)$ associated with the (A_z^-, F_z^-) terms will be identical to that associated with (A_z^+, F_z^+). In order to simplify the derivatives in Equation (A-32) one employs the following relationships.

$$\frac{\partial s}{\partial z} = \cos\delta = \sin\psi; \quad \frac{\partial \xi}{\partial z} = \frac{m}{\rho_g}\cos\delta; \quad \frac{\partial s}{\partial d} = \sin\delta; \quad \frac{\partial \xi}{\partial d} = \frac{m}{\rho_g}\sin\delta. \tag{A-33a);(A-33b) (A-33c);(A-33d)}$$

Employing Equation (A-33) into (A-32), and retaining only terms to lowest order in $\frac{1}{ka}$, one obtains

$$\begin{aligned}\bar{H}_t^m(P_N) \sim\ & \bar{p}_m\cdot\hat{\tau}_1'\hat{\tau}_1\left[\sin^2\delta + \frac{j}{ks}\left(1-\frac{j}{ks}\right)\left(2-3\sin^2\delta\right)\right]v(\xi)G(ks) \\ & + \bar{p}_m\cdot\hat{\tau}_2'\hat{\tau}_1\left[-\cos\delta\sin\delta\left\{1-\frac{3j}{ks}\left(1-\frac{j}{ks}\right)\right\}\right]v(\xi)G(ks) + \\ & + \bar{p}_m\cdot\hat{\tau}_1'\hat{\tau}_2\left[-\sin\delta\cos\delta\left\{1-\frac{3j}{ks}\left(1-\frac{j}{ks}\right)\right\}\right]v(\xi)G(ks) \\ & + \bar{p}_m\cdot\hat{\tau}_2'\hat{\tau}_2\left\{\left[\cos^2\delta+\frac{j}{ks}\left(1-\frac{j}{ks}\right)\left(2-3\cos^2\delta\right)\right]v(\xi)\right. \\ & \left. + f\,\frac{j}{ks}\left[u(\xi)-v(\xi)\right]\right\}G(ks)\ . \end{aligned} \tag{A-34}$$

The above result has the interpretation that the field $\bar{H}_t^m$ propagates along the helical geodesic surface ray path from P_N' to P_N as shown in Figure 1. A second helical geodesic ray path (not shown in Figure 1) which traverses

the cylinder surface in a sense opposite to that shown in Figure 1 also contributes to the total field at P_N; the latter contribution results from the (A_z^-, F_z^-) terms, and it is identical in form to that in Equation (A-34), except that s, α and ξ are now associated with this second path. It is noted that $\hat{\tau}_1'$ and $\hat{\tau}_1$ correspond to $\hat{z}|_{P_N'}$ and $\hat{z}|_{P_N}$, respectively; whereas, $\hat{\tau}_2'$ and $\hat{\tau}_2$ correspond to $\hat{\phi}|_{P_N'}$ and $\hat{\phi}|_{P_N}$, respectively.

Next, one may evaluate E_ρ due to $\bar{M}$ via Equations (A-7), (A-26) and (A-31) as follows.

$$E_\rho \approx -\frac{kp_m^c}{2\pi j}\frac{\partial}{\partial z}\left[u(\xi)\frac{e^{-jks}}{(ks\sin\theta)^2}\right] + \frac{kp_m^c}{2\pi}\frac{\partial}{\partial d}\left[v(\xi)\cot\delta\frac{e^{-jks}}{ks}\right]$$

$$-\frac{kp_m^a}{2\pi}\frac{\partial}{\partial d}\left[v(\xi)\frac{e^{-jks}}{ks}\right] \qquad \text{(A-35)}$$

where $d=a\phi$. One may simplify Equation (A-35) by employing the relations in Equation (A-33); thus, retaining terms to lowest order in $1/ka$,

$$\frac{\partial}{\partial z}\left[u(\xi)\frac{e^{-jks}}{(ks\sin\theta)^2}\right] \approx \frac{u(\xi)}{(ks)^2}\frac{-jk}{\sin^2\delta}\cdot e^{-jks}\cos\delta,$$

and

$$\frac{\partial}{\partial d}\left[v(\xi)\frac{e^{-jks}}{ks}\right] \approx -jk\left(1-\frac{j}{ks}\right)\frac{e^{-jks}}{ks}v(\xi)\sin\delta \quad .$$

Therefore

$$E_\rho(P_N) \approx \frac{k^2 p_m^c}{2\pi j}\left[\left(1-\frac{j}{ks}\right)\frac{e^{-jks}}{ks}v(\xi)\cos\delta + \frac{j}{(ks)^2}\left\{u(\xi)-v(\xi)\right\}\frac{\cos\delta}{\sin^2\delta}e^{-jks}\right]$$

$$-\frac{k^2 p_m^a}{2\pi j}\left[\left(1-\frac{j}{ks}\right)\frac{e^{-jks}}{ks}v(\xi)\sin\delta\right] \quad , \qquad \text{(A-36a)}$$

or in the vector notation of Section II,

$$\bar{E}^m_n(P_N) \sim (Y_o)^{-1} \bar{p}_m \cdot \Big\{ [-\hat{\tau}'_1 \sin\delta + \hat{\tau}'_2 \cos\delta] \hat{n} (1 - \tfrac{j}{ks}) v(\xi)$$

$$+ \hat{\tau}'_2 \cos\delta \hat{n} \tfrac{j}{ks} [u(\xi) - v(\xi)] f \Big\} G(ks). \qquad \text{(A-36b)}$$

One may now develop similar expressions for the electromagnetic surface fields of a radial electric current $\bar{J}$ on a perfectly-conducting circular cylinder. One defines $\bar{J}$ in a manner anologous to that in Equation (A-1),

$$\bar{J} = \bar{p}_e \delta(|\bar{r} - \bar{r}'|). \qquad \text{(A-37)}$$

It is noted that p_e is the strength of the infinitesimal electric current moment which is oriented normal to the surface at $\bar{r}'$. The tangential magnetic field $\bar{H}^e_t(P_N)$ due to $\bar{J}$ may be simply obtained by employing the reciprocity theorem to the fields of $\bar{M}$ and $\bar{J}$; namely,

$$\bar{H}^e_t \cdot \bar{p}_m \Big|_{\text{at } \bar{p}_m} = - \bar{E}^m_n \cdot \bar{p}_e \Big|_{\text{at } \bar{p}_e} . \qquad \text{(A-38)}$$

Consequently, from Equations (A-36b) and (A-38), one obtains

$$\bar{H}^e_t(P_N) \sim -(Y_o)^{-1} \bar{p}_e \cdot \Big\{ \hat{n}' [-\hat{\tau}_1 \sin\delta + \hat{\tau}_2 \cos\delta] (1 - \tfrac{j}{ks}) v(\xi)$$

$$+ \hat{n}' \cos\delta \, \hat{\tau}_2 \tfrac{j}{ks} [u(\xi) - v(\xi)] f \Big\} G(ks). \qquad \text{(A-39)}$$

The radially directed electric field, $\bar{E}^e_n(P_N)$; i.e., the electric field component normal to the surface at P_N, which is generated by the source $\bar{J}$ may be obtained from Equation (A-39) via the equation of continuity. Thus,

$$\tfrac{j}{kY_o} \nabla_s \cdot [\hat{n} \times \bar{H}^e_t(P_N)] = \hat{n} \cdot \bar{E}^e_n(P_N), \qquad \text{(A-40)}$$

where $[\nabla_s \cdot]$ is the surface divergence operator. The above equation simplifies to

$$\bar{E}_n^e(P_N) = \hat{n}\left(\frac{j}{kY_o}\right)\left[-\frac{\partial}{\partial d}(\hat{\tau}_1\cdot\bar{H}_t^e)+\frac{\partial}{\partial z}(\hat{\tau}_2\cdot\bar{H}_t^e)\right] \quad , \tag{A-41}$$

which in turn may be evaluated via Equation (A-33). Without going through the details of the evaluation of Equation (A-41), the final expression for $\bar{E}_n^e(P_N)$ which contains terms only to lowest order in $\frac{1}{ka}$ is given below.

$$\bar{E}_n^e(P_N)\sim-(Y_o)^{-2}\bar{p}_e\cdot\hat{n}'\hat{n}\left\{\left[1-\frac{j}{ks}(1-\frac{j}{ks})\right]v(\xi)+(f)\,\frac{j}{ks}[u(\xi)-v(\xi)]\right.$$

$$\left.-\frac{j}{ks}(1-\frac{j}{ks})[u(\xi)-v(\xi)]\right\}G(ks). \tag{A-42}$$

It is noted that $u(\xi)$ and $v(\xi)$ are special cases of the more general functions $F_s(\xi,y_1,y_2)$ and $F_h(\xi,y_1,y_2)$ which are indicated in Appendix V. It can be shown that if the height of the observation point P above the surface is d_2 (i.e., $|\overline{P_NP}|=d_2$ of Figures 1 and 2) and $d_2\geq 0$, then the functions $u(\xi)$ and $v(\xi)$ in Equations (A-34), (A-36b), (A-39) and (A-42) may be replaced by $F_s(\xi,0,y_2)$ and $F_h(\xi,0,y_2)$, respectively with $y_1=0$ and $y_2=m^{-1}kd_2$, provided $kd_2<<k\rho_g(P_N)$. Furthermore, if the source $\bar{J}$ of Equation (A-37) is also raised above the surface from P_N' to P' (i.e., $|P_N'P'|=d_1$ of Figures 1 and 2) when P_N is raised to P above the surface, then the $u(\xi)$ and $v(\xi)$ in Equation (A-39) and Equation (A-42) must then be replaced by $F_s(\xi,y_1,y_2)$ and $F_h(\xi,y_1,y_2)$, respectively with $y_1=m^{-1}kd_1$ and $y_2=m^{-1}kd_2$, for $kd_1<<k\rho_g(P_N')$ and $kd_2<<k\rho_g(P_N)$. An approximation based on Taylor series is given in Appendix V for $F_{s,h}(\xi,y_1,y_2)$ when h_1, and h_2 are sufficiently small and when $\xi\neq 0$ (also ξ must not be close to zero).

APPENDIX II

ASYMPTOTIC ANALYSIS OF THE SURFACE FIELDS EXCITED BY INFINITESIMAL ELECTRIC OR MAGNETIC CURRENT SOURCES ON A PERFECTLY-CONDUCTING SPHERE

The geometry of this canonical problem is illustrated in Figure 3. The case of an infinitesimal tangential magnetic current source at P_N' will be treated first; a corresponding treatment will be subsequently presented for the case of an infinitesimal radial electric current source at P_N'.

The notation employed in this Appendix for the fields $\bar{E}_n^m$, $\bar{H}_t^m$ due to the source $\bar{M}$ has the same meaning as that in Section II, and Appendix I, respectively. Let the source $\bar{M}$ be $\hat{x}$-directed in Figure 3; then the vector potential $\bar{F}_o$ associated with the source $\bar{M}=\hat{x}p_m\delta(\bar{r}-\bar{r}')$ in free space (i.e., in the absence of the sphere) is given by [14]

$$\bar{F}_o = \hat{x}\,\frac{p_m}{4\pi}\,\frac{e^{-jk|\bar{r}-\bar{r}'|}}{|\bar{r}-\bar{r}'|}\quad , \tag{A-43a}$$

or

$$\bar{F}_o = \hat{x}\,\frac{kp_m}{4\pi j}\sum_{n=0}^{\infty}(2n+1)h_n^{(2)}(kr')j_n(kr)P_n(\cos\theta);\quad |\bar{r}|<|\bar{r}'|, \tag{A-43b}$$

where j_n, $h_n^{(2)}$ and P_n are the usual spherical Bessel, Hankel and Legendre functions. Let

$$\bar{r}' = (a+d_1)\hat{z} = b\hat{z}. \tag{A-44}$$

It is convenient to introduce a new set of potentials $\pi^e\hat{r}$ and $\pi^m\hat{r}$ which satisfy the following differential equation and the field relations [14].

$$(\nabla^2 + k^2)\begin{Bmatrix}\pi^e/r\\ \pi^m/r\end{Bmatrix} = 0\quad ;\qquad r\neq 0\quad . \tag{A-45}$$

$$E_r = \frac{1}{jkY_o}\left(\frac{\partial^2}{\partial r^2} + k^2\right)\pi^e \tag{A-46}$$

$$E_\theta = \frac{-1}{r\sin\theta}\ \frac{\partial \pi^m}{\partial \phi} + \frac{1}{jkY_o r}\ \frac{\partial^2 \pi^e}{\partial r \partial \theta} \tag{A-47}$$

$$E_\phi = \frac{1}{r}\frac{\partial \pi^m}{\partial \theta} + \frac{1}{jkY_o r\sin\theta}\ \frac{\partial^2 \pi^e}{\partial r \partial \phi} \tag{A-48}$$

$$H_r = \frac{1}{jkz_o}\left(\frac{\partial^2}{\partial r^2} + k^2\right)\pi^m \tag{A-49}$$

$$H_\theta = \frac{1}{r\sin\theta}\frac{\partial \pi^e}{\partial \phi} + \frac{1}{jkz_o r}\ \frac{\partial^2 \pi^m}{\partial r \partial \theta} \tag{A-50}$$

$$H_\phi = -\frac{1}{r}\frac{\partial \pi^e}{\partial \theta} + \frac{1}{jkz_o r\sin\theta}\ \frac{\partial^2 \pi^m}{\partial r \partial \phi} \tag{A-51}$$

where E_r, E_θ, and E_ϕ are the $\hat{r}$, $\hat{\theta}$ and $\hat{\phi}$ components of the electric field, $\overline{E}$ which are respectively generated by the potentials π^e and π^m. Likewise H_r, H_θ and H_ϕ are the $\hat{r}$, $\hat{\theta}$ and $\hat{\phi}$ components of the magnetic field, $\overline{H}$ which are respectively generated by π^e and π^m. Let π_o^e and π_o^m denote the value of the potentials π^e and π^m which are associated with the source $\overline{M}$ in free space. Let the fields associated with these potentials π_o^e and π_o^m be denoted by $\overline{E}^{(o)}$ and $\overline{H}^{(o)}$. From [14],

$$\overline{E}^{(o)} = -\nabla x \overline{F}_o \quad ; \qquad \overline{H}^{o} = \frac{\nabla x \nabla x \overline{F}_o}{jkz_o} = \frac{\nabla(\nabla_o \cdot \overline{F}_o) - \nabla^2 \overline{F}_o}{jkz_o} \quad . \tag{A-52a;A-52b}$$

Without going through the details, the following expressions are obtained via (A-43, A-52a;A-52b).

$$\overline{r}\cdot\overline{E}^{(o)} = r\hat{r}\cdot\overline{E}^{(o)} = rE_r^{(o)} = \sin\phi\ \frac{\partial F_o}{\partial \theta} \tag{A-53}$$

and

$$\bar{r}\cdot\bar{H}^{(o)} = r\hat{r}\cdot\bar{H}^{(o)} = rH_r^{(o)} = -\frac{\cos\phi}{jkz_o}\left[\frac{\partial}{\partial\theta}\left(\frac{\partial F_o}{\partial b}+\frac{F_o}{b}\right)\right]. \qquad \text{(A-54)}$$

A useful procedure given by Fock in his development of a modal expansion for the fields of an electric current moment over a dielectric sphere [13] is employed in order to obtain the form in Equations (A-53) and (A-54). The following relations are helpful in arriving at Equations (A-53) and (A-54).

$$F_o = \hat{x}\,\frac{p_m}{4\pi}\,\frac{e^{-jkR}}{R} \quad ; \quad R^2=|\bar{r}-\bar{r}'|^2 = b^2+r^2-2br\cos\theta. \qquad \text{(A-55)}$$

$$\frac{\partial F_o}{\partial r} = \left(\frac{\partial F_o}{\partial R}\right)\frac{\partial R}{\partial r} \quad ; \quad \frac{\partial F}{\partial\theta} = \left(\frac{\partial F_o}{\partial R}\right)\frac{\partial R}{\partial\theta} \quad . \qquad \text{(A-56a;A-56b)}$$

$$\frac{\partial R}{\partial r} = \frac{r-b\cos\theta}{R} \quad ; \quad \frac{\partial R}{\partial\theta} = \frac{br\sin\theta}{R} \quad ; \quad \frac{\partial R}{\partial b} = \frac{b-r\cos\theta}{R} \quad . \qquad \text{(A-57a;A-57b;A-57c)}$$

$$\cos\theta\,\frac{\partial F_o}{\partial r} - \frac{\sin\theta}{r}\,\frac{\partial F_o}{\partial\theta} = -\frac{\partial F_o}{\partial R}\,\frac{\partial R}{\partial b} = -\frac{\partial F_o}{\partial b} \qquad \text{(A-58)}$$

$$\sin\theta\,\frac{\partial F_o}{\partial r} + \frac{\cos\theta}{r}\,\frac{\partial F_o}{\partial\theta} = \frac{1}{b}\,\frac{\partial F_o}{\partial R}\,\frac{\partial R}{\partial\theta} = \frac{1}{b}\,\frac{\partial F_o}{\partial\theta} \quad . \qquad \text{(A-59)}$$

From Equations (A-46), (A-47), (A-53) and (A-54), it can be seen that

$$\sin\phi\,\frac{\partial F_o}{\partial\theta} = \frac{-1}{jkY_o}\,\Delta^*\left(\frac{\pi_o^e}{r}\right) \quad , \qquad \text{(A-60)}$$

and

$$\cos\phi\left[\frac{\partial}{\partial\theta}\left(\frac{\partial F_o}{\partial b}+\frac{F_o}{b}\right)\right] = \Delta^*\left(\frac{\pi_o^m}{r}\right) \quad , \qquad \text{(A-61)}$$

where the operator Δ^* is as defined by Fock [13].

$$\Delta^* = \frac{1}{\sin\theta}\,\frac{\partial}{\partial\theta}\,\left(\sin\theta\,\frac{\partial}{\partial\theta}\right) + \frac{1}{\sin^2\theta}\,\frac{\partial^2}{\partial\phi^2} \quad . \qquad \text{(A-62)}$$

In order to solve for $\pi_o^{e,m}$ in terms of F_o via Equations (A-60) and (A-61), respectively, it is convenient to introduce the following expressions as done previously by Fock [13].

$$\frac{\pi_o^e}{r} = -\sin\phi \frac{\partial A_o}{\partial \theta} \quad ; \quad \frac{\pi_o^m}{r} = -\cos\phi \frac{\partial B_o}{\partial \theta} . \qquad \text{(A-63);(A-64)}$$

Incorporating Equations (A-63) and (A-64) into Equations (A-60) and (A-61), with F_o as in Equation (A-43b), it follows that

$$A_o = -jkY_o\left(\frac{kp_m}{4\pi j}\right) \sum_{n=1}^{\infty} \frac{2n+1}{n(n+1)} h_n^{(2)}(kr')j_n(kr)P_n(\cos\theta) \qquad \text{(A-65)}$$

and

$$B_o = \left(\frac{kp_m}{4\pi j}\right) \sum_{n=1}^{\infty} \frac{2n+1}{n(n+1)} \left\{ \frac{kr'h_n^{(2)'}(kr')+h_n^{(2)}(kr')}{r'} \right\} j_n(kr)\, P_n(\cos\theta) \qquad \text{(A-66)}$$

where $r' = b = a+d_1$.

Using the definitions [13,15]

$$\zeta_n^{(2)}(kr) = krh_n^{(2)}(kr) \quad ; \quad \psi_n(kr) = krj_n(kr) \qquad \text{(A-67);(A-68)}$$

one obtains

$$A_o = -jkY_o\left(\frac{kp_m}{4\pi j}\right) \frac{1}{(kb)(kr)} \sum_{n=1}^{\infty} \frac{2n+1}{n(n+1)} \zeta_n^{(2)}(kb)\psi_n(kr)P_n(\cos\theta) \qquad \text{(A-69)}$$

$$B_o = \left(\frac{kp_m}{4\pi j}\right) \frac{k}{(kb)(kr)} \sum_{n=1}^{\infty} \frac{2n+1}{n(n+1)} \zeta_n^{(2)'}(kb)\psi_n(kr)P_n(\cos\theta) \; . \qquad \text{(A-70)}$$

From the relationships in Equations (A-63) and (A-64), and the results in Equations (A-69) and (A-70), the expressions for π_o^e and π_o^m are completely determined. The relationship $\frac{\partial}{\partial\theta} P_n(\cos\theta) = -P_n^1(\cos\theta)$ may be employed in evaluating $\frac{\partial A_o}{\partial\theta}$ and $\frac{\partial B_o}{\partial\theta}$ in Equations (A-63) and (A-64), respectively.

The potentials π_o^e and π_o^m are the potentials associated with the source $\bar{M}$ in free space; consequently one may introduce π_s^e and π_s^m to denote the potentials resulting from the presence of the conducting sphere such that the total potentials π^e and π^m associated with $\bar{M}$ in the presence of the sphere are obtained via the following superposition.

$$\pi^e = \pi_o^e + \pi_s^e \quad ; \quad \pi^m = \pi_o^m + \pi_s^m \quad . \tag{A-71);(A-72}$$

Let A_s and B_s be introduced as follows,

$$\frac{\pi_s^e}{r} = -\sin\phi \frac{\partial A_s}{\partial \theta} \quad ; \quad \frac{\pi_s^m}{r} = -\cos\phi \frac{\partial B_s}{\partial \theta} \quad . \tag{A-73);(A-74}$$

Equations (A-73) and (A-74) have been chosen to possess the same form as Equations (A-63) and (A-64), respectively. It follows from Equations (A-69) and (A-70), that

$$A_s = -jkY_o\left(\frac{kp_m}{4\pi j}\right) \frac{1}{(kb)(kr)} \sum_{n=1}^{\infty} \frac{2n+1}{n(n+1)} \zeta_n^{(2)}(kb)\tilde{B}_n(kr)P_n(\cos\theta), \tag{A-75}$$

$$B_s = \left(\frac{kp_m}{4\pi j}\right) \frac{k}{(kb)(kr)} \sum_{n=1}^{\infty} \frac{2n+1}{n(n+1)} \zeta_n^{(2)'}(kb)\tilde{A}_n(kr)P_n(\cos\theta) \ , \tag{A-76}$$

where the coefficients $\tilde{B}_n(kr)$ and $\tilde{A}_n(kr)$ must be found by enforcing the boundary condition that $\hat{n}x[\bar{E}^{(o)}+\bar{E}^{(s)}]=0$ on the spherical surface at r=a; here, $\bar{E}^{(s)}$ is the electric field produced by the potentials π_s^e and π_s^m. The total electric field $\bar{E}^m=\bar{E}^{(o)}+\bar{E}^{(s)}$ is produced by $\bar{M}$ in the presence of the sphere. Also, $\hat{r}\hat{r}\cdot\bar{E}^m=\bar{E}_n^m$ of the earlier notation. It is easily verified that

$$\tilde{A}_n(kr) = \psi_n(kr) - \frac{\psi_n(ka)}{\zeta_n^{(2)}(ka)} \zeta_n^{(2)}(kr) \ , \tag{A-77}$$

and

$$\tilde{B}_n(kr) = \psi_n(kr) - \frac{\psi_n'(ka)}{\zeta_n^{(2)'}(ka)} \zeta_n^{(2)}(kr) \ . \tag{A-78}$$

Let $\bar{H}^m$ denote the total magnetic field of $\bar{M}$ in the presence of the sphere. Then, from Equations (A-63), (A-64), (A-65), (A-66), (A-71), (A-72), (A-73), (A-74), (A-75), (A-76), (A-46) and (A-49), it may be seen that

$$\hat{r}\cdot\bar{E}^m = E_n^m = \left(\frac{kp_m}{4\pi j}\right)\left[\frac{-k\sin\phi}{kb}\right] \sum_{n=0}^{\infty} (2n+1)\zeta_n^{(2)}(kb)\, \frac{\tilde{B}_n(kr)}{(kr)^2}\, P_n^1(\cos\theta) \qquad \text{(A-79)}$$

and

$$\hat{r}\cdot\bar{H}^m = H_n^m = \left(\frac{kp_m}{4\pi j}\right)\left[\frac{-jkY_o\cos\phi}{kb}\right] \sum_{n=0}^{\infty} (2n+1)\zeta_n^{(2)'}(kb)\, \frac{\tilde{A}_n(kr)}{(kr)^2}\, P_n^1(\cos\theta), \qquad \text{(A-80)}$$

the sum over n in Equations (A-79) and (A-80) starts from n=0 instead of n=1 for convenience since $P_0^1(\cos\theta)=0$. In order to evaluate Equations (A-79) and (A-80) asymptotically for large ka, it is convenient at this juncture to employ the Watson transform to these equations [5]. As a first step, one may write Equations (A-79) and (A-80) more compactly for later convenience.

$$\begin{Bmatrix} \hat{r}\cdot\bar{E}^m \\ \hat{r}\cdot\bar{H}^m \end{Bmatrix} = \left(\frac{kp_m}{4\pi j}\right) \begin{Bmatrix} (-k\sin\phi) I_e^m \\ (-jkY_o\cos\phi) I_h^m \end{Bmatrix} , \qquad \text{(4-81)}$$

where

$$\begin{matrix} I_e^m \\ I_h^m \end{matrix} = \sum_{n=0}^{\infty} (2n+1) \begin{Bmatrix} \zeta_n^{(2)}(kb)\, \tilde{B}_n(kr)/(kr)^2(kb) \\ \zeta_n^{(2)'}(kb)\, \tilde{A}_n(kr)/(kr)^2(kb) \end{Bmatrix} P_n^1(\cos\theta) \quad . \qquad \text{(A-82)}$$

Employing the Watson transform to Equation (A-82), one obtains

$$\begin{matrix} I_e^m \\ I_h^m \end{matrix} = \frac{1}{2\pi j} \oint_{C_\nu^+ + C_\nu^-} d\nu\, \frac{\pi(-1)^\nu}{\sin\nu\pi}\, (2\nu+1) \begin{Bmatrix} \zeta_\nu^{(2)}(kb)\tilde{B}_\nu(kr)/(kr)^2(kb) \\ \zeta_\nu^{(2)'}(kb)\tilde{A}_\nu(kr)/(kr)^2(kb) \end{Bmatrix} P_\nu^1(\cos\theta). \qquad \text{(A-83)}$$

Contours $C_\nu^\pm$ are shown in Figure A-IV.

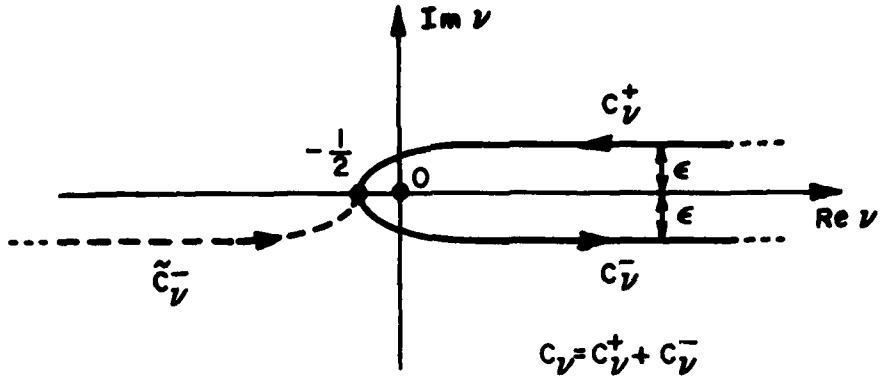

Figure A-IV. Contour of integration in the complex ν plane.

Employing the relationship $(-1)^\nu P_\nu^1(\cos\theta) = \nu(\nu+1)P_\nu^{-1}(-\cos\theta)$, and replacing ν by $-\nu-1$ in the integration over C_ν^+, one obtains

$$I_{e\,h}^{m} = \frac{1}{2\pi j}\int_{-\infty-j\epsilon}^{\infty-j\epsilon} d\nu\left(\frac{\pi}{\sin\nu\pi}\right)(2\nu+1)\nu(\nu+1)\begin{Bmatrix}\zeta_\nu^{(2)}(kb)\tilde{B}_\nu(kr)/(kr)^2(kb)\\ \zeta_\nu^{(2)\prime}(kb)\tilde{A}_\nu(kr)/(kr)^2(kb)\end{Bmatrix}P_\nu^{-1}(-\cos\theta), \tag{A-84}$$

where ϵ is a positive number however small. In arriving at (A-84), use is made of the following relationships.

$$P_{-\nu-1}^{-1}(-\cos\theta) = P_\nu^{-1}(-\cos\theta), \tag{A-85}$$

$$\zeta_\nu^{(2)}(kb)\tilde{B}_\nu(kr) = \sqrt{\frac{\pi^2k^2br}{4}}\,H_{\nu+1/2}^{(2)}(kb)\left[J_{\nu+1/2}(kr) - \frac{\tilde{Q}J_{\nu+1/2}(ka)}{\tilde{Q}H_{\nu+1/2}^{(2)}(ka)}H_{\nu+1/2}^{(2)}(kr)\right], \tag{A-86}$$

$$\zeta_\nu^{(2)\prime}(kb)\tilde{A}_\nu(kr) = kb\tilde{Q}H_{\nu+1/2}^{(2)}(kb)\left[J_{\nu+1/2}(kr) - \frac{J_{\nu+1/2}(ka)}{H_{\nu+1/2}^{(2)}(ka)}H_{\nu+1/2}^{(2)}(kr)\right]\sqrt{\frac{\pi kr}{2}}, \tag{A-87}$$

$$\tilde{Q} = \frac{\pi}{2x}\left(\frac{d}{dx} + \frac{1}{2x}\right) \quad ; \qquad x = \begin{Bmatrix} kb=kr' \\ \text{or}" \\ kr \end{Bmatrix} \quad , \tag{A-88}$$

and the circuit relationships for the cylindrical Bessel and Hankel functions, $J_{\nu+1/2}(x)$ and $H^{(1)}_{(2)\,\nu+1/2}(x)$, respectively. Furthermore, one may employ the following relationships in Equation (A-84); namely

$$\begin{Bmatrix} \tilde{B}_\nu(kr)/(kr)^2 \\ \tilde{A}_\nu(kr)/(kr)^2 \end{Bmatrix} = \left(\frac{\partial^2}{\partial r^2} + k^2\right)\left[\frac{1}{k^2\nu(\nu+1)}\right] \begin{Bmatrix} \tilde{B}_\nu(kr) \\ \tilde{A}_\nu(kr) \end{Bmatrix} , \tag{A-89}$$

in order to obtain integral representations for π^e and π^m, since $\bar{E}^m_n$ and $\bar{H}^m_n$ are simply related to π^e and π^m via Equations (A-46) and (A-47), respectively. Thus, from Equations (A-46), (A-47), (A-81), (A-84) and (A-89),

$$\pi^e = \left(\frac{kp_m}{4\pi j}\right)\left(\frac{-jY_o \sin\phi}{kb}\right)\frac{1}{2\pi j}\int_{-\infty-j\varepsilon}^{\infty-j\varepsilon} d\nu\left(\frac{\pi}{\sin\nu\pi}\right)(2\nu+1)\zeta^{(2)}_\nu(kb)\tilde{B}_\nu(kr)P^{-1}_\nu(-\cos\theta) \tag{A-90}$$

and

$$\pi^m = \left(\frac{kp_m}{4\pi j}\right)\left(\frac{\cos\phi}{kb}\right)\frac{1}{2\pi j}\int_{-\infty-j\varepsilon}^{\infty-j\varepsilon} d\nu\left(\frac{\pi}{\sin\nu\pi}\right)(2\nu+1)\zeta^{(2)\,\prime}_\nu(kb)\tilde{A}_\nu(kr)P^{-1}_\nu(-\cos\theta). \tag{A-91}$$

π^e is next evaluated for the special case of interest; namely r'=b=a (i.e., for d_1=0) and r=a as follows. Let $\mu=\nu+1/2$; then,

$$\pi^e = \left(\frac{kp_m}{4\pi j}\right)\left(\frac{-jY_o \sin\phi}{kb}\right)\frac{1}{2\pi j}\int_{-\infty-j\varepsilon}^{\infty-j\varepsilon} d\mu\left(\frac{-\pi}{\cos\mu\pi}\right)2\mu\,\zeta^{(2)}_{\mu-1/2}(ka)\tilde{B}_{\mu-1/2}(ka)P^{-1}_{\mu-1/2}(-\cos\theta). \tag{A-92}$$

In the shadow boundary transition region (i.e., the penumbra region) and in the deep shadow region, both of which are of interest in this study, the dominant contribution to the integral in Equation (A-92) occurs when $\mu \sim 0(ka)$. Thus, in this region, one introduces the usual transformation $\mu = ka + m\tau$ to approximate the cylindrical functions $\psi_{\mu-1/2}$ and $\zeta^{(1)}_{\mu-1/2}$, $\zeta^{(2)}_{\mu-1/2}$ by the Fock type Airy functions. In particular [15],

$$\psi_{\mu-1/2}(ka) \sim \frac{\sqrt{m}}{2j}\left(W_1(\tau) - W_2(\tau)\right) \quad ; \quad \mu = ka + m\tau \quad ; \quad m = \left(\frac{ka}{2}\right)^{1/3} . \tag{A-93}$$

$$\psi'_{\mu-1/2}(ka) \sim -\frac{1}{2j\sqrt{m}}\left(W'_1(\tau) - W'_2(\tau)\right). \tag{A-94}$$

$$\zeta^{(1)}_{\mu-1/2}(ka) \sim j\sqrt{m}\, W_{1_2}(\tau). \tag{A-95}$$

$$\zeta^{(2)}_{\mu-1/2}(ka) \sim \frac{1}{j\sqrt{m}}\, W'_{1_2}(\tau). \tag{A-96}$$

Noting that $\frac{-1}{\cos\mu\pi} = 2j\, e^{-j(\mu-1/2)\pi} \sum_{\ell=0}^{\infty} e^{-j(\mu-1/2)(2\pi\ell)}$ in Equation (A-92), one may retain only the $\ell=0$ term for large ka as the terms corresponding to $\ell \neq 0$ contribute to the multiply encircling field paths around the sphere; these terms ($\ell \neq 0$) contribute negligibly for large ka. Also, $P^{-1}_{\mu-1/2}(-\cos\theta)$ may be approximated for large ka, $\theta \neq \pi$, and $\mu \sim 0(ka)$ as follows [15],

$$P^{-1}_{\mu-1/2}(-\cos\theta) \sim \frac{\mu^{-3/2}}{2j}\sqrt{\frac{2}{\pi\sin\theta}}\; e^{-j\frac{\pi}{4}}\, e^{j\mu\pi}\left[e^{-j\mu\theta} - je^{-j\mu(2\pi-\theta)}\right] . \tag{A-97}$$

Let

$$\pi^e = \pi^e_+ + \pi^e_- \tag{A-98}$$

where the π^e_+ term is associated with the $e^{-j\mu\theta}$ term in Equation (A-97); and π^e_- is associated with the term $e^{-j\mu(2\pi-\theta)}$ term in Equation (A-97).

Thus, one may write $\pi_{\pm}^{e}$ as:

$$\pi_{e}^{\pm} \sim \pm e^{-j\frac{\pi}{4}} \cdot \frac{kp_m Y_o}{4\pi j} \frac{\sin\phi}{(ka)^{3/2}} \cdot m^2 \left[\int_{-\infty}^{\infty} d\tau \frac{W_2(\tau)}{W_2'(\tau)} e^{-j\xi^{\pm}\tau} \right] \sqrt{\frac{2}{\pi \sin\theta^{\pm}}} e^{-jka\theta^{\pm}} \tag{A-99a}$$

with

$$\xi^{\pm} = m\theta^{\pm} \quad ; \qquad \theta^{\pm} = \begin{Bmatrix} \theta \\ 2\pi-\theta \end{Bmatrix} . \tag{A-99b;A-99c}$$

Simplifying the expression in Equation (A-99a) yields

$$\pi_{\pm}^{e} \sim \pm \frac{jp_m}{k} v(\xi^{\pm}) \sin\phi D^{\pm} G(ks^{\pm}) \tag{A-99d}$$

where $v(\xi)$ is defined in Equation (A-29); it is also discussed in Appendix V. Also, $G(ks)$ is defined in Equation (A-27). Here,

$$s^{\pm} = \begin{Bmatrix} a\theta \\ a(2\pi-\theta) \end{Bmatrix} ; \quad \xi^{\pm} = m \begin{Bmatrix} \theta \\ 2\pi-\theta \end{Bmatrix} ; \quad D^{\pm} = \sqrt{\frac{\theta^{\pm}}{\sin\theta^{\pm}}} = \begin{Bmatrix} \sqrt{\frac{\theta}{\sin\theta}} \\ \sqrt{\frac{2\pi-\theta}{\sin(2\pi-\theta)}} \end{Bmatrix} . \tag{A-100}$$

Clearly $G(ks^{+})$ corresponds to the field propagation along a great circle (geodesic) ray path corresponding to $s^{+}=a\theta$; whereas, $G(ks^{-})$ corresponds to propagation along the ray path $s^{-}=a(2\pi-\theta)$ along the same great circle (geodesic) but in a direction opposite to s^{+}. In this analysis, $0<\theta<\pi$; hence, it is noted that, $D^{-} = \sqrt{\frac{2\pi-\theta}{\sin(2\pi-\theta)}} = j\left|\sqrt{\frac{2\pi-\theta}{\sin(2\pi-\theta)}}\right|$; the factor j outside the radical is the same as that in front of the term $e^{-j\mu(2\pi-\theta)}$ in Equation (A-97), and it results from the crossing of a caustic of the great circle ray paths as they traverse the spherical surface. This caustic occurs at $\theta=\pi$. The asymptotic approximation in Equation (A-99) must be modified near $\theta=\pi$; a simple modification of Equation (A-99) for θ at and near π is discussed in Appendix III on caustic corrections.

Without going through the details, it can be similarly shown that

$$\pi^m_{\pm} \sim \pm \frac{-p_m e^{-j\frac{\pi}{4}}}{4kmY_o} G(ks^{\pm}) D^{\pm} \cos\phi \left\{ \sqrt{\frac{\xi^{\pm}}{\pi}} \int_{-\infty}^{\infty} d\tau W_2'(\tau) \left[W_1(\tau - y_2) - \frac{W_1(\tau)}{W_2(\tau)} W_2(\tau - y_2) \right] e^{-j\xi^{\pm}\tau} \right\} \tag{A-101}$$

for r'=b=a (i.e., $d_1=0$), and

$$y_2 = m^{-1}k(r-a) \triangleq m^{-1}kd_2; \quad r \geq a \tag{A-102}$$

The subscripts $\pm$ on $\pi^m_{\pm}$ have the same meaning as that in $\pi^e_{\pm}$; i.e.,

$$\pi^m = \pi^m_+ + \pi^m_- \quad . \tag{A-103}$$

From Equations (A-50), (A-51), (A-98), (A-99d), (A-101), and (A-103), one obtains the following surface magnetic field associated with π^e_+ and π^m_+ (the field corresponding to π^e_- and π^m_- is obtained by simply replacing s^+ by s^-, and by replacing ξ^+ by ξ^-, etc. in the fields corresponding to π^e_+ and π^m_+). Here, the subscript (+) is dropped for convenience.

$$H_\theta = \hat{t}\cdot\bar{H} = p_m \cos\phi \left[\frac{j}{ks}\left(1 - \frac{2j}{ks}\right) u(\xi) + D^2 \frac{j}{ks} v(\xi) \right] DG(ks) \tag{A-104a}$$

$$H_\phi = -\hat{b}\cdot\bar{H} = -p_m \sin\phi \left[\left(1 - \frac{j}{ks}\right) v(\xi) + j^2 D^2 \frac{u(\xi)}{(ks)^2} \right] DG(ks). \tag{A-104b}$$

$$\bar{H}^m_t(P_N) \sim \hat{t}(\hat{t}\cdot\bar{H}) + \hat{b}(\hat{b}\cdot\bar{H}). \tag{A-104c}$$

In obtaining Equations (A-104a;A-104b) use is made of the following relationships.

$$\frac{\partial}{\partial\theta^{\pm}} \frac{e^{-jks^{\pm}}}{ks^{\pm}} = a \frac{\partial}{\partial s^{\pm}} \frac{e^{-jks^{\pm}}}{ks^{\pm}} = 2m^3 \frac{e^{-jks^{\pm}}}{ks^{\pm}} \left[-j - \frac{1}{ks^{\pm}}\right]; \theta^{\pm} = \begin{Bmatrix} \theta \\ 2\pi - \theta \end{Bmatrix}. \tag{A-105a}$$

$$\frac{\partial}{\partial\theta^{\pm}} D^{\pm}e^{-j\xi^{\pm}\tau}=m\frac{\partial}{\partial\xi^{\pm}}(D^{\pm}e^{-j\xi^{\pm}\tau})=m\left[\frac{\partial D^{\pm}}{\partial\xi^{\pm}}e^{-j\xi^{\pm}\tau}+D^{\pm}(-j\tau)e^{-j\xi^{\pm}\tau}\right]. \qquad \text{(A-105b)}$$

As before, only terms to lowest order in $\frac{1}{ka}$ are retained in Equations (A-104a;A-104b).

In order to obtain $\bar{E}_n^m(P_N)$, i.e., $\bar{E}_r$ due to $\bar{M}$, it is convenient to rewrite Equation (A-46) as

$$E_r = -\frac{1}{jkY_o r^2}\Delta^*\pi^e \quad . \qquad \text{(A-106)}$$

It is noted that Δ^* is as in Equation (A-62), and

$$\left.\frac{\Delta^*}{r^2}\right|_{r=a} = \frac{D^2}{s}\frac{\partial}{\partial s}\left(\frac{s}{D^2}\frac{\partial}{\partial s}\right)+\frac{D^4}{s^2}\frac{\partial^2}{\partial\phi^2}\sim\frac{\partial^2}{\partial s^2}+\frac{1}{s}\frac{\partial}{\partial s}-\frac{D^4}{s^2} \qquad \text{(A-107)}$$

since $\frac{\partial^2}{\partial\phi^2}\to -1$ (due to $\sin\phi$ or $\cos\phi$ variation of $\pi^{e,m}$), and $\frac{\partial}{\partial s}\left(\frac{1}{D^2}\right)$ is neglected as it contributes to terms which are higher order in $\frac{1}{ka}$. One may rewrite Equation (A-106) via Equation (A-107) as follows after operating on π^e with the $\frac{\partial}{\partial s}$ and $\frac{\partial^2}{\partial s^2}$ operators.

$$\left.\frac{-\Delta^*\pi^e}{jkY_o r^2}\right|_{r=a} = \frac{-jp_m}{2\pi}\left[-k^2\left(1-\frac{j}{ks}\right)\frac{e^{-jks}}{ks}+k^2(1-D^4)\frac{e^{-jks}}{(ks)^3}\right]Dv(\xi). \qquad \text{(A-108)}$$

One may conveniently neglect the term involving $(1-D^4)$ in Equation (A-108) which contains a $\frac{1}{(ks)^3}$ dependence as it is vanishingly small for (ks) small (where D→1) and it is also small in comparison to the first two terms for (ks) large. Thus, $\hat{r}\cdot\bar{E}=E_r=E_n^m$ becomes

$$\bar{E}_n^m(P_N)\sim\hat{r}\left(\frac{-jp_m}{2\pi}\right)k^2\left(1-\frac{j}{ks}\right)\frac{e^{-jks}}{ks}\cdot D\,v(\xi)(-\sin\phi);\begin{Bmatrix}\bar{p}_m\cdot\hat{b}'=\\ -\sin\phi\ P_m\end{Bmatrix}. \qquad \text{(A-109)}$$

As before, the field in Equation (A-109) is associated with π_+^e with the subscript (+) dropped for convenience. The term corresponding to π_-^e is the same as in Equation (A-109) except that s^+ and ξ^+ are now replaced by s^- and ξ^-, respectively for the π_-^e case.

One may next develop similar expressions for the electromagnetic surface fields of a radial electric current $\bar{J}$ on a perfectly-conducting sphere. The source $\bar{J}=\bar{p}_e\delta(\bar{r}-\bar{r}')$ as in Equation (A-37). Since $\bar{p}_e=p_e\hat{n}$ at P_N', the tangential magnetic field $\bar{H}_t^e(P_N)$ due to $\bar{J}$ may be simply obtained from $\bar{E}_n^m(P_N)$ due to $\bar{M}$ via reciprocity as indicated in Equation (A-38). Thus,

$$\bar{H}_t^e(P_N)\sim-(Y_o)^{-1}\,\bar{p}_e\cdot(\hat{n}'\hat{b}[1-\frac{j}{ks}]v(\xi))D\,G(ks). \tag{A-110}$$

One may next compute the normal (radial) electric field $\bar{E}_n^e(P_N)$ due to $\bar{J}$ via the equation of continuity (see Equation (A-40)) and Equation (A-110) with the understanding that $\hat{b}=-\hat{\phi}$ in Equation (A-110). Thus,

$$\nabla_s\cdot[\hat{n}\times\bar{H}_t^e]\sim\frac{\partial H_t^e}{\partial s}+\frac{H_t^e}{s} \tag{A-111}$$

after neglecting $\frac{\partial}{\partial s}\,(\frac{1}{D^2})$ as before. Then from Equation (A-40),

$$\bar{E}_n^e(P_N)\sim-(Y_o)^{-2}\,\bar{p}_e\cdot\hat{n}'\hat{n}\left([1-\frac{j}{ks}(1-\frac{j}{ks})]v(\xi)\right)D\,G(ks). \tag{A-112}$$

Once again, referring to Figure 3, it is noted that if $d_2>0$, then $u(\xi)$ and $v(\xi)$ in Equations (A-104), (A-109), (A-110) and (A-112) must be replaced by $F_s(\xi,0,y_2)$ and $F_h(\xi,0,y_2)$ of Equations (A-139) and (A-138) for $kd_2<<ka$. On the other hand, if $d_1>0$ and $d_2>0$ in Equation (A-110) and Equation (A-112); then one must replace $u(\xi)$ by $F_s(\xi,y_1,y_2)$ and $v(\xi)$ by $F_h(\xi,y_1,y_2)$ in these equations when $kd_{1,2}<<ka$. The functions $F_{s,h}(\xi,y_1,y_2)$ are discussed in Appendix V along with an approximation for these functions based on a Taylor expansion which is valid for $kd_{1,2}$ sufficiently small and $\xi\neq0$. Finally, it is once again noted that the results in Equations (A-104), (A-109), (A-110) and (A-112) are not valid at and near $\theta=\pi$. For $\theta\to\pi$, these results must be modified as shown in Appendix III on caustic corrections.

APPENDIX III
CAUSTIC CORRECTIONS FOR THE SURFACE FIELDS ON THE SPHERE

As pointed out at the end of Appendix II, the expressions for the surface field on a sphere due to a source at P_N' on the same sphere (see Figure 3) as given in Equations (A-104), (A-109), (A-110) and (A-112) are not valid at $\theta=\pi$ because $D\to\infty$ as $\theta\to\pi$. The point P_N on the surface corresponding to $\theta=\pi$ is a caustic of the surface rays since at $\theta=\pi$, every great circle path is now a geodesic between the diametrically opposite source and field points, P_N' and P_N, respectively. Such a continuum of geodesic surface ray paths intersect at P_N, thereby producing a point caustic at P_N for $\theta=\pi$. In order to obtain an asymptotic approximation for the surface field which is valid at and near the caustic at $\theta=\pi$, one begins by noting that the approximation in Equation (A-97) is responsible for the singular behavior of D at $\theta=\pi$. Thus, to remedy this singular behavior of D at $\theta=\pi$, one may employ an asymptotic approximation for the Legendre function which is different from that in Equation (A-97) when $\theta\to\pi$; such an approximation is indicated in [15]. Alternatively, one may employ an approximation in Equations (A-104), (A-109), (A-110) and (A-112) for $\theta\to\pi$ which is based on the following physical considerations. Firstly, whenever $\theta\neq\pi$, there are two great circle geodesic surface ray paths between the points P_N' and P_N; these paths are associated with the potentials $\pi_+^{e,m}$ and $\pi_-^{e,m}$, respectively as indicated earlier in Appendix II. Furthermore, the total field is constructed from the sum of these $\pi_\pm^{e,m}$ potentials as indicated in Appendix II, i.e., from $\pi^{e,m}$ with

$$\pi^{e,m} = \pi_+^{e,m} + \pi_-^{e,m} \quad . \tag{A-113}$$

The electromagnetic surface fields resulting from $\pi_+^{e,m}$ are given in Equation (A-104) or (11) and in Equation (A-109) or (15) for the case of the magnetic current source $\bar{M}$ on a sphere; and they are given in Equation (A-110) or (22) and Equation (A-112) or (24) for the electric current source $\bar{J}$ on a

sphere. From (11) it is noted that the total $\bar{H}_t^m$ field, (i.e., including the $\pi_-^{e,m}$ contribution) contains the following combination of D G(ks) type terms.

$$T_{c1} = D^+ G(ks^+) + D^- G(ks^-), \tag{A-114}$$

and

$$T_{c3} = [D^+]^3 G(ks^+) + [D^-]^3 G(ks^-). \tag{A-115}$$

Simplifying T_{c1} and T_{c3} via $G(ks^{\pm})D^{\pm} = \sqrt{\frac{\theta^{\pm}}{\sin\theta^{\pm}}} \frac{k^2 Y_o}{2\pi j} \frac{e^{-jks^{\pm}}}{ks^{\pm}}$ yields,

$$T_{c1} = \frac{k^2 Y_o}{2\pi j}\left[\sqrt{\frac{\theta^+}{\sin\theta^+}}\ \frac{e^{-jks^+}}{ks^+} + \sqrt{\frac{\theta^-}{\sin\theta^-}}\ \frac{e^{-jks^-}}{ks^-}\right], \tag{A-116}$$

and

$$T_{c3} = \frac{k^2 Y_o}{2\pi j}\left[\left(\sqrt{\frac{\theta^+}{\sin\theta^+}}\right)^3 \frac{e^{-jks^+}}{ks^+} + \left(\sqrt{\frac{\theta^-}{\sin\theta^-}}\right)^3 \frac{e^{-jks^-}}{ks^-}\right], \tag{A-117}$$

with the understanding that:

$$\theta^+=\theta\ ;\quad s^+=a\theta\ ;\quad \theta^-=2\pi-\theta\ ;\quad s^-=a(2\pi-\theta). \tag{A-118a;A-118b; A-118c;A-118d}$$

Since $0<\theta<\pi$ is understood in the present development, it is clear that $\sin\theta^-<0$. Furthermore,

$$\sqrt{\frac{\theta^-}{\sin\theta^-}} = \sqrt{\frac{2\pi-\theta}{-\sin\theta}} = j\sqrt{\frac{2\pi-\theta}{\sin\theta}}\ ; \qquad 0<\theta<\pi\ . \tag{A-119}$$

Near the caustic, $\theta\to\pi$; hence, Equations (A-116) and (A-117) may be approximated as

$$T_{c1} \approx \frac{k^2 Y_o}{2\pi j}\left[\sqrt{\pi}\, e^{-jka\pi}\left(\frac{e^{jka(\pi-\theta)}}{\sqrt{\pi-\theta}} + j\,\frac{e^{-jka(\pi-\theta)}}{\sqrt{\pi-\theta}}\right)\right]\frac{1}{ks^+}\ ;\ \theta\to\pi \quad , \tag{A-120}$$

and

$$T_{c3} = \frac{\pi}{\sin\theta}\cdot T_{c2} \quad , \tag{A-121}$$

where

$$T_{c2} \approx \frac{k^2 Y_o}{2\pi j}\left[\sqrt{\pi}\, e^{-jka\pi}\left(\frac{e^{jka(\pi-\theta)}}{\sqrt{\pi-\theta}} - j\,\frac{e^{-jka(\pi-\theta)}}{\sqrt{\pi-\theta}}\right)\right]\frac{1}{ks^+}\ ;\ \theta\to\pi \quad . \tag{A-122}$$

In the above approximations, $\sin\theta = \sin(\pi-\theta) \approx \pi-\theta$ has been used for $\theta\to\pi$; also $\frac{1}{ks^-} \approx \frac{1}{ks^+}$ is used for $\theta\to\pi$. One may now rewrite Equation (A-120) and (A-122) in terms of trigonometric functions as:

$$T_{c1} \approx \frac{k^2 Y_o}{2\pi j}\left[\pi m^{3/2}\, e^{-j2\pi m^3}\left\{\sqrt{\frac{2}{\pi ka(\pi-\theta)}}\cos\left(ka(\pi-\theta)-\frac{\pi}{4}\right)\right\}\right]\frac{2e^{j\frac{\pi}{4}}}{ks^+} \tag{A-123}$$

and

$$T_{c2} \approx \frac{k^2 Y_o}{2\,j}\left[\pi m^{3/2}\, e^{-j2\pi m^3}\left\{\sqrt{\frac{2}{\pi ka(\pi-\theta)}}\sin\left(ka(\pi-\theta)-\frac{\pi}{4}\right)\right\}\right]\frac{2e^{j\frac{\pi}{4}}}{ks^+} \quad . \tag{A-124}$$

with

$$m = \left(\frac{k\rho_g}{2}\right)^{1/3}, \text{ and } \rho_g = a \text{ for the sphere.} \tag{A-125}$$

It is noted that $\sin\left(ka(\pi-\theta)-\frac{\pi}{4}\right) = \cos\left(ka(\pi-\theta)-\frac{\pi}{4}-\frac{\pi}{2}\right)$ in Equation (A-124). Furthermore, one also notes that for $ka(\pi-\theta)>>1$ the trigonometric functions in Equations (A-123) and (A-124) are asymptotic approximations of cylindrical Bessel functions as indicated below.

$$J_o(ka(\pi-\theta)) \sim \left\{ \sqrt{\frac{2}{\pi ka(\pi-\theta)}} \cos(ka(\pi-\theta) - \frac{\pi}{4}) \right\} , \qquad \text{(A-126)}$$

and

$$J_1(ka(\pi-\theta)) \sim \left\{ \sqrt{\frac{2}{\pi ka(\pi-\theta)}} \cos(ka(\pi-\theta) - \frac{\pi}{4} - \frac{\pi}{2}) \right\} . \qquad \text{(A-127)}$$

For small $ka(\pi-\theta)$, one may therefore replace the trigonometric functions in Equations (A-123) and (A-124) by the Bessel functions in Equations (A-126) and (A-127), respectively, thereby making T_{c1} and T_{c2} (and hence T_{c3}) valid for $\theta \to \pi$. This procedure is similar to that employed earlier by Keller [3] in his study of the diffraction by a circular aperture.

Thus, for $\theta \to \pi$, one may employ the following expressions for T_{c1}, T_{c2} and T_{c3} instead of those in Equations (A-120), (A-122) and (A-121), respectively.

$$T_{c1} \approx \frac{k^2 Y_o}{2\pi j} \left[\pi m^{3/2} e^{-j2\pi m^3} J_o(2m^3(\pi-\theta)) \right] \frac{2e^{j\frac{\pi}{4}}}{ks^+} \quad ; \quad 2m^3 >> 1; \quad \theta \to \pi, \qquad \text{(A-128)}$$

$$T_{c2} \approx \frac{k^2 Y_o}{2\pi j} \left[\pi m^{3/2} e^{-j2\pi m^3} J_1(2m^3(\pi-\theta)) \right] \frac{2e^{j\frac{\pi}{4}}}{ks^+} \quad ; \quad 2m^3 >> 1; \quad \theta \to \pi, \qquad \text{(A-129)}$$

$$T_{c3} \approx \frac{k^2 Y_o}{2\pi j} \left[2\pi^2 m^{9/2} e^{-j2\pi m^3} \frac{J_1(2m^3(\pi-\theta))}{2m^3(\pi-\theta)} \right] \frac{2e^{j\frac{\pi}{4}}}{ks^+} \quad ; \quad 2m^3 >> 1; \quad \theta \to \pi, \qquad \text{(A-130)}$$

and $m = (\frac{ka}{2})^{1/3}$ as noted previously.

From Equations (15) and (22) it is noted that the total $\overline{E}_n^m$ and the $\overline{H}_t^e$ fields (i.e., including the $\pi_-^{e,m}$ contribution) respectively contain only the T_{c2} type term; whereas, the total $\overline{E}_n^e$ field corresponding to Equation (24) contains only the T_{c1} type term. Hence, Equations (15) and (22) may be modified for $\theta \to \pi$ by employing T_{c2} of Equation (A-129) in place of Equation (A-122); likewise Equation (24) may be modified for $\theta \to \pi$ by employing T_{c1} of Equation (A-128) in place of Equation (A-120).

APPENDIX IV

NUMERICAL TECHNIQUES FOR EVALUATING THE MULTIPLE SURFACE INTEGRALS ASSOCIATED WITH THE MUTUAL ADMITTANCE BETWEEN TWO IDENTICAL SLOTS ON A CIRCULAR CYLINDER

Consider two identical circumferential slots on the surface of a circular cylinder. Under the "dominant mode" approximation of the aperture fields in the slots, the mutual admittance between the two slots can be expressed as follows:

$$Y_{12}^{c} = \frac{-2a^2}{\ell d} \int_{\phi_1=-\ell/2a}^{\ell/2a} d\phi_1 \int_{z_1=-d/2}^{d/2} dz_1 \int_{\phi_2=\phi_0-\ell/2a}^{\phi_0+\ell/2a} d\phi_2 \int_{z_2=z_0-d/2}^{z_0+d/2} dz_2$$

$$\cos[\frac{\pi a\phi_1}{\ell}] \cos[\frac{\pi}{\ell}a(\phi_2-\phi_0)]\, g_{\phi}^{c}(s,\theta) \quad . \tag{A-131}$$

In the above expression, a is the radius of the circular cylinder, d and ℓ are the slot dimensions; and ϕ_0 and z_0 are the angular and axial separation of the centers of the two slots, respectively. These parameters are illustrated in Figure A-5. The Green's function $g_{\phi}^{c}(s,\theta)$ represents the surface field $\hat{\tau}_2\cdot\bar{H}_t^m$ at (ϕ_2,z_2) due to a unit-strength, $\hat{\tau}_2'$-directed magnetic dipole at (ϕ_1,z_1). The variable "s" is the arc length along the geodesic path joining the source location (ϕ_1,z_1) and the field point location (ϕ_2,z_2); and the variable "θ" is the pitch angle associated with the geodesic helix as shown in Figure A-5. It has been shown in Section II that the surface field $\hat{\tau}_2\cdot\bar{H}_t^m$ is indeed only a function of the arc length "s" and the pitch angle "θ". It is noted that both "s" and "θ" depend upon the relative distance of $|z_2-z_1|$ and $|\phi_2-\phi_1|$. The feature that $\hat{\tau}_2\cdot\bar{H}_t^m$ depends upon only the relative axial and angular separation between the source and field locations suggests an efficient way to perform the

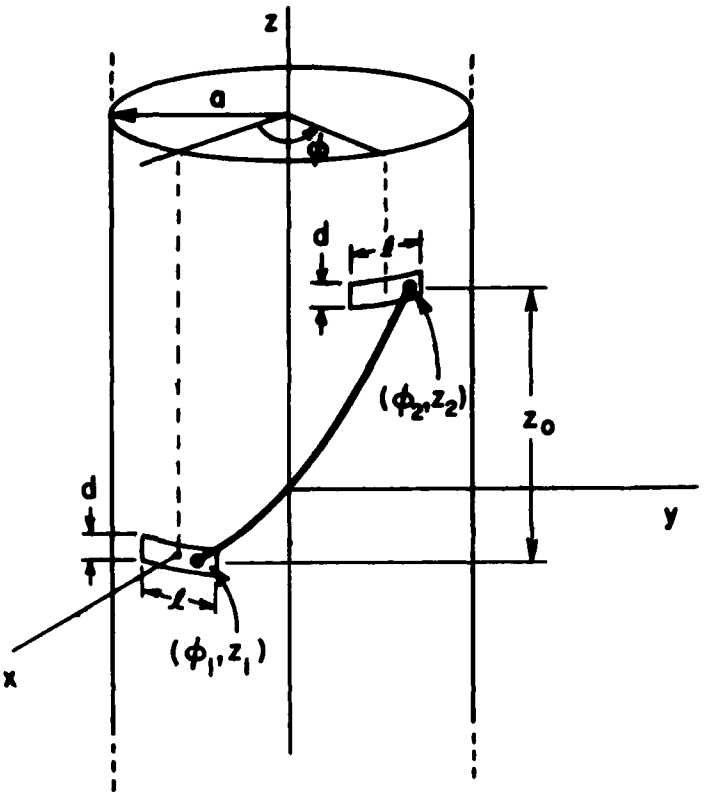

Figure A-V. Slot dimensions and the cylinder geometry.

double surface integration required for the evaluation of the mutual coupling between the slots. In fact, the double surface integration can be reduced to a double line integration via a suitable coordinate transformation. Equation (A-131) can be rewritten as follows:

$$Y_{12}^{c} = \frac{-a^2}{d\ell} \sum_{i=1}^{4} I_i \qquad \text{(A-132a)}$$

where

$$I_1 = \cos\left(\frac{a\pi}{\ell}\phi_o\right) \int_{\phi_1}\int_{\phi_2}\int_{z_1}\int_{z_2} \cos\left[\frac{\pi a}{\ell}(\phi_2+\phi_1)\right] g_{\phi}^{c}(s,\theta)\, dz_1 dz_2 d\phi_1 d\phi_2 \qquad \text{(A-132b)}$$

$$I_2 = \cos\left(\frac{a\pi}{\ell}\phi_o\right) \int_{\phi_1}\int_{\phi_2}\int_{z_1}\int_{z_2} \cos\left[\frac{\pi a}{\ell}(\phi_2-\phi_1)\right] g_\phi^c(s,\theta)\,dz_1\,dz_2\,d\phi_1\,d\phi_2 \qquad \text{(A-132c)}$$

$$I_3 = \sin\left(\frac{a\pi}{\ell}\phi_o\right) \int_{\phi_1}\int_{\phi_2}\int_{z_1}\int_{z_2} \sin\left[\frac{\pi a}{\ell}(\phi_2+\phi_1)\right] g_\phi^c(s,\theta)\,dz_1\,dz_2\,d\phi_1\,d\phi_2 \qquad \text{(A-132d)}$$

$$I_4 = \sin\left(\frac{a\pi}{\ell}\phi_o\right) \int_{\phi_1}\int_{\phi_2}\int_{z_1}\int_{z_2} \sin\left[\frac{\pi a}{\ell}(\phi_2-\phi_1)\right] g_\phi^c(s,\theta)\,dz_1\,dz_2\,d\phi_1\,d\phi_2 \qquad \text{(A-132e)}$$

and

$$s = \sqrt{a^2(\phi_2-\phi_1)^2 + (z_2-z_1)^2} \qquad \text{(A-133a)}$$

$$\theta = \tan^{-1}\left[\frac{z_2-z_1}{a(\phi_2-\phi_1)}\right] . \qquad \text{(A-133b)}$$

It is observed that all four integrals in Equations (A-132b;A-132c;A-132d; A-132e) are similar in form. This appendix is devoted to the discussion of the numerical techniques used to perform only the double surface integration appearing in Equation (A-132b). Similar analysis can be carried out for the rest of the integrals in Equations (A-132c;A-132d;A-132e).

Let us introduce the following coordinate transformations.

$$v = \frac{1}{\sqrt{2}}(\phi_2-\phi_1) \qquad \text{(A-134a)}$$

$$u = \frac{1}{\sqrt{2}}(\phi_2+\phi_1) \qquad \text{(A-134b)}$$

$$t = \frac{1}{\sqrt{2}}(z_2-z_1) \qquad \text{(A-134c)}$$

and

$$w = \frac{1}{\sqrt{2}} (z_2+z_1) \quad . \tag{A-134d}$$

It can be shown that the integral I_1 given in Equation (A-132b), via the transformation defined in Equations (A-134a;A-134b;A-134c;A-134d), can be expressed as follows:

$$I_1 = \cos(\tfrac{a\pi}{\ell}\phi_o) \int_{v_1}^{v_2} \int_{u_1(t)}^{u_2(t)} \int_{t_1}^{t_2} \int_{w_1(t)}^{w_2(t)} \cos[\tfrac{\pi a}{\ell}\sqrt{2}u] g_\phi^c(v,t)\,dt\,dw\,du\,dv. \tag{A-135}$$

The regions of integration in the (t,w) plane and (u,v) plane correspond to the shaded areas illustrated in Figure A-6. The u-integration and w-integration in Equation (A-135) can be readily integrated in closed form and leads to the following expression.

$$I = \int_{v_1=\frac{1}{\sqrt{2}}(\phi_o-\ell/a)}^{v_2=\frac{1}{\sqrt{2}}(\phi_o+\ell/a)} dv \int_{t_1=\frac{1}{\sqrt{2}}(z_o-d)}^{t_2=\frac{1}{\sqrt{2}}(z_o+d)} dt \quad F(t)\left[F(u_2)-F(u_1)\right] g_\phi^c(v,t) \tag{A-136a}$$

where

$$F(t) = \begin{cases} 2t - \sqrt{2}(z_o-d) & ; \quad t \le \dfrac{z_o}{\sqrt{2}} \\ \sqrt{2}\,(z_o+d)-2t & ; \quad t \ge \dfrac{z_o}{\sqrt{2}} \end{cases} \tag{A-136b}$$

and

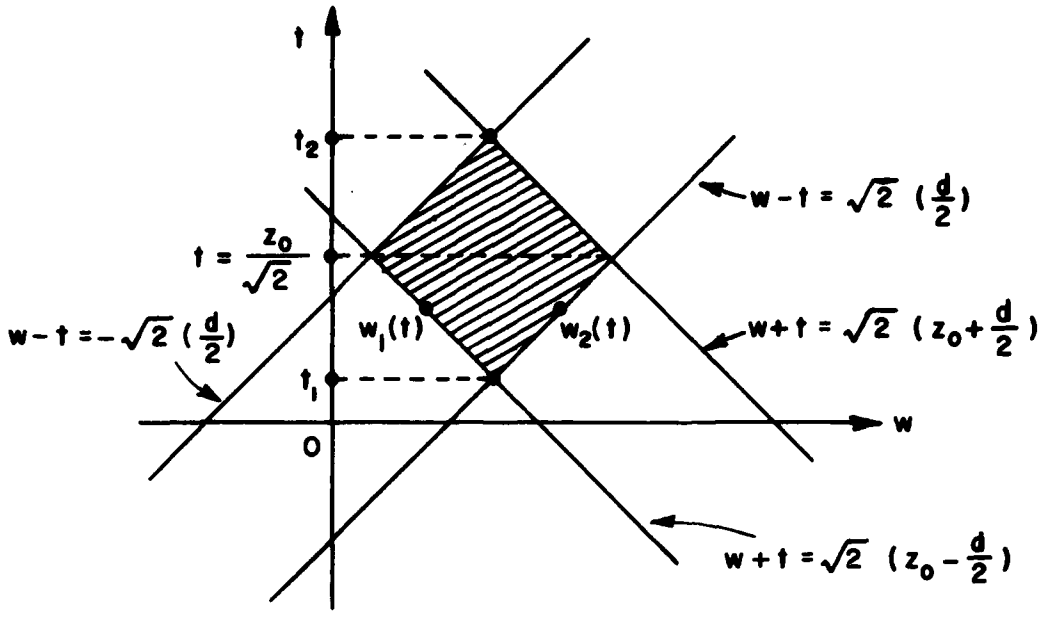

Figure A-VIa. Region of integration in the (t,w) plane.

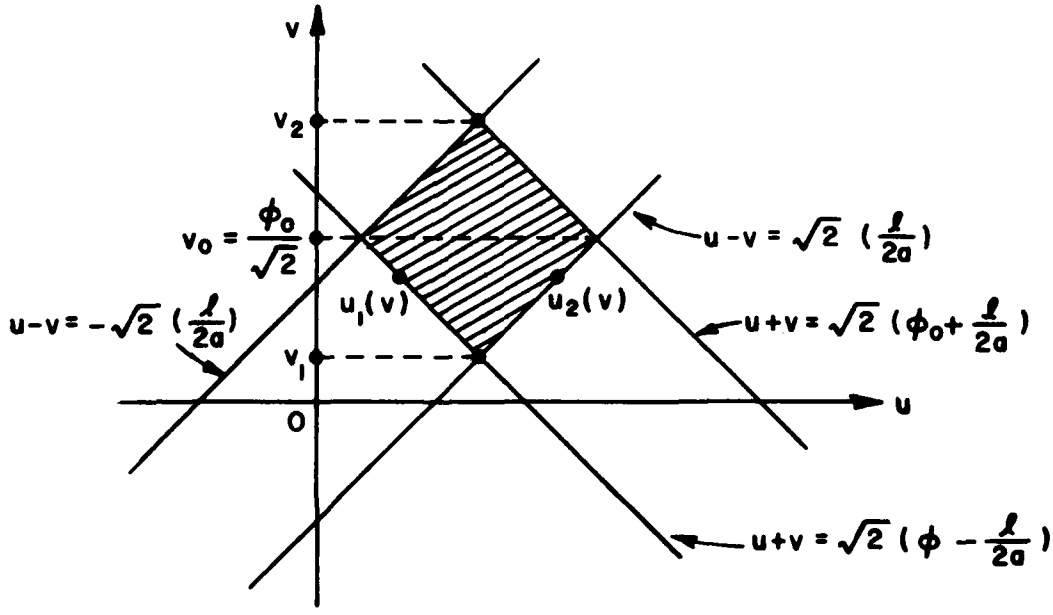

Figure A-VIb. Region of integration in the (u,v) plane.

$$F(u) = \frac{\sin(\sqrt{2}\,\frac{a\pi}{\ell}\,u)}{\sqrt{2}\,\frac{a\pi}{\ell}} \tag{A-136c}$$

$$u_1 = \begin{cases} v - \sqrt{2}\,\ell/2a & v \geq \frac{\phi_o}{\sqrt{2}} \\ \sqrt{2}(\phi_o - \ell/2a) - v & v \leq \frac{\phi_o}{\sqrt{2}} \end{cases} \tag{A-136d}$$

$$u_2 = \begin{cases} \sqrt{2}(\phi_o + \ell/2a) - v & v \geq \frac{\phi_o}{\sqrt{2}} \\ v + \sqrt{2}(\ell/2a) & v \leq \frac{\phi_o}{\sqrt{2}} \end{cases} \tag{A-136e}$$

From Equations (A-132b) and (A-135), one concludes that

$$\int_{\phi_1=-\ell/2a}^{\ell/2a} d\phi_1 \int_{z_1=-d/2}^{d/2} dz_1 \int_{\phi_2=\phi_o-\ell/2a}^{\phi_o+\ell/2a} d\phi_2 \int_{z_2=z_o-d/2}^{z_o+d/2} dz_2 \quad \cos[\tfrac{\pi a}{\ell}(\phi_2+\phi_1)]\, g_\phi^c(s,\theta)$$

$$= \int_{v=\frac{1}{\sqrt{2}}(\phi_o-\ell/a)}^{\frac{1}{\sqrt{2}}(\phi_o+\ell/a)} dv \int_{t=\frac{1}{\sqrt{2}}(z_o-d)}^{\frac{1}{\sqrt{2}}(z_o+d)} dt \quad F(t)[F(u_2)-F(u_1)]\, g_\phi^c(v,t) \tag{A-137}$$

The above equation indicates that the double surface integration in Equation (A-132b) can be reduced to a double line integration via a set of suitable coordinate transformations.

It should be noted that the discussion in this appendix is also valid for the case of two axial slots on the circular cylinder.

APPENDIX V

ON THE SURFACE TYPE FOCK FUNCTIONS

In this appendix we define and list some useful formulas of the Fock functions: $F_h(\xi,y_1,y_2)$, $F_s(\xi,y_1,y_2)$, $v(\xi)$, $u(\xi)$, $v_1(\xi)$, $v'(\xi)$, $u'(\xi)$, and the Airy functions $w_1(t)$ and $w_2(t)$. For a complex τ and real ξ, we define the above functions as follows.

$$F_h(\xi,y_1,y_2) = \frac{1}{2j}\,\frac{1}{\sqrt{4\pi}}\,e^{j\frac{\pi}{4}}\,\xi^{1/2}\cdot$$

$$\cdot\int_{\Gamma_1} d\tau\; W_2(\tau-y_1)\left[W_1(\tau-y_2) - \frac{W_1'(\tau)}{W_2'(\tau)}\,W_2(\tau-y_2)\right]e^{-j\xi\tau}\quad ;$$

$$y_1 > y_2 \qquad\qquad (A\text{-}138)$$

$$F_s(\xi,y_1y_2) = -\frac{1}{2}\,e^{j\frac{\pi}{4}}\,\xi^{3/2}\,\frac{1}{\sqrt{\pi}}\int_{\Gamma_1} d\tau\; W_2'(\tau-y_1)\cdot$$

$$\cdot\left[W_1'(\tau-y_2) - \frac{W_1(\tau)}{W_2(\tau)}\,W_2'(\tau-y_2)\right]e^{-j\xi\tau}\quad ;\quad y_1 > y_2 \qquad (A\text{-}139)$$

where y_1 and y_2 are defined in Sections II and III. For $y_1=y_2=0$:

$$F_h(\xi,0,0) = v(\xi) = \frac{1}{2}\,e^{j\frac{\pi}{4}}\,\xi^{1/2}\,\frac{1}{\sqrt{\pi}}\int_{\Gamma_1} d\tau\,\frac{W_2(\tau)}{W_2'(\tau)}\,e^{-j\xi\tau} \qquad (A\text{-}140)$$

$$F_s(\xi,0,0) = u(\xi) = e^{j\frac{3\pi}{4}} \xi^{3/2} \frac{1}{\sqrt{\pi}} \int_{\Gamma_1} d\tau \frac{W_2'(\tau)}{W_2(\tau)} e^{-j\xi\tau} \quad \text{(A-141)}$$

$$v_1(\xi) = e^{j\frac{3\pi}{4}} \xi^{3/2} \frac{1}{\sqrt{\pi}} \int_{\Gamma_1} d\tau \frac{W_2(\tau)}{W_2'(\tau)} \tau\, e^{-j\xi\tau} \quad \text{(A-142)}$$

$$w_1(\tau) = \frac{1}{\sqrt{\pi}} \int_{\Gamma_1} dz\, \exp(\tau z - \frac{z^3}{3}) \quad \text{(A-143)}$$

$$w_2(\tau) = \frac{1}{\sqrt{\pi}} \int_{\Gamma_2} dz\, \exp(\tau z - \frac{z^3}{3}) \quad \text{(A-144)}$$

where integration contour $\Gamma_1(\Gamma_2)$ goes from ∞ to 0 along the line $arg(z) = -\frac{2\pi}{3}(+2\pi/3)$ *and from* 0 *to* ∞ *along the real axis.*

For $\xi \neq 0$, and y_1, y_2 small, one may approximate F_s and F_h of Equations (A-139) and (A-138) by a Taylor series expansion as follows.

$$F_h(\xi,y_1,y_2) \approx v(\xi) - \frac{j}{4} \xi^{-1} v_1(\xi)[y_1^2+y_2^2]; \qquad \xi \neq 0 \quad \text{(A-145)}$$

$$F_s(\xi,y_1,y_2) \approx u(\xi) + \frac{j}{2} [u'(\xi) - \frac{3}{2} \xi^{-1} u(\xi)]\, [y_1^2+y_2^2]; \qquad \xi \neq 0 \quad \text{(A-146)}$$

For ξ large and positive, one may employ a rapidly converging residue series representation for the Fock functions as follows [6,11,12]

$$v(\xi) = e^{-j\frac{\pi}{4}} \sqrt{\pi}\, \xi^{1/2} \sum_{n=1}^{\infty} (\tau_n')^{-1} e^{-j\xi\tau_n'} \quad \text{(A-147)}$$

$$u(\xi) = e^{j\frac{\pi}{4}} 2\sqrt{\pi}\, \xi^{3/2} \sum_{n=1}^{\infty} e^{-j\xi\tau_n} \tag{A-148}$$

$$v_1(\xi) = e^{j\frac{\pi}{4}} 2\sqrt{\pi}\, \xi^{3/2} \sum_{n=1}^{\infty} e^{-j\xi\tau'_n} \tag{A-149}$$

$$v'(\xi) = \frac{1}{2} e^{-j\frac{\pi}{4}} \sqrt{\pi}\, \xi^{-1/2} \sum_{n=1}^{\infty} (1-j2\xi\tau'_n)(\tau'_n)^{-1} e^{-j\xi\tau'_n} \tag{A-150}$$

$$u'(\xi) = e^{j\frac{\pi}{4}} 3\sqrt{\pi}\, \xi^{1/2} \sum_{n=1}^{\infty} (1-j\tfrac{2}{3}\xi\tau_n) e^{-j\xi\tau_n} \tag{A-151}$$

where τ_n and τ'_n are zeros of $w_2(\tau)$ and $w'_2(\tau)$, respectively, and they are tabulated in Table A-I.

TABLE A-I

Zeros of $W_2(\tau)$ and $W'_2(\tau)$

$\tau_n = |\tau_n|\, e^{-j\pi/3}$ and $\tau'_n = |\tau'_n|\, e^{-j\pi/3}$

τ_n	$\lvert\tau_n\rvert$	$\lvert\tau'_n\rvert$
1	2.33811	1.01879
2	4.08795	3.24819
3	5.52056	4.82010
4	6.78661	6.16331
5	7.94413	7.37218
6	9.02265	8.48849
7	10.0402	9.53545
8	11.0085	10.5277
9	11.9300	11.4751
10	12.8288	12.3848

On the other hand, if ξ is small and positive, one may employ a small argument asymptotic expansion for the Fock functions as follows [6,11,12].

$$v(\xi)\sim 1-\frac{\sqrt{\pi}}{4}e^{j\frac{\pi}{4}}\xi^{3/2}+\frac{7j}{60}\xi^{3}+\frac{7\sqrt{\pi}}{512}e^{j\frac{\pi}{4}}\xi^{9/2}-\cdots \quad \text{(A-152)}$$

$$u(\xi)\sim 1-\frac{\sqrt{\pi}}{2}e^{j\frac{\pi}{4}}\xi^{3/2}+\frac{5j}{12}\xi^{3}+\frac{5\sqrt{\pi}}{64}e^{-j\frac{\pi}{4}}\xi^{9/2}-\cdots \quad \text{(A-153)}$$

$$v_1(\xi)\sim 1+\frac{\sqrt{\pi}}{2}e^{j\frac{\pi}{4}}\xi^{3/2}-\frac{7j}{12}\xi^{3}-\frac{7\sqrt{\pi}}{64}e^{-j\frac{\pi}{4}}\xi^{9/2}+\cdots \quad \text{(A-154)}$$

$$v'(\xi)\ \frac{3\sqrt{\pi}}{8}e^{-j\frac{3\pi}{4}}\xi^{1/2}+\frac{7j}{20}\xi^{2}+\frac{63\sqrt{\pi}}{1024}e^{-j\frac{\pi}{4}}\xi^{7/2}-\cdots \quad \text{(A-155)}$$

$$u'(\xi)\sim\frac{3}{4}\sqrt{\pi}\,e^{-j\frac{3\pi}{4}}\xi^{1/2}+\frac{5j}{4}\xi^{2}+\frac{45\sqrt{\pi}}{128}e^{-j\frac{\pi}{4}}\xi^{7/2}-\cdots \quad \text{(A-156)}$$

For $\xi\geq\xi_0$, the residue series representation with the first ten terms in the summation may be used. For $\xi\leq\xi_0$, the small argument asymptotic expression with the first three terms may be used. In the present study ξ_0 is set to be 0.6 as shown in [11,12].

END 5—79